CRANFIELD UNIVERSITY

Babak Eftekharnejad

Condition monitoring of gearboxes using Acoustic Emission

SCHOOL OF ENGINEERING

PhD THESIS

Supervisor: Dr David Mba

July 2010

CRANFIELD UNIVERSITY

SCHOOL OF ENGINEERING

PhD THESIS

Academic Year 2009-2010

Babak Eftekharnejad

Condition monitoring of gearboxes using Acoustic Emission

Supervisor: **David Mba**

July 2010

Abstract

Acoustic emission (AE) is one of many technologies for health monitoring and diagnosis of rotating machines such as gearboxes. Although significant research has been undertaken in understanding the potential of AE in monitoring gearboxes this has been solely applied to spur gears and slow speed roller bearings. This research presents an experimental investigation that assesses the effectiveness of both AE and vibration technologies in identifying various types of defects on in a helical gearbox; the first known attempt.

Furthermore, the application of advanced signals processing techniques such as Spectral kurtosis (SK) and wavelet analysis were studied on AE and vibration signatures. It is shown that the application of advanced signal processing methods is particularly necessary for monitoring helical gears. The application of SK and wavelet analysis was found to be effective in denoising the acquired signals.

The first chapter of this thesis is an introduction to this research and briefly explains motivation and theoretical background supporting this research. The second chapter summaries the relevant literature to establish the current level of the knowledge in this field. The third chapter describes methodologies and experimental arrangement utilized for this investigation. Chapter 4 discusses helical gear diagnosis for both natural and seeded surface defect. Chapter 5 reports on an experimental investigation in which several technologies such as AE, vibration and motor current signature analysis, were applied to identify the presence of a naturally fatigued pinion shaft in an operating gearbox. Chapter 6 details an investigation which compared the applicability of AE and vibration technologies in monitoring a naturally degraded roller bearing.

It has been concluded that AE is a strong diagnostic tool for early diagnosis of bearings faults. However, the application of condition monitoring for helical gear diagnosis was fraught with some degree of complexity as compared to spur gears. This implies that condition monitoring of the gears using AET can be challenging. On the contrary, the applicability of AET for bearing diagnosis was promising and it offered an absolute advantage over the conventional vibration

diagnosis. Furthermore, the application advanced signals processing methods such as Spectral Kurtosis and wavelet was found to be promising in denoise the recorded AE signals. It was also concluded that the use of different signal processing methods is often necessary to achieve meaningful diagnostic information from the signals.

The results of this research have been published in number of academic journals as listed following:

1. B Eftekharnejad, and D Mba, August 2008, "Acoustic Emission Signals Associated with Damaged Helical Gears," Insight-Non-Destructive Testing and Condition Monitoring, **50**(8) pp. 450-451,452,453.

2. Eftekharnejad, B., and Mba, D., 2009, "Seeded Fault Detection on Helical Gears with Acoustic Emission," Applied Acoustics, **70**(4) pp. 547-555.

3. Behzad, M., AlandiHallaj, A., Bastami, A. R.,Mba, D.,Eftekharnejad, B., 2009, "Defect Size Estimation in Rolling Element Bearings using Vibration Time Waveform," Insight: Non-Destructive Testing and Condition Monitoring, **51**(8) pp. 426-430.

4. Eftekharnejad, B., and Mba ,D.,2009," SHAFT CRACK DIAGNOSTICS IN GEARBOX",

Applied Acoustic ,submitted.

5. Eftekharnejad, B., Carrasco, M. , Charnley, B. , Mba, D. , The application of spectral kurtosis on Acoustic Emission and vibrations from a defective..., Mechanical Systems and Signal Processing (2010), doi:10.1016/j.ymssp.2010.06.010

6. B Eftekharnejad, B Charnley and D Mba," Source location of natural defect on a high speed rolling element bearing using Acoustic Emission", Engineering Fracture Mechanics, submitted.

7. B Eftekharnejad and D Mba ," Monitoring natural pitting progress on helical gear mesh using Acoustic Emission and Vibration", Strain, accepted.

"*Everything should be made as simple as possible, but not simpler*"

Albert Einstein

Acknowledgment

First and foremost I express my gratitude to my parents. I attribute my PhD to their encouragement and effort , without which the completion of this thesis was impossible. I offer my sincerest regards to my supervisor, Professor David Mba, who has supported me throughout my research with his patience and knowledge. One simply could not wish for a better or friendlier supervisor. Lastly, special thank goes to Alan Hutchings, Bernard Charnley and Scott Booden for their technical support over the past few years.

TABLE OF CONTENTS

LIST OF FIGURES

Nomenclature

Symbol	Definition
E	Module of elasticity
E^*	Equivalent module of elasticity
e	Weibull factor
P	Load (MPa)
P_0	Maximum load within contact zone
a	Contact radius
R	Radius of curvature
τ_{max}	Maximum shear stress
Z	Depth beneath the surface of material
S	Probability of survival
N	Integer counter representing number of cycle and
L	Length
$C_{1,2}$	Material dependent exponent
t	time
$S(t)$	Signal in time domain
$S(\omega)$	Signal in frequency domain
μ	Mean of signal
σ	Standard deviation
T	Sampling period (sec)
ω	Frequency
$X(t)$	Averaged signal in time domain
Ψ	Shape factor of mother wavelet
ϑ	Poisson ratio
α	Scale factor
τ	Window length
η	Efficiency of motor
P_{in}	Input power
P_{out}	Output power
P_{loss}	Power loss
I	Electric current
(k)	Filter coefficient
S_{nY}	n statistical of moment of Y
$W(n)$	Window function
$K_f(Y)$	Spectral kurtosis value

1 Introduction

1.1 Background

Today's competitive market together with the revolution in consumer expectations and technology has made companies become more concerned about their productivity and performance [1]. For industries to survive in such a complex and competitive environment it is vital to improve their product reliability whilst cutting down on production cost. Product reliability is an important factor for the manufacturer in the mining, aviation, nuclear and chemical industries where operational failure can lead to a devastating disaster. According to the report issued by Mine Safety and Health Administration (MSHA) [2], 20% of the total fatal mining casualties in the US between 2005 and 2009 were caused by machinery failure. On the other hand, maintenance expenses can directly contribute to the final cost of product. Given the demand for product reliability, as well as the reduction in production cost, it is essential to employ condition monitoring (CM) techniques for firstly predicting the failure prior to the event and secondly preventing unexpected shutdowns of machinery. The former is particularly important in the oil and gas sector where unexpected plant shutdown can result in a major economic loss, while an unexpected failure can result in fatalities in civil aviation. There have been continuous challenges in designing robust CM systems capable of diagnosing damage in its early stages of development and predicting the remaining life of the machine.

Gearboxes are the key part in any rotating machine. In wind turbines the price of the transmission system is usually between 15-20% of the total turbine value [3]. McNiff et al. [4] reported on 20% gearbox related failure on 200 Micron 65 wind turbines over 10,000 hours of operation. There have also been some reports on gearbox related fatalities in aviation. From 1964-1974, 20% of the total helicopter accidents in the UK were due to gearbox malfunction [5, 6]. On 10th April 2009, the BBC News broadcast a report on the death of 16 people in a North Sea helicopter crash because of gearbox failure. The recent interest on condition based and predictive maintenance of industrial assets, together with product safety, has led to a growing interest in the condition monitoring of gearboxes.

There are different technologies being used for the purpose of the condition monitoring of gearboxes. Vibration and wear debris monitoring are among the most popular methods of CM in industry [7, 8]. The wear debris monitoring involves analyzing and measuring the wear particles and contaminates inside the used oil. This method is very time consuming and requires fairly advanced and expensive laboratory equipment [9]. The vibration measurement is not capable of detecting the incipient damage inside the machines because the source of vibration in machines is changes in stiffness. Hence the vibration response of the machine will not show any change unless the extent of the damage is high enough to influence the mechanical integrity and therefore stiffness [10, 11]. For the past few decades there has been an awareness for using Acoustic Emission (AE) technology in monitoring gearboxes [12]. Because of the microscopic origin of AE activity in rotating machines, AE has shown effectiveness in detecting the incipient damage in a more advanced way than wear debris and vibration monitoring. To date, most investigations into the application of AE in gearbox diagnosis have been made on spur gears and slow speed roller element bearings [12, 13]. This research has aimed to build a further insight into condition monitoring of gearboxes by focusing on the application of AE technology in monitoring broader ranges of gearbox components and failures. The outcome of this work is expected to strengthen the position of AE monitoring in industry for health diagnosis of transmissions.

1.2 Project Objectives

The project objectives are listed as follows:

- To assess the capability of AE technology (AET) for detecting the location of defects and their propagation in helical gears and high speed roller element bearings. Others have made similar investigations on spur gears and slow speed bearings [14, 15]; however, this research is the first known attempt with regard to helical gears and high speed roller bearings. The authors believes the task of locating the position of defects on both gear and bearing carries significant diagnostic values as it can help to identify the root cause of the damage as well as the design or assembly problems leading to the failure. An example of such is the presence of misalignment in the gearbox causing an overload and uneven load distribution of bearing race, which can lead to the onset of localized damage on bearing. Finding the position of damage can address the source of misalignment.

- To conduct a comparative study between AE, Vibration and Motor Current Signature Analysis to diagnose the naturally fatigued shaft. This investigation has built on Elforjani and Mba's research [16] in which AET was applied to diagnose cracks on a slow speed shaft. Furthermore, this research is the first of its kind which has studied natural fatigue of a relatively high speed shaft in an operating actual gearbox .

- To study the application of advanced signal processing techniques to enhance the diagnostic effectiveness of AE signals.

1.3 Contributions

This research has provided several contributions to the knowledge:

- Investigation on the applicability of Spectral Kurtosis (SK) in analyzing Acoustic Emission signals; thus far, the application SK has been limited into vibration diagnostic. Given the high level of background noise superimposed to AE signals, it is believed that the use of SK can effectively cancel the back ground noise and offer diagnosis advantages.

- Investigation on AE diagnosis capability in relation to Helical gears. Whilst Others have made the similar investigation on spur gears [13] this research is the first known attempt in which Helical gear diagnosis has been studied.

- Studying the prognosis and diagnosis of high speed roller bearing using vibration and AE; this complimented the work of Elforjani [17] who made the similar contribution for slow speed bearing.
- Diagnosis of natural fatigued shaft in actual transmission system using AE.

- Investigation on the correlation between the volume of removed material from helical gear surface and AE activity.

CHAPTER 2

---

2 Transmission (Gearbox)

Gearboxes are the key parts in any rotating machines and used to transfer the power and rotational speed from a mechanical source to another rotating component. The main components of each gearbox are bearings, shafts and gears, see Figure 1.

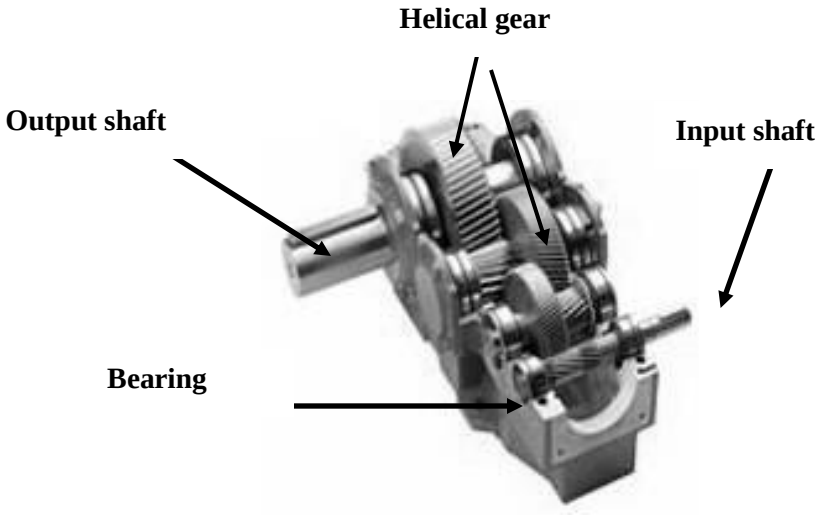

Figure 1 Hansen P4 gearbox

2.1 Gears

Gears are the key components inside the transmission designed to produce mechanical advantages. The gears transfer the rotational motion and torque from the input shafts to output shafts. There are a variety of types of gears being employed in gearboxes; however, where input and output axes are parallel to each other, only spur and helical types of gears are used, see Figure 2. The spur gear teeth are straight and parallel to the axis of rotation. The helical gears can be assumed as an infinite number of spur gears adjacent to each other with relative offset. The helical design involves angled teeth to the rotational axis. This angle provides a smoother and quieter run for a helical gear, making it the perfect choice for large load transmission at high operational speeds whereas the spur gears are suitable for slow speed applications [18].

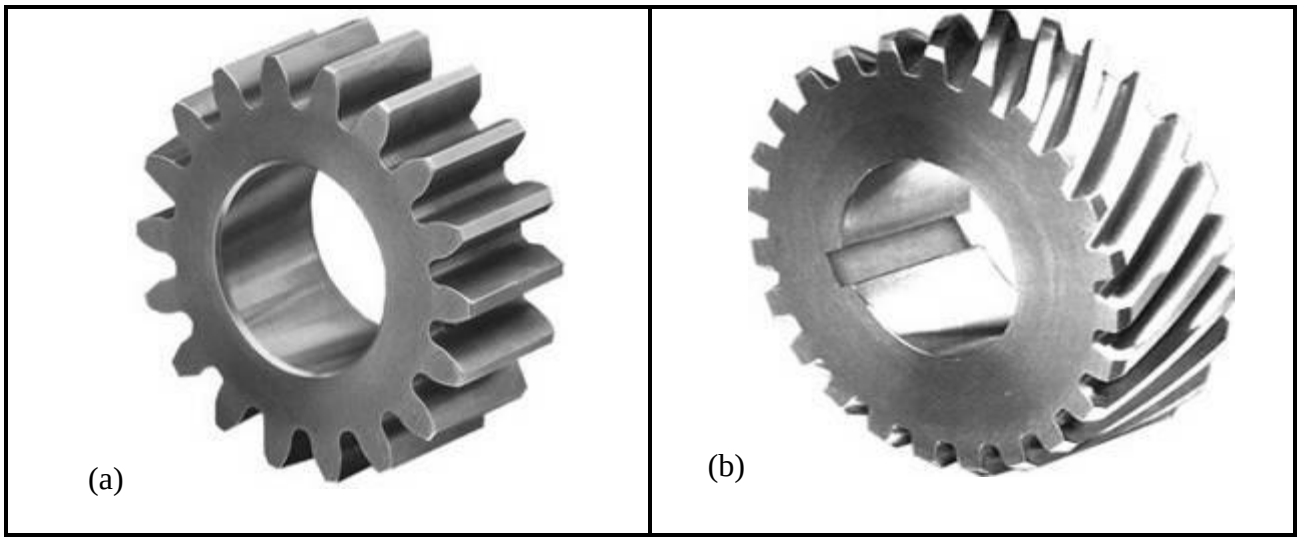

Figure 2 Illustration of spur (a) and helical (b) types of gears

2.1.1 Meshing mechanism

During the gear operation combination of the sliding and rolling, contact occurs at both sides of the meshing teeth. However, the slide-to-roll ratio varies at different position of the tooth surface. For the spur gears, the length of contact is constant and the pure rolling contact is experienced on the pitch line, while the highest slide-to-roll ratio is associated with the beginning and end of contact on dedendum and addendum respectively . The direction of sliding and rolling velocity is the same on the addendum (positive sliding) and opposite on the dedendum (negative). The length of contact for helical gears is progressive and gradually increases and decreases in contact length over a particular tooth. In contrast to those of the spur gear, the pitch points of helical gears are not located on a single line and not passed at same time along the tooth face width. Hence during the helical mesh the continuous pure rolling and varying slide-to-roll ratio are experienced on and away from the pitch point [19-22].

2.1.2 Mode of failures

Gears can be damaged in different ways. Fatigue is the most common type of failure in gears and is categorized into two groups: surface fatigue and bending fatigue. The latter involves the growth of a crack near the tooth root resulting in partial or complete fracture of the tooth [21].

Spalling and pitting are the two main types of surface fatigue. Pitting constantly occurs on an operating gear mesh along the contact zone and is considered to be the initial mode of failure originating from a subsurface crack; spalling is synonymous with the presence of deep craters on the tooth surface [23-25]. The repetitive high contact stresses are responsible for the formation of pits and spalls. The rolling contact between two curved surfaces normally results from a presence of high shear stress concentration further below the surface of materials, see Figure 3. This will result in the initiation of a subsurface crack, from the point of high stress concentration, moving parallel to the surface of the material. The repetitive rolling action can change the path of crack propagation towards the surface of the material resulting in the detachment of wear particles from the main body, see Figure 4. The gear surface is always subjected to the combination of sliding and rolling contact. The presence of sliding contact is associated with the elastic deformation of the surface which itself can influence the stress distribution below the surface of the material. The maximum stress point and the position of the crack will therefore be shifted close to the surface of the material. Furthermore, depending on the direction of the rolling and sliding, the magnitude of the maximum shear stress varies. It is worth to mention that with introduction of the lubricant on sliding surfaces the magnitude of shear stress will be reduced. At the dedendum, where the direction of rolling and sliding are opposite, the localized stress is higher than at the addendum and pitch lines (in spur gears) hence this will result in surface fatigue to be initiated from the dedendum [26]. More recently Tan et al [13] reiterated this phenomena as they showed pitting initiation and growth initially on the dedendum.

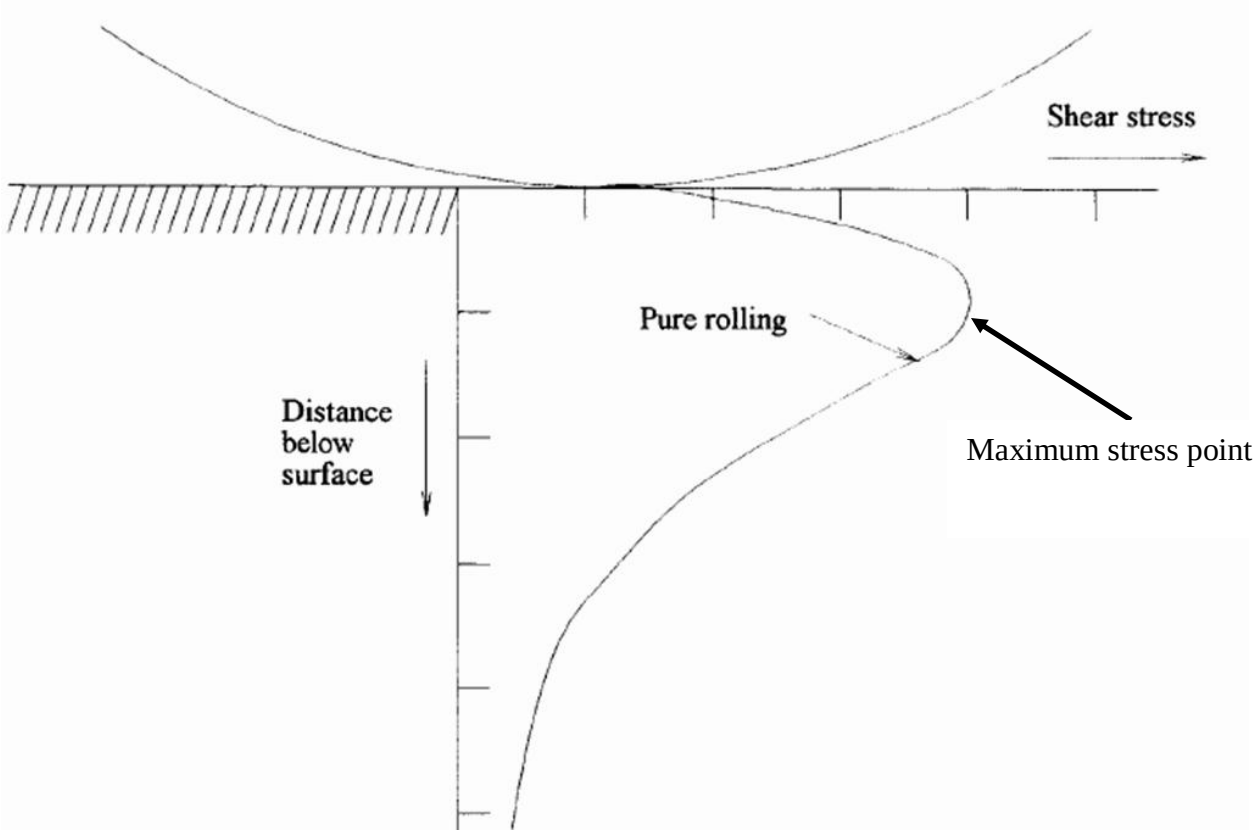

Figure 3 Stress distribution at and near two contacting surfaces under pure rolling [26]

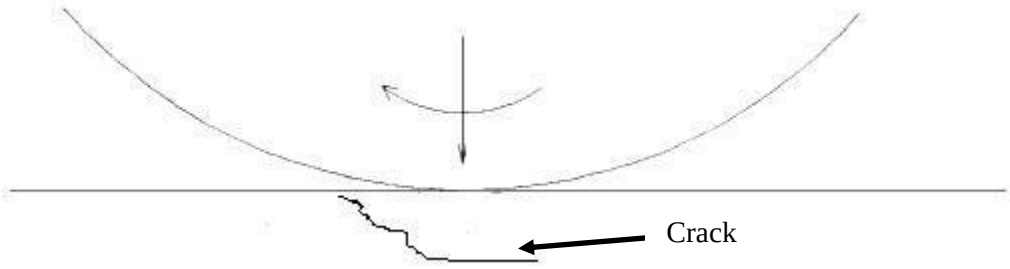

Figure 4 Formation of sub-surface crack [26]

2.1.3 Gear life predication

There are three major standards for calculating the theoretical gear life:

- **BS 436-3:** Method for calculation of contact and root bending stress limitations for metallic involute gears. [27]
- **ISO-6336-02:** Calculation of the surface durability of gears. [28]
- **ANSI/AGMA 2101-C95:** Rating Factors and Calculation Methods for Involute Spur and Helical Gear Teeth. [29]

These methods involve predicting the allowable bending and contact stress for gears. The gear systems are durable if the maximum stress, during the gear operation, is less than the allowable values. Although the given calculation provides no guarantee of undamaged operation for a pair of gears within the estimated service life, it will determine the time after which the gear is likely to be damaged.

2.1.4 Gear lubrication

The lubrication of the sliding bodies is divided into three groups: Boundary, Elastohydrodynamic (EHL) and Hydrodynamic regime. Where the surfaces are counter conformal, i.e. they have line or point contact, the local contact pressure will be very high, resulting in the elastic distortion of the surfaces. This circumstance is known as EHL under which a very thin film, in the scale of a few micrometers, is formed. The pressure distribution in a typical counter conformal contact between a sphere and a plane under EHL condition is presented in Figure 5. Since the mass flow of the oil film between sliding surfaces is constant and given that the presence of Hertzian pressure drops to the ambient level at the edges of the contact zone, the secondary pressure peak is generated to meet the requirement of mass continuity. The position of the secondary peak matches the point of minimum oil film thickness, see Figure 5 [30].

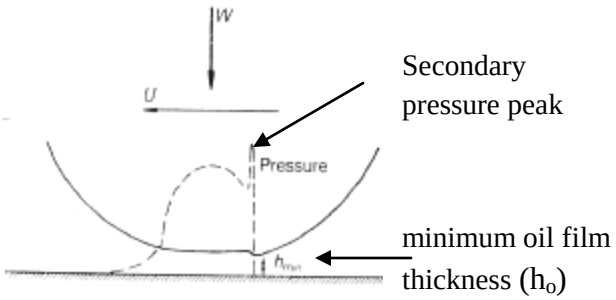

Figure 5 Elastic distortion of sphere under combined normal load and sliding condition [30]

Under abnormal contact stress or very slow sliding speed the EHL film cannot be maintained and the direct surface asperity constant occurs, causing a high rate of wear and friction. Therefore, the EHL is replaced by the boundary lubrication condition which involves the formation of adsorbed molecular film on the surface [31]. The specific oil film thickness (λ) is defined as the ratio of minimum oil film thickness to the r.m.s. roughness of both surfaces. For boundary lubrication, the value of λ is less than one whilst for $1<\lambda<3$ the mixed or partial EHL condition will be dominant under which some asperities come into contact. For the greater values of λ the asperity contacts are negligible [30].

2.2 Rolling element bearing

The rolling element bearings are usually the smallest rotating components within the gearboxes. Although small, failure of these bearings can result in the malfunction of the entire gearbox; i.e., a single bearing failure in a steel mill can result in a £150-£300 financial loss per hour while such failure could involve up to £1-£20 loss per hour in modern power generation systems [32]. The rolling element bearings are divided into two groups of roller and ball bearing; however, both types share a common mechanical mechanism. The roller bearings consist of roller, outer and inner race, see Figure 6. The relative motion of the inner and outer race results in the roller rolling over its pathway; however, this rolling motion is normally associated with a slight sliding element. The rolling element bearings may be lubricated using solid, liquid or grease. Solid

lubrication is normally employed under extreme conditions where the operating temperature and pressure are very high or extremely chilled, i.e. in space application; whereas liquid lubrication is suitable for the high operating speed. The most common method of lubricating roller bearings is by grease lubrication and this is particularly recommended for moderate applications with a speed parameter of less than 600,000 DN [1][33].

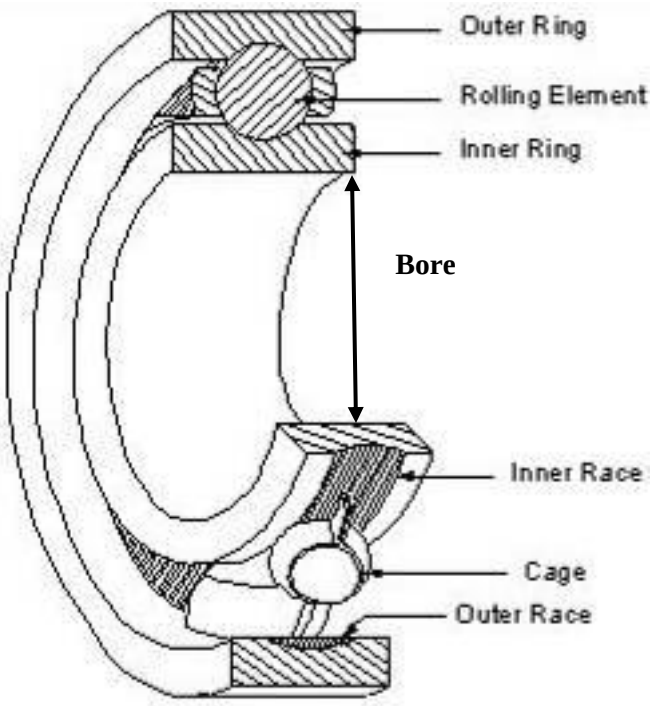

Figure 6 Schematic presentation of a ball bearing with cut through view [34]

2.2.1 Rolling bearing failures

Bearings are damaged mostly because of improper lubrication and assembly, excess vibration, manufacturing abnormalities and wear. Common types of failure mode associated with rolling bearings are as follows [35]:

- Damaged rollers: This type of damag is normally caused by misalignment and manufacturing error and associated with either peeling or chipping of roller.
- Fractured cage: The main reason for cage breakage is improper assembly.

[1] Is a parameter which is equal to the bore in millimetres multiplied by speed in r.p.m.

- Skidding: Appears as uneven wavy wear marks caused by roller slip due to a variable rotating load or local distortion of the races. Also it occurs under a very low radial load under which the clearance between roller and races is significant resulting in roller slip. The presence of roller slip is a prerequisite for the occurrence of skidding; slip results from the speed difference between the roller and rotating inner race.

- Formation of spall on the outer race: The rolling fatigue is responsible for the generation of the subsurface crack which eventually leads to the formation of spall on the outer and inner race.

- Smearing: This type of failure is associated with scuff marks, discoloration and metal transfer on the stationary race way. It is often caused by poor lubrication

Most of the listed damages can be prevented by accurate controlling of lubrication and the machine assembly. However, the formation of fatigue spall is inevitable since the operational bearings have a limited fatigue life and are constantly subjected to repetitive surface stresses. It is worth mentioning that the focus of this research is the diagnosis of naturally occurring fatigue spalls on the outer race.

2.2.2 Bearing life prediction

Rolling bearing contacts are selected with two factors: static load and life (L_{10}). Static load is the maximum load withstood by the stationary bearing for which the total deformation of roller and race is less than the 0.1% of the roller diameter. The dynamic capacity of the bearing (L_{10} life) is the load operational load under which the life of the bearing is 1,000,000 revolutions with a failure rate of 10% [33]. For the grooved race bearing, the standard procedure, as described by BS 5512, 1991, is employed for determining the dynamic load rating (L_{10}) [36]. There are several theories for the determination of the bearing life for the given load and operation speed. For this investigation Hertz contact theory [30] is used to calculate the surface stress and

deformation. Hertz theory determines the contact area between two elastic spheres with respect to the applied external loads. Figure 7 presents the schematic illustration of Hertzian contact between two spheres in which $R_{1,2}$ correspond to radius of curvature for each sphere, a is contact radius and $E_{1,2}$ and are module of elasticity and Poisson ratio respectively. The Hertz theory assumes that the strain between contacting bodies are small and falls within the elastic region and each solid can be considered as an elastic half-space ($a<<R$) [37].If two sphere loaded with load (P) according to Hertz theory the maximum contact pressure between the spheres (P_0) is determined from Equation 1-4 [37]:

$$E^* = \left(\left(\frac{1-\upsilon_1^2}{E_1}\right) + \left(\frac{1-\upsilon_2^2}{E_2}\right) \right)^{-1}$$ **Equation 1**

$$R = \left(\frac{1}{R_1} + \frac{1}{R_2}\right)^{-1}$$ **Equation 2**

$$a = \left(\frac{3PR}{4E^*} \right)^{-1}$$ **Equation 3**

$$P_0 = \left(\frac{6P E^{*}}{\pi^3 R^2} \right)^{1/3}$$ **Equation 4**

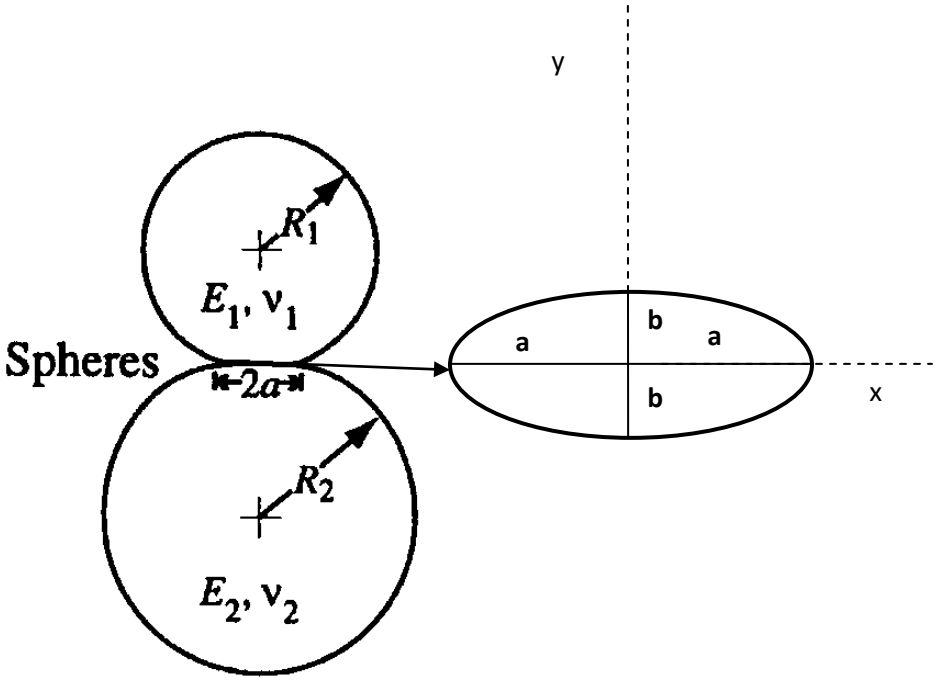

Figure 7 Schematic illustration of Hertzian contact between spheres [37]

To determine the subsurface stress the Thomas and Hoersch theory [38] was employed. Applying the latter the maximum shear stress (τ_{max}) and its location (Z) along the principal axis (z) are determined using Equations 5 and 6. Appendix C lists the indicative values of pressure in the contact zone as compared to yield and ultimate stress of different materials.

$$\tau_{\max} = 0.31 P_0$$ **Equation 5** [37]

$$Z = 0.48a$$ **Equation 6** [37]

Having determined the maximum subsurface stress the Lundberg-Palmgren theory [39] was used for fatigue life evaluation, see Equation 7.

$$\ln \frac{1}{s} \approx \frac{\tau_{\max}^{C_2} N^e aL}{Z^{C_1 - 1}}$$ **Equation 7** [39]

Where

s: Probability of survival (Reliability factor)

N: Life (Number of cycles)

L: Length of running track of the race

e: Weibull factor

$C_{1,2}$: Material depended exponents

Wiebull factor, e, is equal to 1 assumes the constant failure rate over defined period of time; the values less than and greater than 1 are correspond to decreasing and increasing failure rate respectively .$C_{1,2}$ are material dependent exponents with the values are function of elasticity, fracture and fatigue limit. For steels these values are normally close to 0.3 [39].

2.3 Shaft

Fatigue is the most common type of failure associated with transmission shafts. The fatigue crack normally initiates from the critical points where stress concentration is higher, i.e. the stress raiser points [40, 41]. The keyways roots and the edges resulting from a sharp change in the cross section area are among the most typical stress raiser points in circular cross section shafts [18], see Figure 8. Berndt and Bennekom [42] categorised shaft fatigue into three groups among which rotational bending is the most observed type of fatigue in the circular shaft; rotational bending fatigue normally occurs when the shaft is subjected to the oscillating tensile and compressive stress within its circumference. Figure 9 presents a schematic illustration of the fatigues in a shaft cross section under high and moderate stress concentration; (a) and (c) are associated with the case in which the fatigue was initiated from a single origin whereas (b) and (d) correspond to a mode where several origins contributed to the formation of multiple fatigue crack. Multiple origin fatigue type normally starts from the centre of the shaft while the single origin fatigue involves 15 º angles between the symmetric axis of the loaded zone and the vertical axis on the fractured surface, see Figure 9.

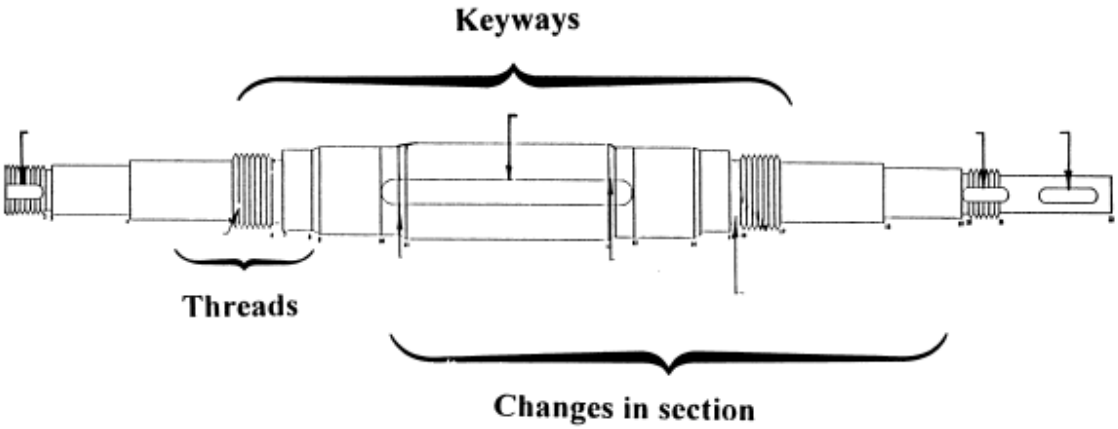

Figure 8 Typical stress concentration sites on shafts. [42]

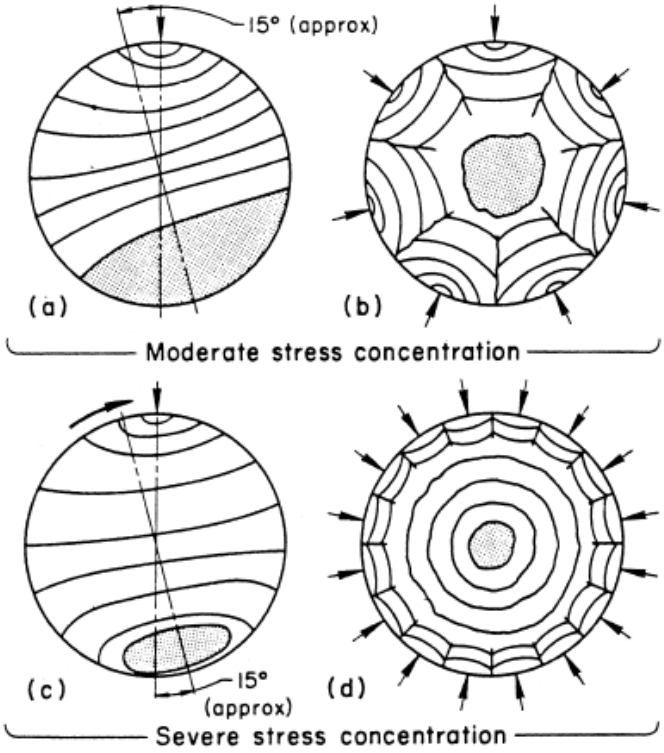

Figure 9 Schematic illustration of a fatigues shaft cross section. [24]

2.4 Condition monitoring technologies applied to mechanical transmissions

There are different technologies being used for the purpose of the condition monitoring (CM) of gearboxes. Vibration and wear debris monitoring are among the most popular methods of CM in industries [7, 8]. Wear debris monitoring involves analysing and measuring the wear particles and contaminates inside the used oil. This method is very time consuming and requires fairly advanced and expensive laboratory equipment [9]. For the past few decades there has been an increased awareness of using Acoustic Emission (AE) technology in monitoring gearboxes [12]. Because of the microscopic source of AE activity in rotating machines, AE has shown an effectiveness in detecting the incipient gear and bearing damage that is more advanced than wear debris and vibration monitoring. Motor current signature analysis (MCSA) is another monitoring technology mainly used for online monitoring of machinery. In some applications, where access to the machine is restricted, this method of monitoring is relatively advantageous over other monitoring technologies. MCSA is based on the fundamental premise that any torsional vibration in a system manifests itself in the frequency spectrum of the current signature as proposed by Yacamini et al. [43]. Apart from oil analysis, other methods involve the measurement of the real time analogue signal from the transmission component using special sensors. The key focus of this project is to assess the diagnostic capability of the former three technologies in relation to transmission.

2.4.1 Signal processing methods

Measurements from sensors are normally in analogue format and appear as a time varying electric voltage. Data acquisition systems are employed to convert the acquired analogue signal into digital. Signal processing methods are a range of techniques used to interpret and identify the source of recorded digital signals. Digital signals are usually presented and analysed in time, frequency or time-frequency domains.

2.4.1.1 Time domain analysis

Different features can be extracted from time domain signals. These features are used to compare the change in signal characteristics over the specified period of time.

2.4.1.2 Root mean square (r.m.s.)

Signal r.m.s. is a measure of signal intensity over a defined duration of time and is determined using Equation 8. The change in signal r.m.s. can be associated with change in machine integrity or dynamic behaviour; for some machinery, the vibration r.m.s. beyond the designated threshold level is an alarming factor, suggesting the termination of machine operation.

$$r.m.s = \sqrt{\frac{\int_{t_1}^{t_2} |S(t)|^2 \, dt}{t_2 - t_1}} \qquad \textbf{Equation 8}$$

S(t): Signal in time domain

t: Time

2.4.1.3 Kurtosis

Relative peakedness of probability distributions of signals is compared using kurtosis. For the normal probability distribution, the kurtosis value is 0. Equation 9 estimates the kurtosis values for time domain signals. Kurtosis is also a degree of signal impulsiveness which can be associated with the presence of impact pulses resulting from a machine component. Dyer and Stewart [44] first proposed the use of kurtosis for bearing defect detection. For an undamaged bearing with Gaussian distribution, the kurtosis value is close to 3. A value greater than 3 is judged by itself to be an indication of impending failure and no prior history is required. However, one disadvantage is that the kurtosis value comes down to the level of an undamaged bearing (i.e. 3) when the damage is well advanced [45].

$$Kurtosis = \frac{\int_{-\infty}^{+\infty}(t-\mu)^4 S(t)dt}{\sigma^4}$$ **Equation 9** [46]

μ: Signal mean

σ: Standard deviation

2.4.1.4 Crest factor

The crest factor (CF) is defined as the ratio of the peak value divided by the signal r.m.s. which gives an indication of signal peak-to-average ratio. CF is a traditional method of measuring the smoothness of a signal. For instance, in bearing diagnosis, the presence of a fault often generates a spiky signal profile resulting in an increase in CF; however, upon the development of the defect the CF decreases due to an increase in the levels of signal r.m.s. [47, 48].

2.4.1.5 Signal count

Count is a statistical feature of a signal which counts the number of crossings of a specific level for that signal. The factor is related to the distribution of peaks in a given period of time [49].

2.4.1.6 Time synchronous averaging (TSA)

The acquired signals often contain noise which results in a lower signal to noise ratio (SNR); the presence of noise within the signal makes machine diagnosis rather challenging and it is therefore important to reduce the noise level prior to the application of any signal processing method. One way to cancel the noise in the time domain is by the use of the TSA technique. This method involves averaging the recoded signal over the specified of time duration; in machine

diagnosis, this duration is usually attributed to the period of a shaft's rotation, see Equation 10 and Figure 10. The TSA method can only be applied to signals recoded from the machinery with synchronous input; synchronous operated machines are rare in industrial application due to load or voltage fluctuations [50]. To overcome this problem, Jafarizadeh et al. [50] introduced a coefficient to correct the asynchronously averaged signals. They corrected each shaft revolution period according to arbitrarily selected duration using the developed correlation factor.

$$TSA(t) = \left(\frac{1}{N}\right)\sum_{m=0}^{N-1} s(t - mT)$$ **Equation 10** [50]

N: Number of averages

T: Shaft rotational period

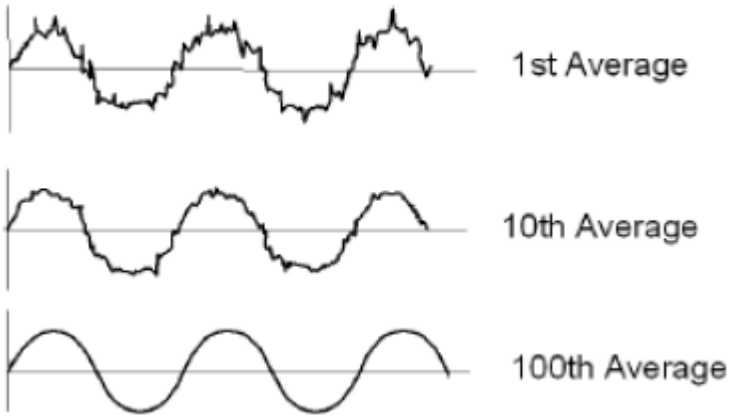

Figure 10 Illustration of the effect of Time Synchronous Averaging [51]

2.4.1.7 Frequency domain analysis

It is often necessary to study the frequency content of the signals. In condition monitoring of machines, the recoded signals are usually diagnosed for a particular frequency band associated with machine elements such as gears, shafts and bearings. This is based on the fact that each machine element has a characteristic rotational frequency; defect on any of the bearing component is manifested as an increase in energy of the particular frequency band associated with defective element [52]. Throughout this research the concept of Fast Fourier Transform (FFT) has been widely employed to generate the frequency spectrum of the acquired signals. This methods works on the basis of Fourier transform which involves representing a polynomial function or a signal by the sum of sinusoid functions with different frequencies [53]. Equation 6 determines the Fourier transform of signal *S(t)* and the frequency spectrum of a signal is generated by plotting the amplitude of each sinusoid function, that equals to real parts of *S(ω)*, against its frequency.

$$S(\omega) = \int_{-\infty}^{+\infty} S(t) e^{-2\pi i t\omega} dt$$ **Equation 11** [53]

ω: Frequency

S(ω): Signal in frequency domain

2.4.2 Complementary signal processing techniques for gearbox diagnosis

2.4.2.1 Time-Frequency domain analysis

Although effective, the application time or frequency domain analyses are limited to non-stationary signals. Since rotating machines are often subjected to variation in operational conditions or dynamic fluctuation, the resultant output signals may possess some degree of non-stationary. These non-stationary features may contain important information which can provide advantages for the significant diagnosis, hence the application of time-frequency analysis has

gained interest as an effective tool in analysing non-stationary signals [54]. There are different methods of analysing signals in time-frequency domain analysis among which Wavelet transform, Winger-Ville distribution (WVD) and Short Time Furrier Transform (STFT) are widely used. Meng and Qu [55] have reported on an application of WVD in processes vibration signature from a faulty rolling bearing and pair of gears. It was shown that WVD was more successful in detecting the source of modulation compared to conventional frequency and time domain analyses. Throughout this research Wavelet analysis has been employed for the purpose of time-frequency domain analysis. Multi-resolution analysis using wavelet transform has gained ground as an effective signal processing tool. The fundamental idea is to decompose the signal into several frequency ranges with finer resolutions, thereby achieving a better understanding of the time-frequency content of the signal [56]. In signal processing, two types of continuous (CWT) and discrete (DWT) wavelet transforms are employed. The function of CWT is to break up the signals into scaled and shifted versions of a transient type of signal known as the mother wavelet, ψ. The scale, a, and frequency of each wavelet are reversely correlated with each other so that the higher scale corresponds to the low frequency version of same wavelet. The coefficient, C, for each segment of the signals is determined based on the difference in energy of scaled and shifted versions of the mother wavelet and that of a particular segment, see Equation 12 [56].

$$C(a,\tau) = \frac{1}{\sqrt{a}} \int_{-\infty}^{+\infty} x(t)\psi\left(\frac{t-\tau}{a}\right)dt \qquad \textbf{Equation 12} \text{ [56]}$$

To save calculation time, discrete wavelet analysis, DWT, was developed; it is performed by discrete scaling and shifting the mother wavelet along the signals. In signal processing application, DWT is often used to decompose the signal into several frequency bands and thereby each frequency band can be treated as an independent signal for which separate analysis can be implemented. Orthogonal wavelets have been found to be a convenient tool due to their good time and frequency localisation. Daubechies wavelet is known to be more effective than other Orthonormal wavelets such as Biof, Coiflet, Haar and so on, in analysing AE signature, as

it provides full details of the localised energy of the signal [56-58]. Some applications of wavelet transforms in manufacturing processes using AE have been discussed in detail and are well documented [59, 60]. Whilst there are limited publications on the application of wavelet to acoustic emissions generated from rotating machinery, a review of these studies has been provided in chapter 2.Throughout this research the choice of best mother wavelets was selected by carefully assessing the effectiveness of broad range of wavelets over the acquired AE and vibration signals. As it was expected Daubechies wavelet of order 8 (db8) exhibited better time-frequency resolution in compare with lower order of same type as well as the other type wavelets. The higher order of Daunechies wavelet did not offer any diagnostic advantageous over db8.The number of decomposition level were also chosen based on the sensor measurement range, the excepted characteristic frequency of gear box and sampling frequency. However, it is worth to mention that one way of automatically establishing the optimum wavelet parameters is to use the Shannon entropy; Shannon entropy is a measure of uncertainty between to discrete parameter. This is particularly useful method in online intelligent monitoring systems. This method involves selecting the mother wavelet and correct scaling factors based on the minimum Shannon entropy; this is to match the wavelet with mechanical impulse characteristic [56, 60].

Although successful, there are some drawbacks associated with the application of wavelet for signal processing purposes. As such, is the dependence of diagnosis outcome to the type of mother wavelet; appropriate selection of the mother wavelet largely enhances the resolution of time-frequency representation towards detecting the transient features. In addition, because the different scale of a single mother wavelet is used to determine the wavelet coefficient, the resultant wavelet coefficient may carry the distorted version of the original signal which can affect the accuracy of fault detection. Furthermore, due to the high level of overlapping in calculating the wavelet coefficient, a large amount of redundant information is likely to present in the decomposed bands. Presence of these extra features may influence the spectral resolution and therefore result in a false failure alarm or signal misinterpretation [61, 62].

2.4.2.2 Amplitude demodulation

Signals may be amplitude modulated for several reasons. Amplitude modulation is the product of a higher frequency carrier signal and low frequency modulating massage signal; the frequency spectrum of the amplitude modulated signal is composed of a peak at carrier frequency and sideband spaced at modulating frequency [63]. Samuel and Pines [64] reviewed a report by Stewart [65] in which the presence of a localised tooth crack resulted in the growth of side bands around GMF and its harmonics. Later McFadden [66] suggested the use of amplitude demodulation for early detection of gear tooth crack. McFadden proposed a method in which the vibration signals were band pass filtered around the GMF then the analytical signals were determined by applying the Hilbert transform [67, 68] on the filtered signals. Hence, the amplitude demodulated signal was derived by calculating the envelope of the signal; the envelope is the magnitude of the complex analytical signals. Figure 11 presents a schematic illustration of the demodulation process as proposed by McFadden. McInerny and Dai [63] reported on the use of a similar demodulation procedure to achieve a direct measure of defect frequency in a roller element bearing.

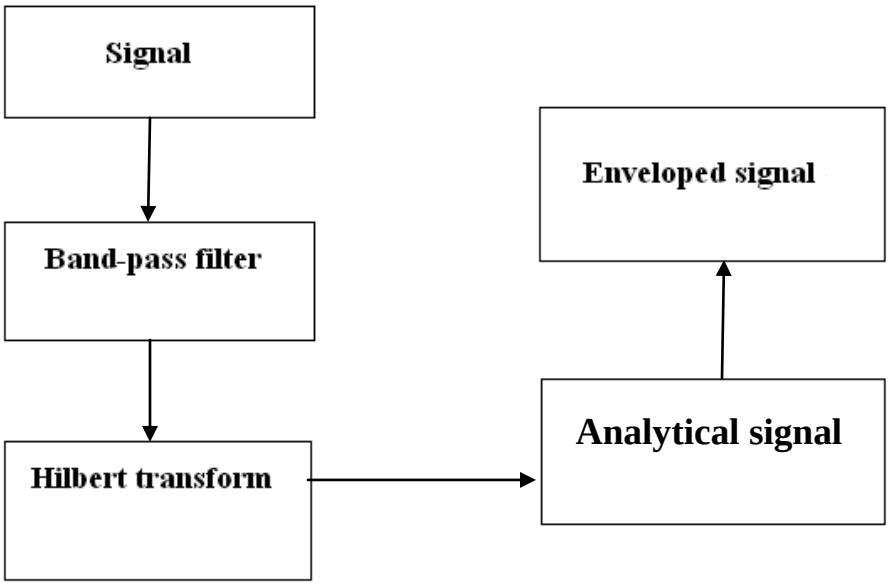

Figure 11 Schematic representation of the signal demodulation procedure

2.4.2.3 Spectral Kurtosis

Spectral Kurtosis (SK) as an effective signal processing method is gaining ground in vibration analysis. To determine SK, the signal is firstly decomposed into the time-frequency domain after which the Kurtosis values are determined for each frequency band [69]. The concept of SK analysis was first developed by Dwyer [70] as a tool which was able to trace non-Gaussian features in different frequency bands using the fourth order moment of the real part of the Short Time Fourier Transform (STFT). Dwyer investigated the application of SK on stationary processes but did not account for non-stationary vibration signatures typical of rotating machines. To date the most comprehensive calculations of the SK has been developed by Antoni [71] as the fourth order cumulant of the spectral moment *(K)* :

$$K_Y(f) = \frac{S_{4Y}(f)}{S_{2Y}^2(f)} - 2 \quad f \neq 0 \qquad \textbf{Equation 13} \ [71]$$

and

$$S_{nY}(f) \overset{\Delta}{=} \langle \left| Y_W(t, f) \right|^n \rangle \qquad \textbf{Equation 14} \ [71]$$

$Y_W(t, f)$ is estimated using the short time Fourier Transform:

$$Y_W(t, f) \overset{\Delta}{=} \sum_{-\infty}^{\infty} Y(n) \cdot W(n - t) e^{-j2\pi nf} \qquad \textbf{Equation 15} \ [71]$$

Where *Y(n)* is the sampled version of the signal, *Y(t)*, and *W(n)* is the window function having zero value outside a chosen interval. For the above calculations to be valid, the size of window (*Nw*) should be smaller than the length between two repetitive impulses and longer than the length of each impulse. In other words, the analysed signal should be locally stationary. Using the definition offered by Antoni [71] , Antoni and Randall [72] developed the concept of the Kurtogram to detect non-Gaussianity in a signal. A Kurtogram simply maps the STFT-based SK values as functions of frequency and window size. To generate a kurtogram a window size is firstly defined. The STFT of the signal based on the given window size is determined afterwhich

the SK is calculated according to Equation 13.This procedure is repeated for range of window size until kurtosis values are mapped as a function of frequency and window size to from the Kurtogram,see Figure 12. Antoni [71, 72] suggested the use of the Kurtogram for designing a band-pass filter which can be applied to increase the signal-to-noise ratio, thereby preserving the impulse-like nature of the signal. Additional authors aimed to find ways to automatically determine the optimum frequency band for envelope analysis. For this research the frequency and window size (bandwidth) at which the Kurtogram is maximum was employed to build a band-pass filter which was applied to measured AE and vibration data. In a separate investigation, Antoni [73] proposed an algorithm for fast computation of the Kurtogram. In this method instead of using STFT at different window lengths, the signal is decomposed by the means of quasi-analytic low-pass and high-pass filters to generate a pyramidal filter-banks tree with bands in each level (*k*). The Kurtogram is computed via calculating the kurtosis of all frequency bands, see Equation 16.

$$S^{i}{}_{nY}(f) \overset{\Delta}{=} \langle \left| C_k^i(n) \right|^n \rangle \qquad \textbf{Equation 16} \text{ [73]}$$

Where $C_k^i(n)$ is the sequence of the coefficient from the *i*th filter at *kth* level.

In this research zero overlap was set to calculate the STFT and therefore Spectral Kurtosis of the signals. Higher overlap values resulted into lower signal to noise ratio on filtered signals; however the reason for this is still unclear. In addition, among different type of band-pass filters window filter was found to be most effective in canceling the background noise and improving signal to noise ratio within the envelop spectrum.

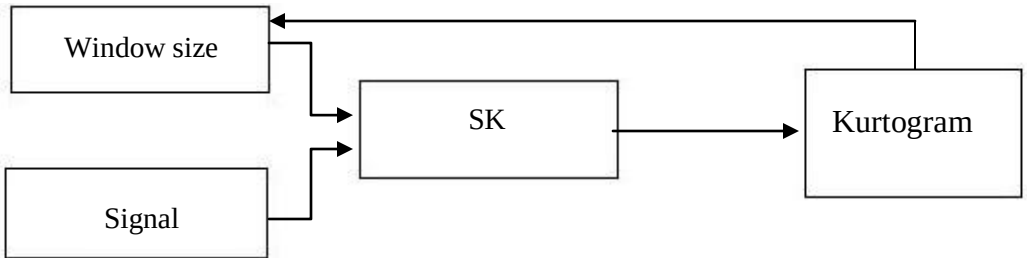

Figure 12 Schematic representation of the procedure for generation of Kurtogram

---

CHAPTER 3

---

3 Literature Review

3.1 Acoustic Emission

3.1.1 History

The first application of Acoustic Emission (AE) was registered around 6500 BC when potters used it to examine the quality of their products. The cracking sound of the clay vessels cooling within the furnace was considered to be a criterion for distinguishing the faulty products [74] In relation to metals, AE was first observed in 'tin cry'. The earliest statement on the observation of tin cry was reported by Jabir ibn Hayyan who described the sound emitted from a tin as a crashing noise. Miller [74] reported on the experiment performed by Anderson [75, 75] who noted the emission of sound during the tensile test of an aluminum beam beyond its yielding point; the sound was emitted after the cyclic load was increased.

However, the recognition of AE as an NDT tool was started from 1945 with the introduction of the Kaiser Effect by Joseph Kaiser. Kaiser discovered that AE activity is not observed within the material until the applied stress exceeds its previous value [76]. In 1968, Balderston [77] reported on a response from a transducer with high energy content, as compared to a background noise level of around 90 kHz. Balderston stated that this response and its associated resonance frequency can be potentially used as a diagnostic tool. Later Board [78] and Bloch [79] addressed the potential of AE diagnostics over conventional vibration techniques in detecting incipient failures.

The improvement in AE technology such as broadband sensors, high speed data acquisition systems and advanced signal processing methods have resulted in AE gaining popularity in the field of Non-Destructive testing (NDT). Monitoring the integrity of pressurised equipment in the nuclear and petrochemical industries was among the first industrial applications of Acoustic Emission Technology (AET) [80]. Stahlkopf and Green [80] performed hydro-tests on a range of pressure vessels using AET, indicating that AE is a very effective tool for Hydrostatic testing of vessels. Dwight Parry from the National Reactor Testing Station of Phillips Petroleum used

AET, aiming to find an effective NDT tool for the early diagnosis of coolant loss in nuclear reactors. After a year of continuously monitoring the system, Dwight successfully diagnosed a failure in reactor vessels from the acquired AE signatures [74]. Currently AE is being used for process monitoring in the petrochemical industry and is also employed to monitor the welding process in manufacturing [12, 76]. The recent advancement in the industrial application of AET has led to the formation of several organisation, among which, Acoustic Emission Working Group (AEWG), aims to promote the research and development of AET in the field of non-destructive testing.

3.1.2 Theory

AE is defined as the range of phenomena that results in the generation of structure-borne and fluid borne (liquid, gas) propagating waves due to the rapid release of elastic energy from localized source within and/or on the surface of material [74]. Different sources of AE activity in machinery are listed in Table 1. Since the origin of AE activity is microscopic, the AE signal is of a broadband nature making it a sensitive tool for incipient damage detection. Figure 13 compares different NDT technologies based on their operational frequency range. The typical frequency range associated with AE signature is normally between 100 and 1,000 kHz. Due to the high frequency content of AE and given that the structural dynamics operate below 1 kHz, the captured AE signatures are less likely to be influenced by background noise and structural resonances.

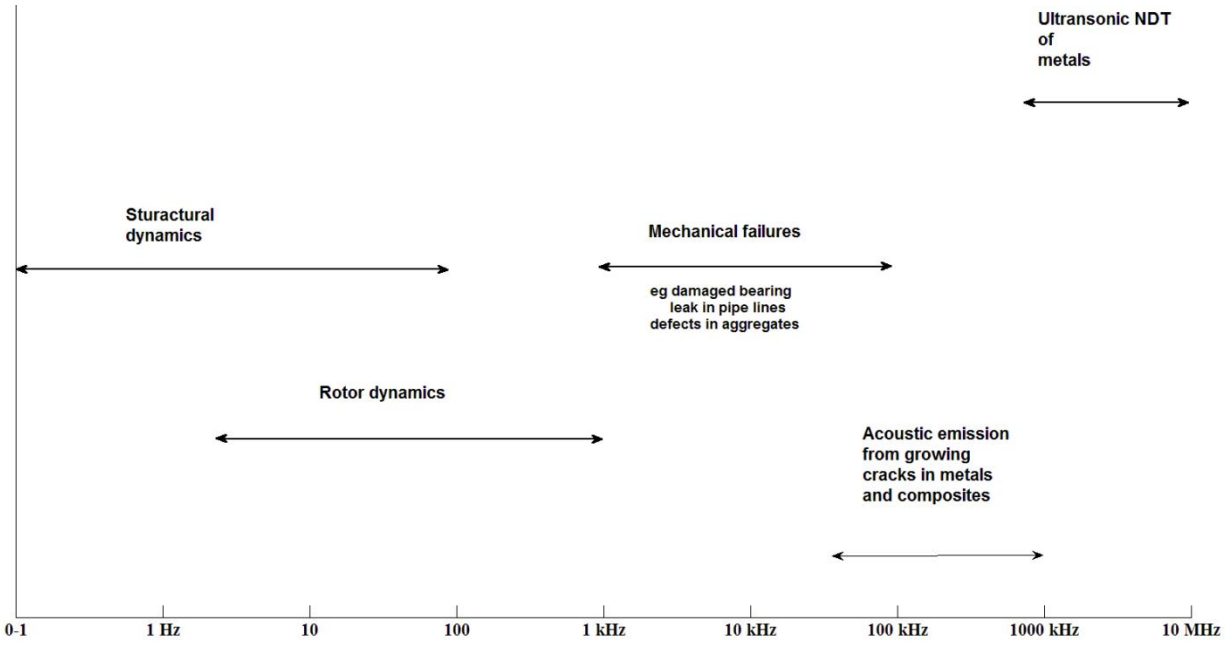

Figure 13 Spectrum of vibration and sound used for inspection and testing [80]

Table 1 Typical sources of AE in machinery [76]

Source description	Physical mechanism
Impact	Localized surface displacement at point of impact
Friction	Local release of stored elastic strain at moment when two contacting points slip
Cavitation	Principally collapse of bubbles plus some activity from bubble formation and coalescence
Turbulence	Collapse of vortices

The AE sensors are Piezoelectric transducers which convert the elastic energy, carried by the propagating surface waves, into electric signals. The sensor consists of a thin disk (Piezoceramic element) with conductive sides incorporated in a metallic cylinder to providing electromagnetic interference shielding, see Figure 14. The Piezoceramic material in composed of titanate and zirconate crystals mixed with other materials such as gallium phosphate or tourmaline; voltage is generated by the variation of dynamic strain within the Piezoceramic element. The sensor is normally attached to the surfaces using a mechanical clamp, grease or silicon epoxy [81]. AE sensors are sensitive to local surface displacement and, depending on the type of transducers, surface displacement as small as 0.1 of a picometre can be detected. Table 2 lists the different types of sensor and associated sensitivity ranges [74]. Although sensitive, there is always a significant amount of noise superimposed on output signals. To increase the SNR ratio, pre-amplifiers with a built-in band-pass filter are coupled with AE sensors [82]. Figure 15 illustrates a schematic view of a typical instrumentation setup employed to acquire the AE signal from a surface.

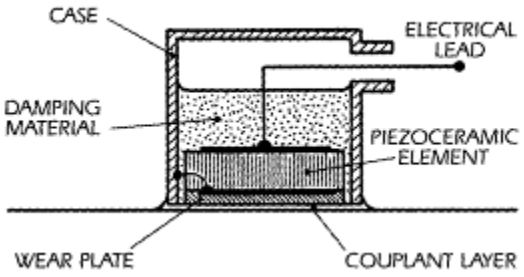

Figure 14 Schematic diagram of typical AE sensor [74]

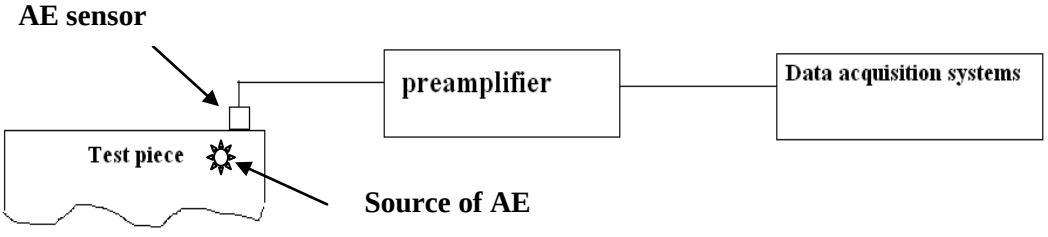

Figure 15 Instrumentation for acquisition of AE signals

Table 2 Bandwidths and minimum detectable signals for AE transducers [74]

Transducer type	Pass band (MHz)	Sensitivity (metre)
Air gap capacitor	DC to 50	10^{-12}
Electromagnetic/Acoustic	0.5 to 15	2×10^{-14} (per microsecond)
Damped PZT	0.1 to 2	10^{-13}
Resonant PZT	0.1 to 3	10^{-14}

The captured AE waveforms are normally in three forms of Burst, Continuous and Mixed (Burst super imposed on the background of the continuous waveform), see Figure 16 [76]. The AE activity is often described as a series of HIT[2]s and events. An Acoustic Emission HIT is normally described by several parameters such as threshold, duration, counts and rise time. The AE signal duration is the time between the first and last amplitude threshold crossing, while the rise time is the time between the start of the HIT and the instant at which the maximum amplitude of HIT is reached, see Figure 17. Additionally, a single AE event can be produced by a number of AE HITs and is defined by local material change giving rise to acoustic emission activity. The AE event is defined by three parameters of HIT definition time (HDT), HIT lockout time (HLT) and peak definition time (PDT). Correctly setting the PDT will result in an accurate measurement of peak amplitude while the appropriate definition of HDT will ensure that each signal generated from the structure is reported as one HIT. This defines the period over which a HIT can be acquired. With an accurate setting of HLT, any spurious measurements made during the signal decay will be avoided; essentially it defines the period between successive HITs, and its other function to inhabit the measurement of reflections [81].

Like any other NDT technology, there are some drawbacks associated with application of AE as a diagnostic tool. As such, the AE signal is subjected to attenuation as it travels through different interfaces. This requires the sensor to be mounted close to the emission source. Furthermore,

[2] The process of detecting and measuring an AE signal on channel'.[81]

different sources may give rise to AE activity at the same time, making locating and identification of the sources a rather challenging task [74].

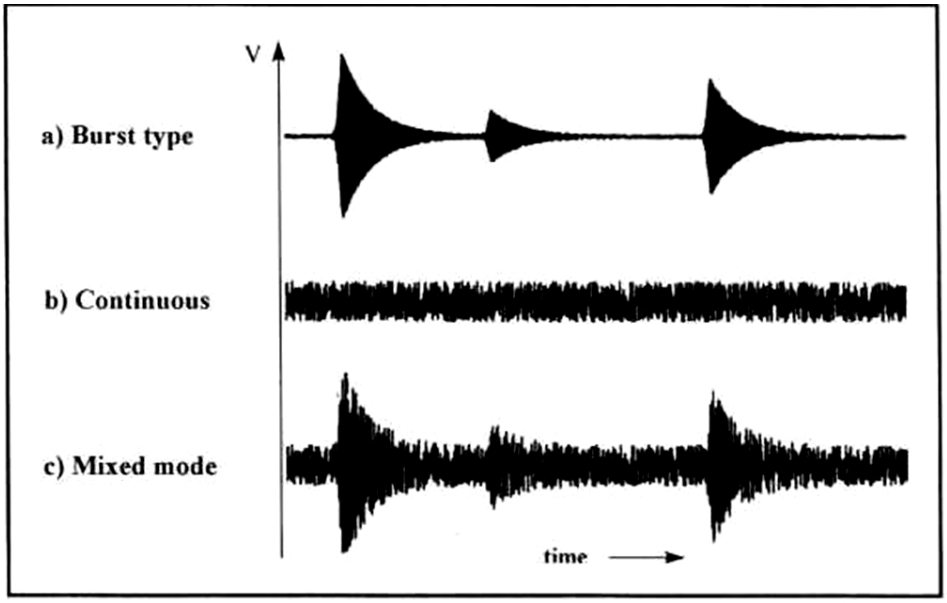

Figure 16 Schematic representation of different types of AE waveforms [76]

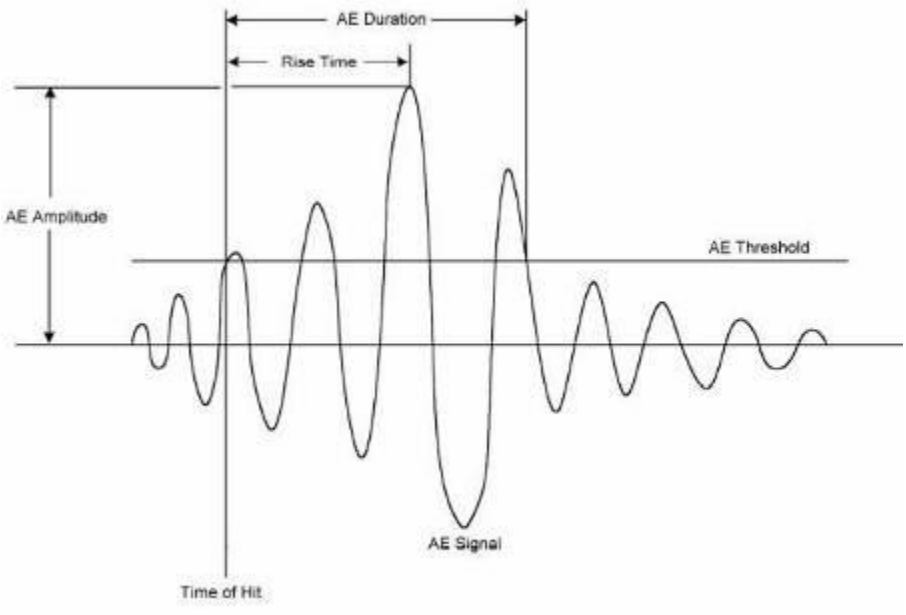

Figure 17 Schematic representation of an AE Hit [81]

3.1.3 Application of Acoustic Emission in monitoring gears and gearboxes

There are numerous publications investigating the applicability of AET for gear diagnostics. While some focused the fault diagnosis capability of AE, others have investigated the mechanism and parameters influencing AE activity during gear mesh .The following sections will categorise and briefly describe these investigations.

3.1.3.1 Bending fatigue diagnosis

Some researchers have studied the application of AE in the detection of the fractured tooth. Wheitner et al. [83] conducted a bending fatigue test on gears, with different surface roughness, material and heat treatment. This was to assess the capability of the stiffness and AE in monitoring the crack initiation and propagation. The test procedure and instruments were in accordance with the guidelines given by the Society of Automotive Engineering (SAE) for single tooth fatigue tests [84]. An AE sensor with a resonance frequency of 300 kHz was glued on the base of the tooth under examination while an accelerometer was placed on test-rig fixture. A cyclic sinusoidal load with a frequency of 10Hz and load ratio of 0.1 was applied and the run out life was set to 10^6 cycles. At the start of the experiment, the authors noted non-zero AE counts which were associated with the background noise. The registered count values showed a further steady increase with the propagation of the crack; however, the rate of increase was higher towards the termination of the test. Similar observations were noted for stiffness measurements. Wheitner et al. concluded that both the AE and stiffness measurements were successful in motoring crack progress, despite AE offering better effectiveness in the early diagnosis of the crack.

Miyachika et al. [85] performed a series of bending tests on normalised and case carbonised spur gears with identical geometry. An AE sensor was clamped on the test gear. Throughout the test different AE features such as cumulative event count, count rate, peak amplitude, and event energy were recorded. In this experiment different loading conditions were tested and the size of the propagating crack was constantly measured. In the case of the carbonised gears, both

cumulative event count and event count registered a sharp increase just before the crack initiation; however, such behaviour was not noted for the normalised gears. The authors argued that this observation was associated with the high noise ratio of the carbonised gears. They also noted that a decrease in the magnitude of load resulted in an increase in the number of cycles to the point where a sharp increase in cumulative event was recorded. In a separate research Miyachika et al. [86] repeated the same procedure on the super carbonised gears using wavelet transform and cumulative energy count to analyse the signals. AE was found to be successful in detecting the crack on supercarbonised gears.

Singh et al [87] undertook a comparative study between the effectiveness of AE and vibration technologies to monitor the crack propagation using a single tooth bending machine. An AE sensor, together with an accelerometer, was incorporated close to the gear tooth. During the test, a cyclic sinusoidal load of 40Hz was applied while the raw AE waveform and fatigue cycles were recorded. The test was terminated after the detachment of the tooth. The amplitude of the AE signal started to increase after the gear reached 90% of its estimated life. Upon the complete detachment of the tooth, the AE registered a burst with very high amplitude whereas the vibration level only began to change after the complete loss of the tooth integrity. Singh et al. concluded that AE offers better effectiveness in early detection of root crack

Most of these aforementioned studies showed the advantages of AE over vibration in early crack diagnosis. However, the experiments were conducted on the bending machine and on non-meshing gears; there is no such report on meshing gears. Due to the difference in the dynamic behaviour of the meshing gear, as compared to non-meshing gears, it important to assess the applicability of AE in monitoring tooth cracks under operational conditions. It is important to mention that during the meshing of gears, different sources may give rise to AE activity which may affect identifying quality of AE towards crack diagnosis.

3.1.3.2 Diagnosis of meshing gears

3.1.3.2.1 Failure detection

Surface damage is the most common type of failure associated with meshing gears and there has been of growing interest in monitoring surface deterioration using AET. Siores and Negro [88] reported on an investigation in which various type of failures such as worn and missing teeth, misalignment, scuffing and backlash were introduced in an experimental gearbox. The gearbox consisted of a pair of spur pinions (45 teeth) and a wheel (20 teeth) with a contact ratio of 1:65. The face width of the teeth and pressure angle were 21.5 mm and 20^{o} respectively. The gearbox was coupled with a DC motor connected to a variable speed controller. An AE sensor with resonance frequency of 175 kHz was mounted on the gearbox casing and the AE signals were acquired with a sampling rate of 640 Hz. Prior to the start of the test, the test rig was run at four one hour intervals under full load conditions. This was to run-in the gear; during the run-in period the surface asperities were flattened. The test was performed at two speeds of 300 and 600 r.p.m. Siores and Negro [88] plotted the acquired signal features of r.m.s., standard deviation, and duration against root cause of each failure. The calculated feature showed a distinct difference between defect free and defective condition. The authors concluded that AE can be correlated with different types of failure. The possible use of AET for online monitoring and predictive maintenance was also suggested. Although defective modes were successfully differentiated, Siores and Negro employed a basic signal acquisition instrument with a very low sampling frequency in comparison with the resonance frequency of the AE sensor.

Singh et al. [89] assessed the applicability of AET in the diagnosis of both natural and seeded surface pitting on spur gears. For the purpose of a simulated pitting test, a UH1H generator drive, consisting of driver and idler gears, was employed. An AE sensor with a resonance frequency of 280 kHz together with an accelerometer were both placed on the gearbox housing. The test was started with no defect on the idler gear after which a simulated pit with a depth and width of 1.25 mm was introduced on the idler gear using an electronic discharge machine. The test was carried out under a combination of loads and speeds. Although the presence of the simulated defect on both AE and vibration waveform was evident, AE offered a better signal-to-noise ratio. However, under high loads or at high speeds both techniques showed limited success in detecting

the defect. The authors attributed this lack of diagnosis capability to the increase in the level of noise and a simultaneous decrease in signal amplitude, associated with the pitted zone, under these specific circumstances. In a separate attempt, a back-to-back gearbox was employed to investigate the diagnosis of natural pit. The same kind of AE sensors were mounted on the housing of the test and slave parts and also on the bearing housing between two parts. The test was run under 1770 r.p.m. with no defect on gears. After 30 min of continuous running, pits started to grow on the pinion teeth. The development of the pits was associated with the presence of periodic occurring peaks on AE signatures. After 15 min into the operation, the occurring peaking becomes closely spaced, suggesting the extension of the pits on to further teeth. Unlike the simulated case, the presence of the periodic teeth peak was not evident in the vibration waveforms. Furthermore, based on the observations from the different AE sensors, the authors concluded that to achieve better diagnosis effectiveness the sensor should be incorporated as close as possible to the gears.

Raad et al. [90] performed a long-term fatigue test on an industrial gearbox consisting of a pair of spur gears with 20 teeth. Two AE sensors of wideband and resonance type and an accelerometer were placed on the bearing pedestal. The operational load was set further above the recommended rated value to accelerate the teeth failure. The gearbox was visually inspected on daily basis while the signals were recorded at one hour intervals and analyzed using kurtosis and enveloping techniques. After two weeks of continuous running the test was terminated due to a presence of cracks close to the roots of two teeth. Comparing both AE and vibration waveform, coincidentally occurring burst with a growth in spall size was evident on the AE signature; the burst disappeared with prolonged running of the gearbox under defective conditions. The AE kurtosis started to increase after 300 cycles whilst an increase in vibration was noted after 5,000 cycles. The spectral density of both AE and vibration was also increased in energy before and after the detection of spall. In addition, the presence of the teeth failure was manifested at twice the shaft frequency in the envelope spectrum of AE and vibration signature; whereas for the AE, this was only evident in the logarithmic scale spectrum. Raad et al. concluded that the application of AE in the early detection of defects was promising; however, they suggest using other signal processing techniques for validation of these findings.

Sentoku [91] investigated the applicability of AE in monitoring the pitting of meshing gears. The test rig consisted of a pair of spur gears operating under forced lubrication system. Throughout the test the oil temperature was maintained at constant value to ensure the constant oil film thickness during the test. An AE sensor was mounted on the wheel and connected to a slip ring allowing the acquisition of the signal while the gearbox was operational. Two sets of tests were performed. The first test was conducted on a pair of hardened gears with a pinion speed of 990 r.p.m. and under applied stress of 960 MPa, measured by a strain gauge mounted on the teeth root while the second test was performed with pair of heat treated gears. For the case of the hardened gear, the AE registered no particular changes though for the second heat treated gears an increase in AE energy simultaneous with defect growth was noted. Sentoku attributed this observation to the increase in friction because of growth in the pitting area. Finally, the author concluded that AE is potentially effective in monitoring the pitting progress. This was influential research, as it clearly addressed the correlation between the AE level and the extent of occurring surface damage on gears.

Badi et al. [92] performed a fault classification analysis on both vibration and AE signals. A test rig consisting of pneumatically loaded spur gears was employed. Several AE sensors and accelerometers were placed at different locations on the test rig. Badi et al. simulated the tooth scuffing and pitting by seeding the ‘blip’ and ‘shaved’ fault on the gear. The captured signals associated with defective and defect free conditions from the sensors were compared using kurtosis and the Crest factor. The blip fault was diagnosed from both AE and vibration measurement, while the shaved tooth was only detected by AE. It was also noted that the waveforms associated with blip damage were of an impulsive nature. Badi et al. concluded that employed signal processing methods can be best applied on the signals with a high degree of spikiness. The authors suggested using more advanced signal processing techniques to better explore the diagnostic strength of the employed techniques.

Tandon and Mata [93] performed a seeded defect test on an IAE lubricant testing machine in which a pair of spur gears were lubricated by a jet of oil. An AE sensor and an accelerometer were placed close to the bearing pedestal. The test was run at 1.000 r.p.m. and the load varied from 0-10 Kg. Pitch line defects with a radius ranging from 250-2,200 μm and a constant depth of 500 μm were seeded on a gear tooth using spark erosion. Throughout the test peak amplitude,

the ring down count and energy for the AE signals were determined. From the results an increase was observed in the calculated AE parameter in tandem with an increase in load and defect size though the ring down count offered better sensitivity in that respect. Also noted were the advantages of AE in detecting the small defects as compared to vibration. It was concluded that the presence of a defect would result a broader distribution of an AE event versus ring down count and peak amplitude.

A similar test was carried out by Toutountzakis et al. [94] using a test rig with a back-to-back arrangement. The test rig consisted of a set of spur gears of 49 and 65 teeth with a contact ratio of 1:77. Two wideband AE sensors with flat responses between 100 kHz-1 MHz were mounted on a pinion and bearing pedestal. A slip ring was used to allow measurement from the rotating pinion. To ensure the identical start point for the captured waveform, Toutountzakis et al. applied an external triggering system so that the acquired waveforms corresponded to a time frame encompassing 16 teeth. Prior to the start of the experiment, the test rig was run-in for 15 hrs under full load. The test was started by recording the AE signals under three different loading conditions of 0, 55 and 100 Nm and at 745 r.p.m. after which a pitch line defect of 1 mm in diameter was introduced on the pinion; the AE signal for the defective condition was acquired under the same circumstances as for the defect free condition. Subsequently, a second defect (12 × 3 mm) seeded on the addendum of the same tooth. The recorded waveforms contained 16 consecutive bursts which were attributed to 16 meshing teeth. In order to detect the defective tooth, the position of each individual burst within the time frame was carefully compared with the physical location of the corresponding tooth on the pinion. It was shown that the burst with the highest peak amplitude was not necessarily correlated with the defective tooth as it did not always occur at the same position under different loading conditions. The captured waveforms were divided into 5, 8 and 16 regions respectively and the r.m.s. level associated with each region was calculated. A reduction in r.m.s. level with a growth in defect size was observed; however, regardless of position of the sensor and the operational load, no distinct r.m.s. peak corresponding to the location of defect was noted. The authors drew their conclusion by addressing the difficulties of seeded defect diagnosis. Their conclusion contradicted the findings of the researchers who claimed success in seeded defect diagnosis [89, 92, 93]. Toutountzakis et al. argued that the reason for such diagnostic limitation was due to the presence of mounds and protrusions around the seeded defect so that the flattening action of these resulted in the

generation of AE activity. This activity was different from typical AE activity during the sliding of gears originated from asperity contacts. Tan and Mba [95] built on Toutountzakis et al.'s investigation by performing a similar procedure with a larger dedendum defect under broader ranges of load and speed. Tan and Mba's findings were in complete agreement with those noted by Toutountzakis et al. and they confirmed the limitations of AE in seeded defect diagnosis.

Al-Balushi and Samanta [96] benefited from the energy-based features when studying the AE signals from a spur gear mesh. Al-Balushi [97] introduced the concept of the energy index (EI) as the square ratio between the r.m.s. value associated with a defined segment of a signal to the overall r.m.s. value of the entire signal. In addition to EI, Crest factor and kurtosis were also employed. In this experiment, three miniature AE sensors were placed close to the bearing pedestals and the signals were acquired at a sampling rate of 1 MHz. The gearbox was run for 40 hrs after which the gears were damaged. The results showed that EI offered better effectiveness in diagnosis of the tooth pitting and breakage in comparison with the other two techniques.

Tan et al. [13] presented conclusive research in which the applicability of AE in monitoring the natural progressive pitting was investigated. They employed a back-to-back gearbox to study the accelerated surface pitting on spur gears while a comparative study between the effectiveness of spectrometric oil analysis, AE and vibration techniques was undertaken. The experimental arrangement was similar to that employed in by Toutountzakis et al [94]; however, an accelerometer was also placed on the bearing pedestal.Throughout this investigation, natural pitting was allowed to occur and the criteria for termination of the test was set to a 50% pitted area on any tooth. The test was performed at 745 r.p.m. and under 73,147 and 220 Nm operational torques. To ensure the repeatability of the results, two set of tests under at each load investigated. At regular intervals the test rig was stopped and the pinion teeth visually inspected while oil samples were taken from the oil sump. AE and vibration r.m.s. along with Fe concentration, from the atomic emission oil analysis, were trended against the test duration and pitting percentage. It was observed from the results that regardless of loading conditions, the AE measurement from the pinion was linearly correlated to the pitting rate. Furthermore, it was noted that the AE from the pinion exhibited the highest sensitivity toward pitting growth when compared to the AE measurement from the bearing pedestal. However, when comparing the sensitivity of AE and vibration signature, taken from the bearing pedestal, and also the Fe

concentration, the AE was found to have more sensitivity only under the higher applied torque of 220 Nm, whereas the vibration remained the most sensitive indicator for the other two torque levels. Tan et al [13]. suggested a better prognosis capability for AE due to its linear correlation with pitting time and rate. Despite being determinative, their research did not report on the type of statistical fit which could have resulted in a better correlation between the signal r.m.s. and pitting extent as compared to the linear fit. Moreover, this was research which only involved the application of r.m.s. to compare the signals, whilst the application of advanced signal processing techniques could enhance the sensitivity of the AE measurement from the bearing pedestal.

Loutas et al. [98] performed the first conclusive research in which advanced signal processing methods were employed to interpret the acquired AE signal from a set of meshing gears. They [98,99] employed both AE and vibration to diagnose a seeded transverse root crack in a single stage spur gearbox. A test which involved prolonged running of a experimental gearbox. Throughout the test the AE was measured from the shaft, bearing and the wheel using the slip ring that had been developed by the same authors [100]. The vibration signals were also acquired from two sides of the gearbox casing. The signals were analysed using the parameters extracted from time and frequency domains as well as the decomposed signal resulted from application of Discrete Wavelet Transform (DWT). It was noted that the energy of both the vibration and AE signal at the third level of wavelet decomposition was capable of diagnosing the root crack. Furthermore, the correlation between the extracted AE signal features, at the same levels, and pitting rate appeared to be linear. The authors drew conclusions suggesting the better diagnostic quality of AE in the early diagnosis of root crack as compared to vibration analysis.

Aiming to study a novel approach to acquire AE signal from rotating gears, Loutas et al. [100] developed mechanism to incorporate the AE sensor on the gear without any requirement of using expensive slip rings to transmit the signals to the data acquisition system. The application of this mechanism was validated by performing a seeded defect test using experimental gearbox. The test involved measuring the AE signal from three conditions of no defect, one defected tooth and two defected teeth respectively. In addition, different loading condition was applied throughout this experiment. The AE r.m.s values of the acquired AE signals was reported to be successful in

discriminating different loading condition and defect modes. Also reported, was sensitivity of AE r.m.s to oil temperature.

3.1.3.3 Influence of operational parameters on AE activity

While investigating the diagnosis of seeded defect, Tan and Mba [95] conducted further tests to better understand the limitations of the AE technique for defect identification. The same experimental setup was employed; however, the AE r.m.s. and energy value were continuously recorded while the oil temperature was measured at 15 min intervals. The test was run at 745 and 1,460 r.p.m. and under three different loading conditions of 0, 55 and 110 Nm. The duration of the test was set to the time between the cold start and the point where the oil temperature had remained constant for 1 h. From the results it was noted that the average variation in both AE r.m.s. and energy values were approximately around 50% and 125% at 745 and 1,460 r.p.m. respectively. Based on this observation, the authors argued that AE signals acquired during the seeded defect test were greatly influenced by the effect of the load and oil temperature which resulted in a variation of oil film thickness and therefore rate of asperity contact. This was an important finding as, until then, there was no published work reporting on the influence of temperate on AE activity. This research clearly showed that the notion of temperature must be taken into consideration while using AE as a diagnosis tool. Tan and Mba went further and studied the effect of load and speed under constant temperature. It was found that the effect of load on the generation of AE activity was negligible while the change of speed from 745 to 1,460 r.p.m. almost doubled the amplitude of the recorded AE activity. Although this research recommended further discussions, the authors postulated that this increase in the level of measured AE can be associated with higher oil temperature at the higher rotation speed.

In a separate investigation, Tan and Mba [101] repeated the test under different loading circumstances and in a broader range of speeds. The results were in agreement with their previous observations. The minimal effect of load on the AE level was attributed to the correlation between load, speed and oil film thickness according to which the influence of load is minimal in comparison with speed. Observation of the results under the fixed loading conditions contradicted the EHL theory, according to which an increase in speed will lead to an increase in

oil film thickness and asperity contact, and therefore AE activity. Tan and Mba addressed this discrepancy by attributing the increase in AE r.m.s. to the larger strain rate and also the larger background noise level experienced by surface asperities at higher speeds. This explanation was different from that given earlier by the same authors in Ref [95] in which the higher temperature at higher speed was suggested as a reason for the increase in AE activity. The authors made further investigations to identify the source of both burst and continuous type AE activity from possible sources of tooth resonance, secondary pressure peak and asperity contact. The tooth resonance was determined at 75 kHz which was far below the operational range of the AE sensor. However, in order to differentiate between the secondary pressure peak and asperity contact, additional experiments were undertaken. The first experiment was performed by running the back-to-back gearbox under dry conditions. This was to exclude the possible effect of pressure peak on AE generation. Tan and Mba noted that the continuous AE activity is associated with sliding contact away from the pitch line while the pure rolling action on the pitch line is responsible for the generation of transient burst.

Raja Hamzah and Mba [22] performed an experiment to assess the influence of load and speed on the generation of AE activity in spur and helical gear mesh. They used a stranded back-to-back to gearbox designed to accommodate both helical and spur gears. For the spur pair the pinion with 49 teeth meshed with a wheel of 65 teeth, while for the helical gear set, the pinion and wheel had 51 and 70 teeth respectively. A wide band AE sensor and two J type thermocouples were glued on to the pinion. The third thermocouple was placed inside the oil bath. A slip ring was used to allow AE and temperature measurement from the rotating pinion. The AE measurement was undertaken using two different gain values of 20 dB and 40 dB for spur and helical gears respectively. To reduce the influence of temperature on the AE measurement the test rig was run for approximately 30 min until the oil temperature stabilised. The same procedure was repeated prior to the start of each test. The first test was run on both spur and helical gears at a fixed speed of 700 r.p.m. and under five different and increasing loading conditions of 60, 120, 180, 250 and 370 Nm. The second test was conducted under fixed loads of 60, 120, 250 and 370 Nm at varying speeds of 700, 1,450 and 2,850 r.p.m. Throughout the test the temperature measurement from the pinion was taken to calculate the specific oil film thickness (λ). The first test revealed that an increase in load from 60 to 370 Nm resulted in 187% and 177% increases in the AE r.m.s. levels for the spur and helical gears respectively,

contradicting the findings of Tan and Mba [95, 101] who suggested a negligible influence of load on AE activity. The authors argued that this contradiction was associated with different lubrication regimes under which the two authors had conducted their experiments. Raja Hamzah added that it was likely that Tan and Mba had experienced a boundary lubrication regime where the effect of load on the rate of asperity contact was insignificant. On the other hand, the results of the second test showed an increase in AE r.m.s. with increased speed. It is worth mentioning that the maximum temperature variation experienced by Raja Hamzah during the second test was 9.6^{o} causing minimal variation of oil film thickness. Furthermore, the Tan and Mba noted that the AE showed higher sensitivity to change in specific oil film thickness from the spur gears as compared with the helical mesh. This was explained with reference to the findings of Boness and McBride [102] and Boness et al., [103] according to which AE exhibited higher sensitivity under the sliding in comparison to the rolling contact. Raja Hamzah also stated that the spur gear experiences a combination of sliding and rolling contact, whereas the helical gear mesh involves a continuous rolling action on the pitch point that results in less sensitivity to change in oil film thickness. Eventually, Raja Hamzah used the results from two tests to develop an equation correlating load, speed and AE r.m.s. for both helical and spur gears. Nevertheless, this equation was based on assumptions of the minimal change in temperature and surface roughness during the experiment. Whilst the source of AE for spur gears was clearly and conclusively identified in ref [101], Raja Hamzah linked the continuous AE activity in helical gear mesh to the continuous rolling action on pitch points resulting in a series of closely spaced AE transient. It was argued that the continuous variation in contact length directly affects the loading distribution along the contact line and results in a variation of oil film thickness and subsequently the amplitude of AE signals on the waveforms. This research was the first known published attempt in which the generation of AE activity from both spur and helical gear mesh were compared. It was clearly shown that the AE activities associated with spur gears are more sensitive to change in operational conditions when compared to helical gears.

Raja Hamzah and Mba [104, 105] and Raja Hamzah [106] further expanded their research by performing an investigation on a range of oil film thickness using the same experimental arrangement. The authors reduced the oil film thickness by changing the surface temperature of the meshing gears. This was done by spraying liquid nitrogen inside the running gearbox. The injection of liquid nitrogen was stopped when the gear temperature approached zero. This

procedure was followed under a combination of loads and speeds using two types of lubricant with a different viscosity. The specific oil film thickness was calculated at the pitch line based on the temperature measurements taken from the oil bath and pinion surface. It was observed that under any operational conditions, the AE r.m.s. was increased with an increase in specific oil film thickness (λ). It was also noted that there was an absence of meshing features and transient burst from the AE waveform at time of minimum temperature (0^{o}C). Both these observations were explained by holding the asperity contact as the main source of AE activity during the gear mesh. It was found that AE is more sensitive to changes in pinion surface temperature as compared to the oil bath temperature. The authors concluded that AET can be a potential tool for online monitoring of the level of asperity contact in the gearing application.

Apart from work of Raja Hamzah and Mba [22, 105] who studied the influence of operational conditions on both spur and helical gears, there is no published attempt at reporting on the application of AE in helical gear diagnosis. The meshing mechanism in a helical gear is different to that of spur gears. The meshing of helical gears is progressive due to the gradual increase and decrease in contact length over a particular tooth face width whilst the spur gear mesh has a constant contact face width throughout the gear mesh. Therefore the AE signals generated from the helical gears are relatively more continuous in nature in comparison with the signals from spur gears in which the presence of transient burst, representing the meshing teeth, is completely evident, see Figure 18. The difference in the nature of the AE signal from both spur and helical gears will influence the effectiveness of AE in monitoring natural and seeded pitting.

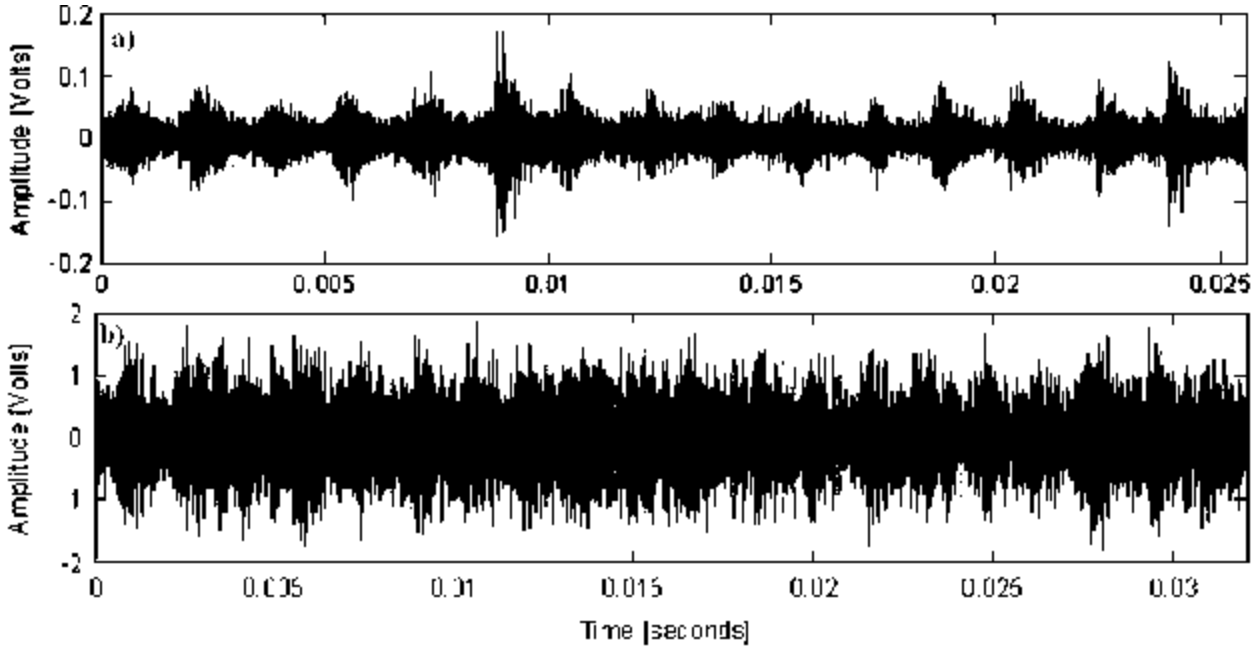

Figure 18 AE signals at 250 Nm and 700 rpm a) Spur gear b) Helical gear [22]

3.1.4 Application of AE in rolling element bearing diagnosis

There is a range of phenomena resulting in the generation of AE activity in roller bearings, i.e., formation of sub surface crack, rubbing of mating surfaces as well as oil film deterioration. The propagation of generated AE activity is normally influenced by several parameters of microstructure, non-homogeneities and transmission paths. There have been reports suggesting that bearing defects normally cause modulation in higher frequencies, matching the AE range, while other types of defect such as misalignment, lossless and imbalance normally influence the structural resonant further, i.e. below 10 kHz. Given the rapid attenuation of high frequency AE signals, it is possible to diagnose the defect, reflected in the high frequency range of the AE signal, by placing the sensor close to the bearing so that the signatures from other machines' components will be subjected to attenuation upon the approach to the AE sensor [12, 107].

3.1.4.1 Defect diagnosis

The earliest application of AE in monitoring the bearing was reported by Balderston [77] in which both vibration and AET were applied to diagnose the range of simulated defects on a test bearing. The vibration signatures were measured in two ranges of audible and resonant (>100 kHz); it was suggested that the resonant frequency associated with each individual component remain unchanged after the assembly, though some damping effect may be experienced. The difficulty in discriminating the source of excitation was also suggested, as the presence of a defect on any component would excite the resonant frequency of the entire machine. In addition, the magnitude of the excitation tends to be minimal under the low rotational speed, resulting in a lower signal-to-noise ratio. Addressing the difficulties associated with resonant range measurement, Balderston recorded the signals from the bearings, with different defective conditions of damaged roller, inner and outer race, under both lubricated and unlubricated conditions. It was noted that the AE signals re-coded from the defective bearing were of a burst type though the waveform evolved to continuous type during the dry run. Also noted was the increase in resonant amplitude with a growth in defect size. The author concluded that AE would find a strong place in condition monitoring with advancements in sensor technologies.

Rogers [108] performed a comparative study between the diagnosis capability of AET and vibration in detecting a range of defects in a slow speed bearing. The employed AE sensor was of a resonance type with a measurement range between 100-300 kHz. The AE signals were identified from different sources including rubbing, grinding and roller impact. Comparing the results of AE and vibration, the kurtosis values of AE signals were found to be more successful in monitoring the bearing.

Tandon and Nakra [109] performed an experiment in which AE counts and peak amplitude from a bearing with an outer race defect were monitored. Throughout the test the load, speed and defect size were varied. It was noted that AE counts were increased with increases in both load and speed. The AE count was found to have a limited diagnosis range – only capable of detecting defects with less than 250 μm in diameter – whilst the AE peak amplitude was capable of detecting the defect without any restriction in size. A similar procedure was repeated by Choudhury and Tandon [110] but with broader ranges of speed, load and bearing size. For the

undamaged bearing, the AE count was found to be less than noted for the damaged case. However, an increase in speed resulted in an increase in count level for damaged and undamaged bearings; such behaviour in AE response was in contrast to the observation made by Tandon and Nakra [109] according to whom the AE count, for both damaged and undamaged cases remained unchanged with variations in load. The inconsistency associated with the observation of the AE count under varying operational conditions has been disscussed by Tan [111] and Tan et al[13] who employed a range of methods to find optimum count parameters as well as threshold levels. Tan argued that the effectiveness of AE count monitoring is affected by a number of factors including the selected threshold level, signal frequency and amplitude of AE pulses, which influences the count rate. It was observed that the registered count rates exponentially increased with an increase in speed and defect size, contradicting the limited sensitivity of AE count to defect size variation as noted in ref [109].

Yoshioka et al. [112] performed a series of long term fatigue tests resulting in the generation of spall on the inner race. Each test lasted approximately 130 hrs and was run at 1520 r.p.m. Throughout the tests vibration r.m.s. and AE counts were monitored. It was observed that upon generation of spall the vibration r.m.s. sharply increased whereas the AE count registered a steady increase 5 hrs before the vibration began to rise. This was first experimental research in which AE was shown to be more effective in the early diagnosis of spall, as compared to vibration.

Aiming to establish the optimised threshold level for AE count calculation Morhain and Mba [113] performed an investigation in which a series of defects were seeded on the outer and inner races of a split copper spherical bearing. The test was run under a combination of load and speed with varying defect sizes. Through the experiment, AE r.m.s., energy and count were monitored. The AE count was determined based on varying percentages of defined amplitude. From the results it was observed that the AE count, irrespective of the applied threshold, increased with the increase in load though this observation only held true for the defect on the outer race, whilst the increase in speed resulted in an increase in AE count for any threshold level and type of damage. Furthermore, the increase in AE count was noted with growth in the outer race and defect size. Morhain argued that the signal attenuation on the AE race may limit the applicability of AE in monitoring the defect size growth on the inner race. In contrast, as noted in ref [109],

the AE count appeared to be effective in detecting the defect with a length up to 15 mm and a width of 1 mm. A conclusion was drawn, suggesting that there is no generic threshold level applicable on all operational conditions and it was advised to investigate background noise levels under a range of operational speeds; however it was proposed that the 30% of maximum amplitude of the background signal, at minimum load and speed, was the optimum threshold for AE count calculations, though the relation between AE count and defect size was found to be independent of the chosen threshold.

Sakishima et al. [114] employed both vibration and AE to diagnose the artificiality seeded defect on the inner race of a ball bearing. The test was run under an applied load of 1 and 2 KN. The measured AE and vibration signals were band pass filtered and passed through an analogue envelope detector after which the envelope spectrum of the resulting signal was generated. The magnitude of defect frequency within the envelope spectrum of both vibration and AE was increased with the growth in defect size. The authors suggested similar diagnosis effectiveness for AE and vibration.

Price [115] utilised a four-ball machine to study the different wear modes on a roller bearing. Throughout the test, AE r.m.s., vibration, friction and temperature were monitored. The AE detected the ball distress before the level of friction began to increase. Price also suggested that the further growth in the extent of the damage would lead to an increase in friction level.

One of the most influential studies comparing the applicability of AE and vibration for bearing diagnosis was performed by Shiroishi et al. [116]. In their investigation the defect width with a constant length of 2.54 mm and varying width ranging from 15.4 to 408.48 μm was introduced on both inner and outer races. Throughout the test, r.m.s., Crest Factor, kurtosis and peak ratio for vibration and AE data were monitored. The peak ratio was defined as the sum of peak values of defect frequency and its harmonics across the envelope spectrum to the mean value of spectrum. For both inner and outer race defects, the peak ratio of the vibration data exhibited the highest linear correlation with defect size. Moreover the AE data appeared to be less sensitive to defect growth on the outer race while being completely insensitive to the inner race defects. Shiroishi et al. argued that the peak ratio can be an effective diagnosis tool for localised defects with particular frequency bands across the envelope spectrum; however for the distributed types

of damage with no evident frequency, i.e. such as debris denting, an overall level measurement such as r.m.s. is more favoured.

Al-Ghamdi et al., [117, 118] built on Shiroishi et al.'s [116] investigation by performing a comparative study between AET and vibration in defect size identification. The same experimental setup as used in ref [113] was employed. The authors performed two set of tests; the first aimed to establish the source of AE in roller bearings while the second was to assess the prognosis capability of AE and vibration in defect size estimation. Al-Ghamdi simulated two types of defective condition on an outer race. The first condition was associated with surface discontinuity without any material protruding, while the second defective condition involved material protrusion above the surface roughness; in total four defects including smooth defect, point defect, line defect and rough defect were seeded. The test was run under a fixed load but with varying speeds. From the observation of raw AE data it was noted that the transient burst spaced at defect frequency; this was only evident on the signals associated with last three types of seeded faults. Also evident was the increase in r.m.s., peak amplitude and kurtosis of AE, with an increase in speed and defect size. However, this increase in parameter and the presence of transient burst was only noted from pointing to the rough defects and there was no distinct difference between recorded background noise and the waveform associated with smooth defects. Given that the AE did not discriminate the background noise and smooth defect condition, Ghamdi [117] concluded that the source of AE in the seeded defect test was the material protrusions. The vibration signature exhibited different trends as compared to AE. This was because that, irrespective of type of damage, the defect induced transient feature as noted on AE waveforms was absent in the vibration signature; in addition the r.m.s. and peak values of vibration signals did not register any change in the extent of seeded defects, though a sharp increase was noted only upon the introduction of rough surface damage. Al-Ghamdi carried on with the second test by seeding seven different defects with varying widths and lengths. The duration of defect induced transient AE bursts were measured for each defective case. A linear correlation between the defect length and burst duration was observed; also noted was the correlation between the continuous part of the signal and the defect width. Building on Ghamdi et al.'s research, Al-Dossary et al. [119] performed a seeded defect test using a similar experimental arrangement. Circumferential defects varying in length and width were seeded on both inner and outer races. The results revealed that the increase in defect size on the inner and

outer race resulted in an increase in AE signal energy. However, Al-Dossary et al. noted some diagnostic limitations particularly associated with inner race defects. As such the inner race defect frequency was not always reflected in the recorded AE signals; this was attributed to the attenuation of the AE signals due to variation in transmission paths. The authors also noted a direct correlation between the defect size on the outer race and transient burst duration, evident in AE waveform, confirming the observation reported by [117, 118]. In addition, the ratio between the maximum amplitude of each burst and underlying noise levels appeared to be correlated with defect width. The authors suggested that the observed correlation is potentially an effective tool for AE prognosis.

Aiming to find a method to determine the remaining life of the operating bearing Li et al. [120] performed accelerated fatigue tests on bearings operated at 1,600 rpm under 167% of rate load. The process of fatigue was accelerated by seeding an initial defect on the outer race using an electric discharge machine. Throughout this investigation AE and vibration signals were continuously recorded. Noted from the results was the increase in both vibration and AE r.m.s. with a growth in defect severity. Li et al. developed the spall propagation process model; coupling the model with the correlation achieved, from AE and vibration r.m.s., a recursive least square algorithm was adopted which was capable of predicting the spall progress on the outer race.

Sundt [121] utilised both AE and vibration technologies to detect foreign particles and hairline outer race cracks on a roller element bearing. It was found that a tiny hairline crack modulated the AE signals above 100 kHz while such a modulation, irrespective of any frequency bands effect, was not evident from vibration measurments. Furthermore, it was noted that AE r.m.s. increased upon the introduction of sand particles inside the bearing. Barclay et al. [122] used the spectral emitted energy (SEE) method to diagnosis the metal to metal contact in rolling bearings that resulted from oil film breakdown. The method involved band pass filtering the measured AE signal between 250-350 kHz and generating the envelope spectrum of the filtered signal so that energy of the resulted spectrum could be calculated. The application of SEE was found to be effective in bearing defect diagnosis.

Jamaludin et al. [123] assessed the applicability of AE in detecting the various types of seeded defects on a bearing running at extremely slow speed (1.12 rpm). In this investigation, a range of

defects including line defect, representing early stage defect, localised defect, resembling actual pitting, and operation with contaminated grease were introduced on the bearing. During the test, AE r.m.s., energy and peak amplitude were used to classify the acquired data based on the transmission path; the data classification was conducted with the aid of the Euclidian distance algorithm. Jamaludin et al. noted that early stage defect under slow operation speed is likely to be hidden until it has been well developed. However, it was concluded that there is an exclusive transmission path for each type of defect and it can provide diagnosis advantages. In addition, the authors mentioned the efficiency of the classification method for diagnosis purposes.

Williams et al. [124] conducted an experiment in which number of ball bearing were naturally fatigued. The bearings were tested at high constant and variable speed conditions ranging from 3400-6000 rpm. In this research, the formation of defects on roller and both innerand outer raceswas experienced. Throughout the test both vibration and AE signals were captured and processed using time domain features of r.m.s., kurtosis and Crest factor. In addition, the frequency content of the re-coded signal was studied from the generated envelope spectrums. The results indicated that the vibration measurement was successful in diagnosing the range of defects in both time and frequency domains whilst the AE showed limited success in diagnosing the roller and outer race defect.

Elforjani and Mba [15, 17, 125] performed an experiment in which the propagation of natural spall on a conventional slow speed (70 rpm) thrust bearing was monitored. This research carried a significant contribution, as it was the first case study reporting on the application of AE in monitoring the natural spall progress on the outer race; the previous researches of a similar kind [112, 124] involved the termination of the experiment upon the formation of spall. In this experiment four Pico AE sensors were circumferentially placed at the back of the stationary outer race. After 20 hrs of continuous running, the outer race was found to be badly damaged from two different locations. Elforjani and Mba assessed ranges of signal processing methods in both time and frequency domains to establish the best method to monitor the spall propagation. Among the time domain features, information entropy (IE) was found to be the most effective in monitoring the development of spall while other methods of r.m.s., Crest factor and kurtosis were only able to detect the onset of failure. Moreover, comparing different spectral techniques, it was found that the enveloped frequency spectrum generated, based on Prony Energy methods,

was more successful in the early detection of the defect frequency as compared to the conventional Fast Furrier Transform spectrum. Application of Continuous Wavelet transform also revealed the periodicity of a defect frequency; however the wavelet analysis did not provide any distinct diagnostic advantages over the other employed methods. This research was the first published attempt in which AE was used to determine the size and relative location of naturally occurring spall. The size of spall was calculated by measuring the duration of transient burst as suggested by other researchers [119]. The location of two localised defects was identified relative to the position of sensors; the defect location was determined by knowledge of AE wave velocity and the signal arrival time on each sensor.

Couturier and Mba [126] conclusively examined the influence of load and speed variation on generation of AE activity. Couturier performed two sets of test using split cooper type roller bearing. For each test either one the parameters of load or speed remained fixed while the other parameter varied. Noted from the results, was the increase in AE activity as the result of increases in load or speed; however, the AE activity showed a higher sensitivity to the change in speed; this observation was attributed to the fact that speed is the greater contributor to change in specific oil film thickness as compared to load.

Mba and Rao [12] reviewed an investigation performed by Tavakoli [127] in which the AE was employed to monitor slow speed bearings (80 rpm) under three different operational conditions of lubricated, unlubricated and missing roller. It was noted that the mean spectral density was able to discriminate all the working condition. Tavakoli clarified that the source of AE in roller bearings in rollers are the interaction and friction between the roller and races.

Miettinen and Andersson [128] used AE to monitor the contaminate within the grease lubricated bearing. In this investigation, a range of greases, classified by the type and concentration of the contaminates, were tested using a roller bearing test rig with a deep groove ball bearing. Four types of contaminate with different hardness including quartz, iron, iron oxide and steel with grain size ranging from 5-40 μm were used to prepare the contaminated grease mixture. The authors used an AE count measurement to determine the lubrication condition in the bearing. It was observed that upon the introduction of a contaminated grease sample, the AE count level as well as the standard deviation was largely increased. In addition, it was noted that the decrease in AE count with an increase in the size of contaminates and an increase in hardness resulted in a

higher spikiness of AE signals. The correlation between the grain size and AE activity was attributed to the higher tendency of finer particles towards agglomeration as compared with larger size grains; the agglomeration action of particles resulted in the generation of high AE activity. Miettinen and Andersson performed a further test to explore the effect of re-greasing on lubrication conditions. The bearing which had been run with contaminated grease was cleaned and re-greased with an un-contaminated grease. It was observed that the level of AE activity dropped to half of the level associated with the previous contaminated condition. The authors therefore concluded that the re-greasing action of a damaged bearing can relatively restore the lubrication condition.

Jamaludin et al. [129] presented an investigation in which the authors aimed to develop a non-intrusive method to determine the lubrication conditions in a slow speed bearing. The fact that the stress waves propagating within and along the surface of material are subjected to attenuation was used as the backbone of this investigation. Two stress wave (AE) sensors were placed inside the bearing tests rig. The first sensor was placed on the rotating shaft which was used to transmit a Dirac stress plus on to the system at a defined shaft position. The second sensor was incorporated on the bearing housing to capture the resultant stress waves. Throughout the experiment, two different greases with different viscosities and varying amounts were tested. In this investigation typical time domain features of AE r.m.s., energy and peak amplitude were monitored while the clustering process, based on Euclidean distance for the purpose of grouping the data, was employed. The results indicated that the transmutability of stress waves through the surface is influenced by the viscosity of the lubricant. The effectiveness of the presented method in establishing the amount of grease and lubrication condition requirements for operational bearings was also shown. The authors suggested that 'this technique can also be applied to other slow speed rotating machinery provided that the end shaft is accessible and the shaft rotates at a speed that will allow the transmitting transducer to be mounted onto the rotating shaft.'

To date, apart from the work of Elforjani and Mba [15, 17, 125], Williams et al. [124] and Yoshioka et al. [112] who studied the application of AE in the diagnosis of natural defects, most researches have focused on simulated fault diagnosis. Yoshioka was among the first who studied the applicability of AE in detecting naturally degraded roller bearings. However, the number of rollers employed in Yoshioka's research was limited to three which was not representative of

operational bearings. Later, Elforjani and Mba conducted an experiment which built on Yoshioka's work. The work of Elforjani and Mba was the first published attempt in which the location of naturally generated spall was successfully identified. Although conclusive, this research was performed at a slow rotational speed (72 r.p.m.); it is believed that at a higher speed the level of superimposed noise on the acquired AE signal is more pronounced and this could make source location significantly more challenging as compared to low rotational speeds. In addition, the presence of gyroscopic effects and roller spin at higher speeds, are likely to influence the diagnosis quality. William et al.'s works were performed under a range of speeds but the results revealed limited success in detecting the formation of roller and outer race defect. This can be due to the fact that the employed signal processing methods were not adequate to effectively extract the useful features from the acquired AE signal.

3.1.5 Shaft diagnosis using Acoustic Emission technology

Although the application of Acoustic Emission (AE) in relation to gearboxes is well documented, the majority of applications have been focused on gear and bearing failure diagnosis. The only conclusive published work was reported by Elforjani and Mba [16] who performed an accelerated fatigue test on the slow speed shafts. To accelerate the fatigue process a V-notched shaft was employed. The shaft was supported by two tapered roller bearings while the operational load was applied through a single row bearing using a hydraulic jack. The shaft was immersed inside a cylindrical oil bath and an AE sensor was placed on the oil bath casing; this was to allow for the measurement of the rotating shaft. Elforjani and Mba performed two sets of tests at 72 rpm and under 4 and 8 KN radial loads. The tests were terminated upon fracture of the shaft. Prior to complete loss of integrity, observation of a developed crack was reported by the authors. They also noticed a sharp rise in levels of AE absolute energy (ABS), count and amplitude – almost 1 h prior to the termination of the tests. During the first test, the AE waveform also registered some transient bursts simultaneously with the increase in the measured feature. Furthermore, an early increase in the level of measured AE features lasting for 1 hour was noticed. The authors attributed this early variation in measured signatures to the resulting elastic energy upon the initiation of the crack. Such observation was not mirrored for the second

test which was performed under the higher load (8 KN). It was argued that, due to the higher applied load, the microscopic phase transfer from initiation until the propagation of the crack was not observed. This research has conclusively addressed the diagnosis potential of AET in the detection of fatigue crack on shafts; however, the test rig arrangement was not as complex as actual transmissions. In practice, the transmission shafts normally accommodate numbers of meshing gears which will result in several sources of AE, such as asperity contact in gears, to contribute in generating AE activity, hence causing the fatigue crack diagnosis to be fraught with some difficulties.

3.2 Vibration diagnosis

3.2.1 Source of vibration in gearboxes

Aiming to study the vibratory characteristic of the gearboxes, Drosjack and Houser [11] developed a model based on an assumption that the presence of pitting on the gear pitch can contribute to the variation of gear stiffness; this was because the pitch point damage reshapes the Hertzian contact zone and causes impulsive contact between meshing gears. The model successfully determined the vibrational behaviour of the gear and was also validated with experimental results. The authors concluded that both the impulsive reaction of meshing teeth and the reduction in tooth stiffness are the main sources of change in the vibratory response of the machine. A similar study was performed by Yesilyurt et al. [10] in which the correlation of wear and tooth stiffness was investigated using both analytical and experimental methods. Their study involved the development of a model in which the vibration measurement was employed to assess the extent of occurred wear damaged. In addition, the experimental investigation showed that an increase in gear wear is linearly correlated with a reduction in tooth stiffness. Given the observation from both the experimental investigation and the results from the model based analysis, Yesilyurt et al. concluded that the gear tooth surface deterioration will cause changes in vibration characteristics by influencing the gear stiffness. Choy et al. [130] developed a model showing the gear tooth damage influence phase and amplitude of overall gearbox vibration; their findings were verified through sets of accelerated fatigue tests on different gears.

Tandon and Choudhury [52] reviewed different literatures explaining the mechanism of vibration in bearings. They concluded that the bearings induce vibration due to the instantaneous variation in stiffness as the result of change in the position of load carrying rollers. It was also stated that presence of both localised and disturbed damages will result in a variation contact force leading to an increase in vibration levels.

3.2.2 Different vibration monitoring techniques

Vibration monitoring is the most widely used method for gearbox diagnosis. McFadden [131] suggested the use of the TSA method to remove the noise and non-periodic transient of the vibration. Ismail et al. [132] proposed a technique in which a kurtosis beta function was used to monitor tooth crack. Use of some further statistical methods such as r.m.s and Crest factor were also presented by other researchers [64]. Lebold et al. [8] reviewed different vibratory analysis methods and concluded that an understanding of the different sensitivities associated with each method is an important step towards the evaluation of diagnostic and prognostic capability. Behzad et al. [45] employed the vibration measurement to determine the size of defects in rolling element bearings. Throughout the test, the inner race defect was artificially seeded while the outer race defect was naturally generated through a continuous running of the test rig. To estimate the defect length on the inner and outer rings, threshold levels have been specified and the rate of crossings was employed. Experimental results showed that the level crossing parameter has an acceptable linear correlation with the defect length on the rolling bearing rings.

With regard to shaft diagnosis, the vibration based method has been classified into signal based and modal based methods [133]. In the signal based approach, the vibration signature of the machine is recorded and analyzed where observations of 1X and 2X components of the vibration signals represent the presence of a defect on the shaft [134, 135]. The modal based method concerns simulating the behavior of the cracked shaft using the finite elements and correlating the results with measured vibrations during the machine operation. Sabnavis et al. [133] have reviewed the theoretical models for cracked shaft diagnosis and noted that the assumption of linearity of crack in the model-based method causes an inaccurate estimation of the vibration

response due to several reasons, such as crack switching, impact closure of cracks, as well as variation in instantaneous stiffness. Furthermore it was stated that the most important issue in simulation of cracks is the right modelling of the local flexibility. Prabhakar et al. [136] employed DWT to diagnose the vibration signals from artificially damaged bearings. They seeded a range of defects on the races of several roller element bearings. The initial observation of the kurtosis and r.m.s. values associated with damaged conditions, revealed an increase with an increase in defect size. However, the frequency spectrum of the vibration signals showed limited success in diagnosing the inner race, and combined defect on both the inner and outer race. Therefore the authors went further and decomposed the signals using the Daubechies wavelet. The transient features spaced at defect frequencies were clearly evident on the decomposed signal bands; such observation was noted on the original waveforms prior to decomposition. In the case of the combined defect on both inner and outer races, two sets of impulses, repeated with a different frequency, were noted in a second level of wavelet decomposition. Prabhakar et al. suggested the use of DWT as an effective tool for the diagnosis of single and multiple defects.

Antoni and Randall [72] were among the first who applied spectral kurtosis (SK) to vibration for diagnosis of natural degradation on gear teeth in a single stage gearbox. The SK was calculated within the range of 0-40 kHz and trended for 10 days of an industrial gear operation. Towards the end of the operational period, the SK values increased at a higher frequency range, suggesting the presence of severe pitting of the gear face. Although this investigation reported success in detecting gear damage it did not provide any prognostic information on the extent of the damage. The same authors, in a separate investigation, reported on the application of SK in detecting the seeded ball and outer race defect in a single stage gearbox. The values of the overall kurtosis of vibration signals for the defective cases were close to zero; this was due to the masking effect induced by the gear vibration. However, for both the defective cases, the SK values showed abnormal activity at the frequencies above 7.5 kHz. The estimated values of SK were used to build Wiener and Match filters after which the signals were filtered using the adopted filters. The results were promising, as the presence of a defect frequency for both cases was completely evident on the filtered waveform. Antoni and Randall performed further analyses by comparing Match, Wiener and SK-based band pass filtering on signals from separate bearing running under different operational circumstances. It was noted that SK-based band pass filtering

offered a better resolution for the diagnosis of outer race defects when compared to the other two filtering methods. Finally the authors stated that 'This result is of great importance for practical application, and refutes the common belief that envelope analysis must rely on excessive user participation'. Combet and Gelman [137] employed SK to build an optimal de-noising Wiener filter. The filter was applied to the residual signal from a two stage helical reduction gearbox with natural-like pitting seeded on five of the teeth at equal angular intervals; the residual signal was obtained by removing mesh harmonics using the time synchronous average method. The SK based residual analysis was found to be effective in detecting small pitting damage on the gear teeth.

Barszcz and Randall [138] reported on the failure of a planetary gear in a wind turbine. The authors studied the recorded signal prior to the turbine failure. The motivation was to find a robust method which could set the alarm prior to a complete malfunction of the turbine's operation; this failure was not reflected in the typical signal features normally employed to monitor wind turbines. For this investigation, a comparative study between the applicability of TSA and Kurtogram was made. Kurtogram was used for the purpose of optimum band-pass filtering while the TSA was employed to obtain the meshing pattern. The results showed no diagnostic success for TSA, whereas the application of SK was promising. The maximum kurtosis value showed an increasing trend from a certain point in the turbine operation time. Moreover, the filtered waveforms exhibited the spikes spaced at roll-over frequency; this frequency was associated with the passage of a planetary gear over a cracked tooth. The authors recommended the use of SK analysis as a standard condition monitoring procedure for cracked tooth diagnosis in wind turbines.

Immovilli et al. [139] applied SK on the vibration signature to detect the generalised roughness on rolling element bearings. The generalised roughness was seeded in different severities by using chemical and abrasive materials. The authors defined SK energy as the energy of the band-pass filtered signal based on the optimum centre frequency and bandwidth derived from Kurtogram. The results showed that the SK energy increased as the function of defect severity and operational speed, while the maximum kurtosis from Kurtogram did not mirror such correlation.

Sawalhi and Randall [140] reported on the application of SK diagnosis of an inner race defect. They filtered the signal using an autoregressive filter after which the Kurtogram of the filtered signals was generated based on the filter bank method suggested by Antoni [73]. The filter bank was built using the complex Morlet wavelet transform with varying octave number. The resulting Kurtogram suggested the optimum frequency and octave number to be used to band-pass filter the signals. The envelope spectrum of the filtered signals clearly discriminates the defect frequency.

3.2.3 Accelerated fatigue test

Dempsey et al [141] performed a prolonged fatigue using 500 hp Helicopter Transmission stand. The purpose of the test was to monitor the crack propagation of gear teeth however the test rig was failed due to an two unexpected triplex ball bearing failure. Prior to the termination of the test vibration signals were continuously acquired while the oil debris data were collected every 15 minutes. Dempsey employed envelop analysis to identify the bearing characteristic frequency from the vibration signals. The vibration data as well the oil debris result were fused together using Fuzzy logic. It was concluded that the combined oil analysis and vibration measurement is effective in diagnosis the bearing failure.

Dempsey et al [142] conducted an investigation aiming to the find optimum threshold level for monitoring pitting progress on the gear tooth surface. Series of accelerated surface fatigue tests were performed on an experimental gearbox. Throughout the test two parameter of Kurtosis and M8A were calculated for the signals; M8A was defined as eight statistical moment to fourth power of variance. The criteria to find the optimum threshold level was set based on the minimum false alarm rate and maximum sensitivity to pitting progress. The finding from the experimental rig was then applied to actual flight data from a helicopter gearbox. It was found that 4 and 394 value for kurtosis and M8A can be an effective threshold level with optimum sensitivity and minimum, false alarm rate. Also found that the similarity between probability density function of both test data and flight data for no damage condition. Dempsey went further and pointed that studying the data distribution from the damaged and undamaged conditions can be an alternative approach to threshold setting.

Dempsey et al [143] reported on an experimental investigation to develop a diagnosis tool for tapered roller bearing. Series of long term fatigue test was conducted on an experimental test rig consisting of a shaft, tapered bearing and salve roller bearing. The test rig was loaded on axial direction and the tests were run with undamaged and pre-damaged bearings. Throughout the test oil debris parameter and vibration signals from three different locations were recorded. The data from both oil analysis and vibration measurement were fused together to built an integrated condition monitoring system for bearing diagnosis. The fusion technique showed an improved diagnosis capability in compared with using each individual monitoring technology.

Dempsey and Zakrajsek [144] presented a study in which the effect of load on measured vibration signals was set to minimum. Dempesey employed the spur gear test rig [142] to perform a long term fatigue test. The signals from the test rig were averaged and the meshing components were filtered from the averaged signals afterwhich the kurtosis of the residual signal were calculated. It was shown the resultant parameter is more sensitive to pitting progression whereas insensitive to load variation. This was an important finding and is particularly useful in the applications where the speed and load constantly varies. In such applications the overall vibration is subjected to fluctuation. This fluctuation in vibration level can itself influence the sensitivity of monitoring parameters to damage progression.

3.3 Motor current signature analysis (MCSA)

Motor Current Signature Analysis (MCSA) is a monitoring technique mainly used for online monitoring of machinery. In some applications where access to the machine is hard to come by, such as nuclear application, this method gains advantages over other monitoring technologies such as AE, vibration etc. Application of other techniques requires mounting the sensor (Accelerometer, AE transducers, Eddy current, etc.) on a specific part of the machinery thus the generated signal is attenuated as it travels through the interfaces between the source of excitation and the sensor. Additionally since different sources participate in generation of the diagnosis

signals, it makes it difficult to localize the specific source of excitation corresponding to a particular part of the machine [145]. MCSA is one monitoring technique which provides the solution for the aforementioned difficulties [146].

3.3.1 Theory

The input power delivered to any three-phase motor can be expressed by Equation 17 [147]. Assuming that the efficiency and mechanical integrity of the motor itself remains unchanged during the normal operational circumstances, then any increase in the amount of power loss is caused by the driven system; according to Equation 18, any change in the amount of power loss can directly influence the current drawn from the supply line. The mechanical fluctuation in the system normally causes an imbalance on the rotor; this results in the disturbance of magnetic flux within the motor cage. Hence the motor itself can act as a transducer, detecting the dynamical variation of a machine as a function of time, so that any torsional vibration at a specific frequency will also be manifested in the current spectrum [146, 148].

$$P = \sqrt{3}EI\cos\theta \qquad \textbf{Equation 17}$$

Where

P: Input power

I: current in a single line

θ : Angele between current and voltage

E : Line voltage between any two phases

Also

$$\eta = \frac{P_{out}}{P_{in}} = \frac{P_{in} - P_{Loss}}{P_{in}}$$ **Equation 18**

Where

η : Efficiency of the motor

P_{in} : Delivered input power

P_{out} : Mechanical power at the motor shaft

P_{Loss} : Power loss

Likewise

$$P_{Loss} = P_M + P_S$$ **Equation 19**

P_M : Power loss from motor components

P_S : Power loss from the driven system

From equations 18 and 17:

Equation 20

$$I = \frac{P_{Loss}}{\sqrt{3}E\cos\theta(1-\eta)}$$

3.3.2 Application of MCSA as a diagnosis tool

One of the first applications of MSCA technology was developed and documented by Kryter and Haynes[149] in the Oak Ridge National Laboratory in which the MSCA technology was used to monitor the motor-driven nuclear power plant safety equipment[149]. Later, in 1990, Haynes and Eissenberg [146] submitted a patent explaining an approach to monitor a motor-operated valve in nuclear power plant and chemical process systems. In their case study a typical conventional current transformer was connected to the control centre of the electric motor which drives whole the valve assembly. The current signal from the transformer was fed to a simple frequency analyzer to generate the frequency spectrum of the current signature. The motor slip frequency, shaft frequency and worm gear meshing frequency, which controls the valve itself, were clearly evident in the frequency spectrum of the signal. The authors claimed success in applying this method in order to monitor different components in valve assemblies by comparing the frequency contents of the captured current signal at different intervals.

There are numerous published articles discussing the applicability of MCSA technology to monitor typical failures inside the induction motor, such as abnormal air gap eccentricity, stator winding faults and broken rotor bars [148, 150-152]. While other researchers have focused on the application of MCSA as an online tool to monitor different machining processes [151-153]. Among those, Oh et al. [156] applied MCSA to control the drilling torque using spindle motor current and studies its effect on tool wear by assuming that increasing the cutting torque level would lead to a significant rise in tool wear and operating temperature. They measured both cutting torque and spindle motor signature using Dynamometers and current Hall-effect sensor respectively. Their results showed that spindle motor current signature perfectly reflects the cutting torque variation. Furthermore, the estimated cutting torque based on the motor current equation was in agreement with the reading from the Dynamometer.

The theory behind the MSCA technology, as it applies to gear diagnostics, is similar to the vibration based monitoring and its theoretical fundamentals have been reviewed in ref [157]. Rajagopalan et al. [157] were among the first who studied the applicability of MCSA technology

to monitor gear mesh. In their experiment the authors used a pair of worm gears, and stainless steel worm meshing with a plastic wheel and was coupled to a six pole torque-controlled BLDC motor. There was no external load applied on the gears and the motor supply frequency was 180 Hz. The gear ratio was 22:1 with 66 teeth on the wheel. Throughout the experiment, three different forms of gear failure, i.e., localised damaged tooth, scoring as a result of loss in lubrication and debris in lubricant, were seeded on the gears and the current and voltage waveforms were recorded. A localised damaged-tooth was introduced to the gear assembly by deforming two adjacent teeth on a plastic wheel using pliers. Impulses representing the localized damaged were completely evident in the real time current signature. Similarly, the defect appeared in the current and voltage frequency spectrum in the form of rich harmonics spaced at the frequency of the rotation of the toothed gear wheel (2.8 Hz); this was completely in agreement with the theoretical calculation.

The test was continued by seeding scoring defects using soap and water to remove the lubricant. The gear fault was characterized by the two sidebands in both the current and voltage frequency spectrum spaced about the 2.8 Hz from the fundamental frequency; the amplitude of the sidebands was increased by 10% of the fundamental. Thus the authors concluded that the harmonics around the fundamental frequency exhibit identifying qualities towards the detection of excessive friction due to lubrication loss. The debris was experimentally seeded by inserting small pieces of paper into the gear while the gears were meshing; the result was similar to the localised tooth damage fault. Rajagopalan concluded that gear fault frequencies are completely evident in both current and voltage spectra and can be easily distinguished from a typical motor fault. Furthermore, it was mentioned that detecting gears faults from the motor voltage is particularly helpful in applications that have only a current control loop; this is because the fault frequencies are more evident.

The second major effort in this regard was performed by Kar and Mohanty [154] in which a four stage gearbox was monitored using MCSA technology. In this research a two-pole three-phase induction motor with 7.5 kW capacity was coupled with a four-speed automobile gearbox. A DC generator was connected to the output shaft and coupled with a 5.625 kW variable resistance load thus the operational load could be adjusted by means of an electric control throughout the test. To study the effect of faults in gears, two defects were seeded; the defects were seeded by

removing two consecutive teeth using an EDM machine. Vibration signals were acquired with an accelerometer mounted near the tail-end bearing of the gearbox casing based on two different sampling rates of 200 Hz and 4.096 kHz for low range frequency (0-100 Hz) and High range frequency (0-1,000 Hz) respectively. The rotation speed of the motor was measured with a photo-electric probe. Four different loading conditions, 5.625, 3.75, 1.875 and 0 kW were applied throughout the test so that the MCSA signatures were acquired at two or three different operational conditions of 5.625 to no load, 3.75 to no load and 1.875 to no load. Fast Furrier Transform (FFT) was applied on both vibration and current readings in two High (0-1,000 Hz) and Low (0-100 Hz) frequency ranges. The shaft frequencies appeared in the vibration spectrum while the corresponding sidebands were evident around the supply line frequency. The motor eccentricity was also evident in the remaining sidebands of supply line frequency. The authors noted frequency variations at order of 30 r.p.m. in two different loads for no defect conditions; Amplitude which decreased as the load became smaller. They argued this phenomenon is due to the vibration from the gearbox casing being retransmitted into the gearbox through the rolling element bearings causing a large excitation of the whole gearbox assembly and large speed fluctuation.

The gear mesh and supply line frequency were also observed in the higher frequency portion of the spectrum. The current signal was decomposed using Daubechies wavelet of the order of 8 up to 4 level with a maximum frequency of 2 kHz after which the frequency spectrum of the second level of decomposition (500-1,000 Hz) was generated, in which the sideband of gear mesh frequencies was evident across the supply line frequency. In addition, the peak-at-shaft frequency and its harmonics were observed in the spectrum; the presence of these peaks was not completely evident in the spectrum of the original signal. Kar and Mohanty postulated that monitoring the amplitude of the second meshing frequency in the D2 spectrum of the current is quite effective in diagnosing the defects. To show whether the defect can be detected through transient analysis of the motor current signature, the authors acquired current signature with a sampling rate of 20 kHz. A similar wavelet (db8) was applied to decompose the signals up to 10 levels. The load fluctuation was clearly evident in the D8, D7 and D3 level decompositions while transient events spaced at defect frequencies were observed in D4. It was also noted that load fluctuation predominantly affected the D8 level which contained the supply line frequency (50 Hz). Based on this observation, the authors concluded that defects in the gearbox can be sensed

by imparting very high load fluctuation that will excite the D4 and D3 level of decomposition. CWT analysis was also applied on the current signature using a similar wavelet. Transients, due to load, were found around particular scale bands, whereas the defect induced transients were not evident in the CWT counter plot, irrespective of any scale.

Thus far, most of the research for works on the application of MCSA in gear diagnosis has focused on the detection of seeded gear defects. However, no investigations have been reported where MCSA has been applied to neither crack shaft diagnosis nor the monitoring of the natural pitting progress on the gear face width.

CHAPTER 4

---

4 Experimental setup and test procedures

4.1 Test rigs

Throughout this research two independent test rigs were used to perform natural and seeded defect tests on roller bearings and gears.

4.1.1 Back-to-Back gearbox

For the purpose of research on gear diagnosis, an experimental gearbox was utilised. The gearbox used in this experiment was a back-to-back arrangement consisting of two main parts: the test and slave helical (214M15) steel gears, details of which are provided in Table 3 and Figure 19. The concept behind the application of the back-to-back arrangement is to allow the torque to be maintained inside a closed loop so that the power requirement overcomes frictional losses only. Hence, highly loaded gears can be rotated by a relatively small electric drive, see Figure 20 [13]. Twisting the loading plates against each other, using a side bolt, will allow a static torque to be applied across the gearbox, see Figure 21. The loading plate consists of two half flanges bolted to each other; one of the flanges has a threaded hole. The loading plates were calibrated using an optical strain gauge with rosette arrangement mounted at the opposite shaft, connecting test and slave pinions together. The test rig assembly was driven by a 3 phase 1KW electric motor at a nominal speed of 690 rpm. The splash lubrication method was used to lubricate the gears during the experiment. According to Drago et al [21], splash lubrication is suited to an application with less than 25.4 m/s pitch line velocity. The pitch line velocity in this research was approximately 5.4 m/s and met the requirements for splash type lubrication. For the purposes of lubrication, Mobilegear 632 was used, the specification of which has been detailed in Table 4 . This is high performance oil intended for use in gearboxes with a splash lubrication system.

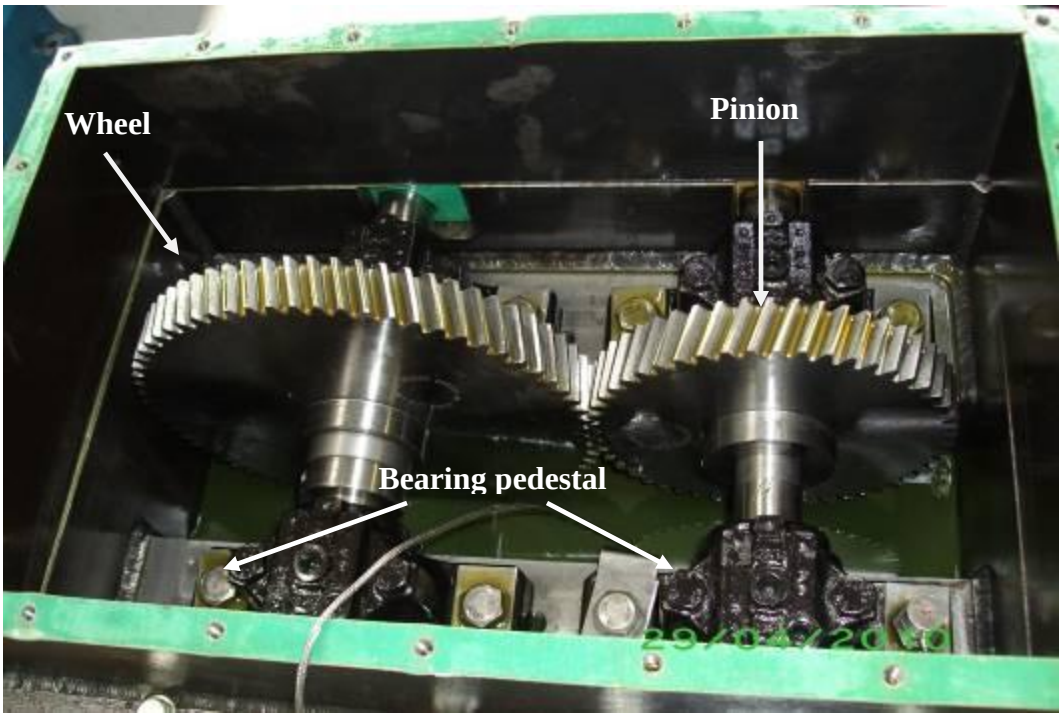

Figure 19 Helical gears

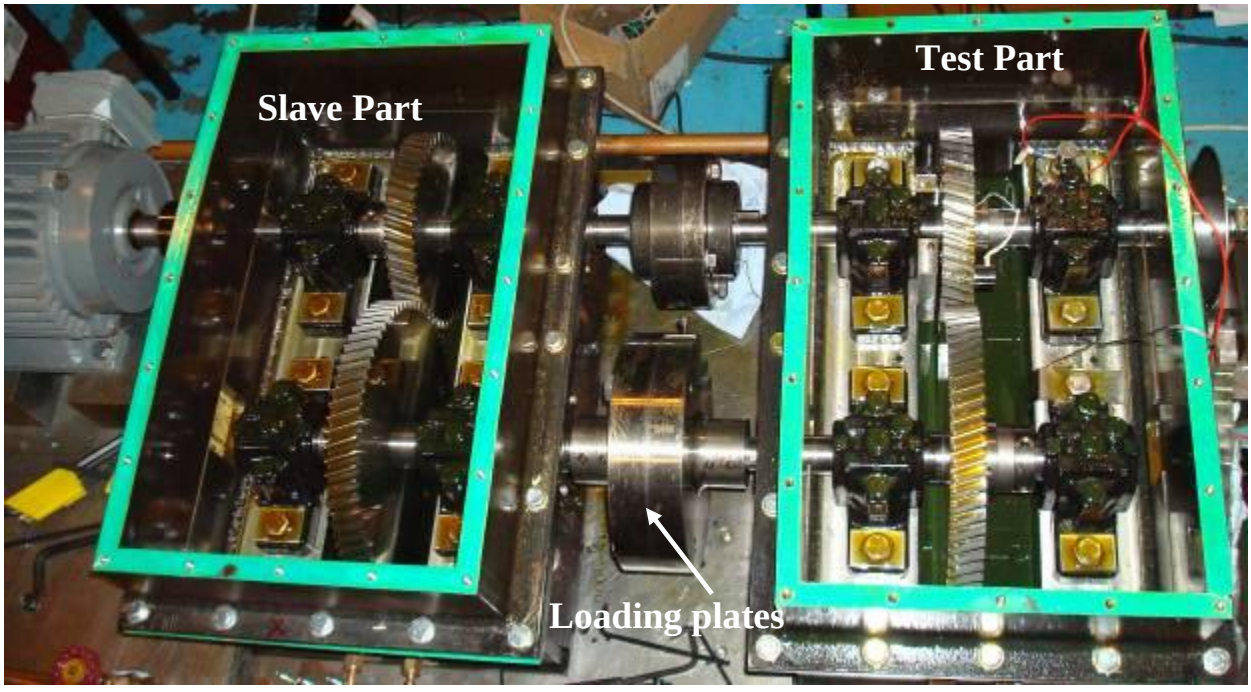

Figure 20 Back-to-back gearbox test rig

Figure 21 Loading plates

Table 3 Specification of the gears

	Pinion	Wheel
Number of teeth	51	70
Module	3mm	3mm
Pressure angle	20º	20º
Helix angle	17.5º	17.5º
Contact ratio	1.7	1.7
Face width	25.1mm	25.1mm
Direction	Rh	Lh
Hardness	137 Hv30	137 Hv30
Surface roughness	1.327 µm	1.327 µm
Pitch diameter	160 mm	220 mm

Table 4 Physical properties of gearbox lubricant

	Mobilegear 632
Kinematic Viscosity @ 100°C, cSt (ASTM D-445)	24.5
Kinematic Viscosity @ 40°C, cSt (ASTM D-445)	320
Viscosity Index (ASTM D-2270)	97
Density @15.6º C, ASTM D 4052, kg/l	0.89

4.1.2 Bearing fatigue machine

The bearing test rig has been designed to simulate varying operating conditions and accelerate natural degradation on thrust roller bearings. The test rig used in this experiment is displayed in Figure 22. The chosen bearing for this study was an SKF single thrust ball bearing, model number SKF51210. To ensure accelerated failure of the race, the standard grooved race was replaced with a flat race, model number SKF 81210TN, see Figure 23. This caused a point contact between the ball elements and the flat race, resulting in faster degradation of the race and early initiation of sub-surface fatigue cracks. The load on the test bearing was applied by a hand operated hydraulic pump (Hi-Force No: HP110-Hand pump-Single speed-Working Pressure: 700 BAR). The test bearing was placed between the fixed thrust loading shaft and the rotating disk which housed the grooved race. The flat race was fitted onto the loading shaft in a specifically designed housing, see Figure 24.

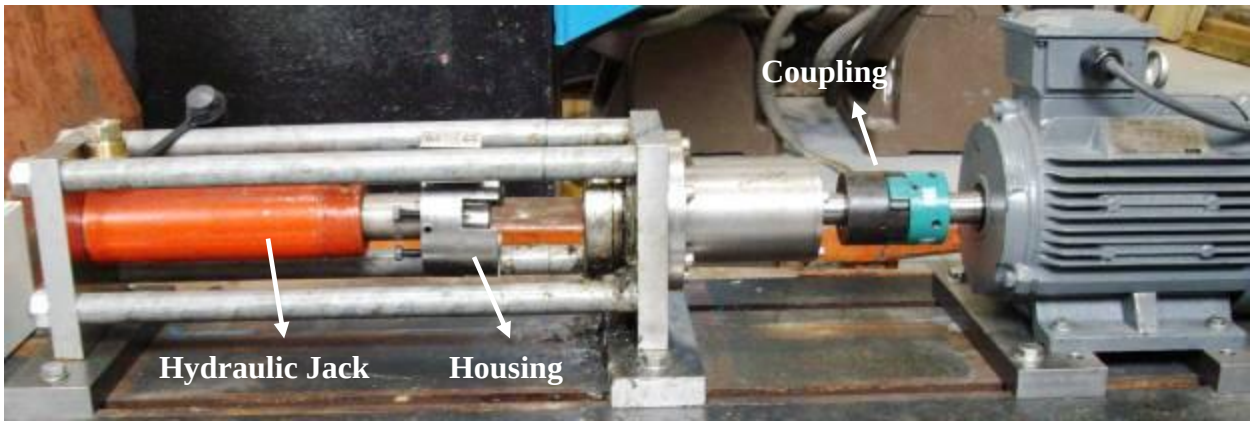

Figure 22 The bearing fatigue rig assembly

Figure 23 The test bearing

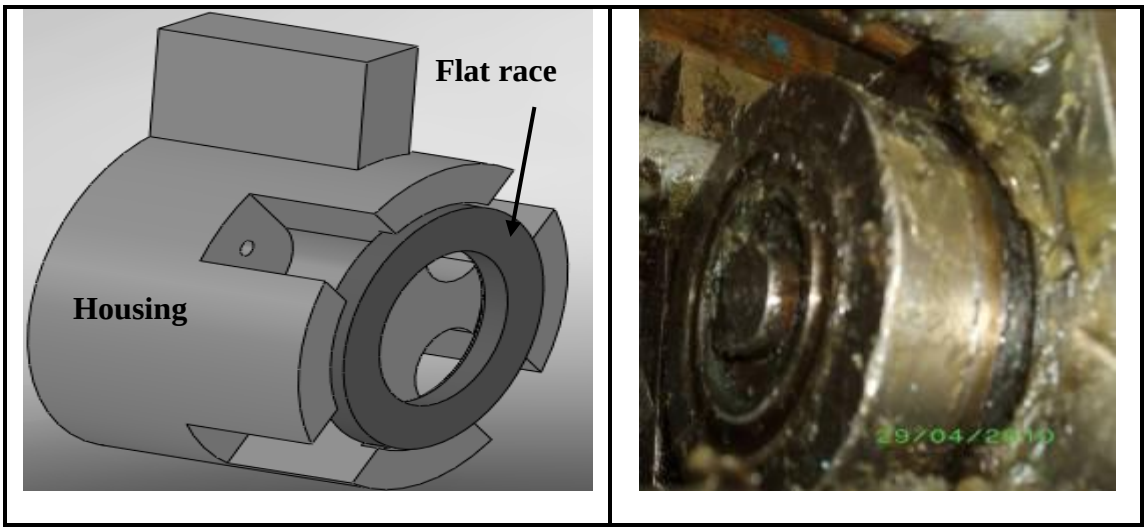

Figure 24 Left) the housing and fitted flat race Right) Rotating disk

4.1.3 Instrumentation

Two separate instrumentation setups were used for data acquisition on each of the rigs. However, similar data acquisition systems were employed to acquire AE and vibration signals from both test-rigs. In total three types of AE, vibration and current signals were recorded using the acquisition devices.

4.1.3.1 Data Acquisition systems

Throughout the test, the AE signals were recorded using AE DSP-32/16 and PCI-2 data acquisition cards produced by the Physical Acoustic Co (PAC). The AE raw waveforms , at 10 MHz sampling rate , were captured using AE DSP-32/16 and software, MI-TRA, released by the PAC. Other signal features such as AE r.m.s., absolute energy, ASL and AE waveforms , at 2 MHz sampling rate , were recorded with the PCI-2 system operated with a special software package, AEWIN. The PCI-2 system contains six independent channels and is capable of acquiring AE data with 16-bit resolution. The vibration and current signals were captured with an analogue-to-digital card (ADC), NI-6009, supplied by the National Instrument Co. The card allows the measurement of up to 40 kHz sampling rate with 14-bit resolution. An in-house

LabView script was developed to initialize the ADC card and to capture the signals at regular intervals.

4.1.3.2 Instrumentation arrangement for gear diagnosis

Figure 25 presents a schematic view of the sensor arrangement for the back-to-back gearbox; furthermore the details of each sensor have been included in Table 5. In order to measure the AE signal, two-wideband differential sensors were placed on the pinion gear (S1) and on the gearbox casing (S2). The sensor on the pinion was fed through a longitudinal hole inside the shaft and connected to a slip ring, thus the signal could be recorded while the gearbox was operational, see Figure 26. The slip ring was a 12-channel sliver contact type supplied by IDM Electronic Ltd. Signals from both AE sensors were fed into a pre-amplifier[3]; in addition AE waveforms were recorded at a sampling rate of 2MHz at 15 minute intervals. Moreover, the AE r.m.s. was constantly acquired ; the time constant for calculation of r.m.s was set to 90 msec. A secondary AE acquisition system (AE-DSP 32/16) was also used to capture the signal at a higher sampling frequency of 10MHz. An external triggering system was employed to ensure that the subsequent acquired data were taken from a defined circumferential point of the pinion for every revolution. AE signals were also acquired with the AE-DSP 32/16 card where the signals were sampled at 10 MHz sampling rate, see Figure 25. The triggering system consisted of a metal disc with a 2 mm diameter hole and an optical sensor. Each time the hole passed through the optical sensor a pulse was generated. The pulse was then sent to the secondary AE acquisition system and the raised edge triggered the system, see Figure 27.

The vibration signals were measured with accelerometers placed on a bearing pedestal (S3) and gearbox casing (S5). The signals from the vibration sensors sampled at 10 kHz and a charge amplifier (Endevco 2721B) were employed; vibration waveforms were acquired at 10 minute intervals. A current probe (S4) from Chauvin Arnoux was employed to measure the electric

[3] The pre-amplifier was equipped with an in-built band-pass filter with band widths of 10 kHz-2 MHz and 10 kHz-900 kHz at 40 and 60 dB gains respectively.

current drawn by the motor from the supply line. Measurements from the current probe (S4) and the vibration sensor (S5) were acquired with the same procedures employed for sensor S3.

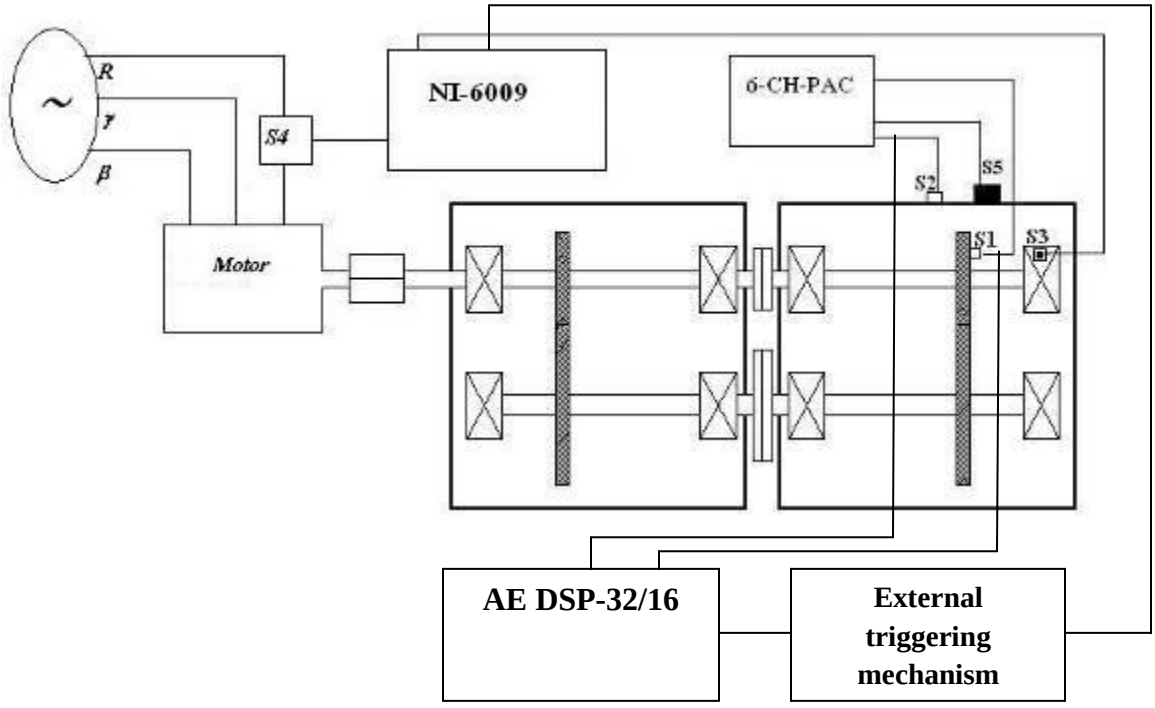

Figure 25 Schematic view of the gearbox and sensor arrangement

Table 5 Sensor specifications

Sensor	Type
S1&S2	Wide band differential AE sensor with a relative flat response between 100kHz-1MHz.
S3	Accelerometer-Endevco 236 ISO base with 10-8000 Hz response range.
S4	Chauvin Arnoux current probe-MN60
S5	Accelerometer-B&K 4370 with 0-4800Hz response range

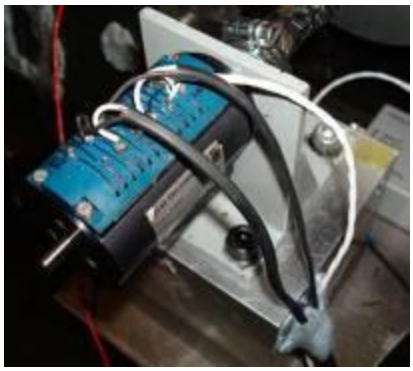

Figure 26 Slip ring

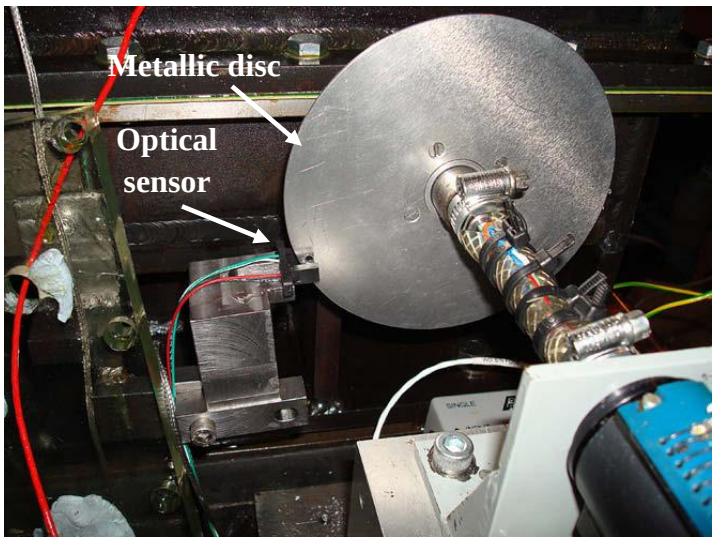

Figure 27 Data acquisition triggering mechanism

4.1.3.3 Instrumentation arrangement for bearing diagnosis

The bearing fatigue machine was equipped with four commercially available piezoelectric sensors (Physical Acoustic Corporation type 'PICO') with an operating range of 200–750 kHz at temperatures ranging from 265 to 1770C. All four AE sensors were mounted at the back of the flat race test bearing and connected to a data acquisition system through a preamplifier (40 dB gain). AE waveforms were taken every three minutes throughout the test duration at the sampling rate of 2 MHz, see Figure 28. The data acquisition system was set to continuously acquire AE absolute energy (atto-Joules) over a time constant of 10 ms at a sampling rate of 100

Hz. The absolute energy is a measure of the true energy and is derived from the integral of the squared voltage signal divided by the reference resistance (10 k-Ohms) over the duration of the AE signal. For these tests, a fixed sample length (250msec) of AE waveforms was captured every 60 seconds at 2 MHz sampling frequency. Throughout the test AE HITs were also acquired. The timing parameters employed for defining an event during these experiments included the HIT definition time (HDT), HIT lockout time (HLT) and peak definition time (PDT) and these were set at 500 µsec, 500 µsec and 100 µsec respectively.

An accelerometer was mounted on the flat race housing (see Figure 29) and vibration measurements were acquired at a sampling of 10 kHz at three-minute intervals using the NI-6009 USB analogue to digital data acquisition card. The specification of the accelerometer was the same as the S3 sensor detailed in Table 5.

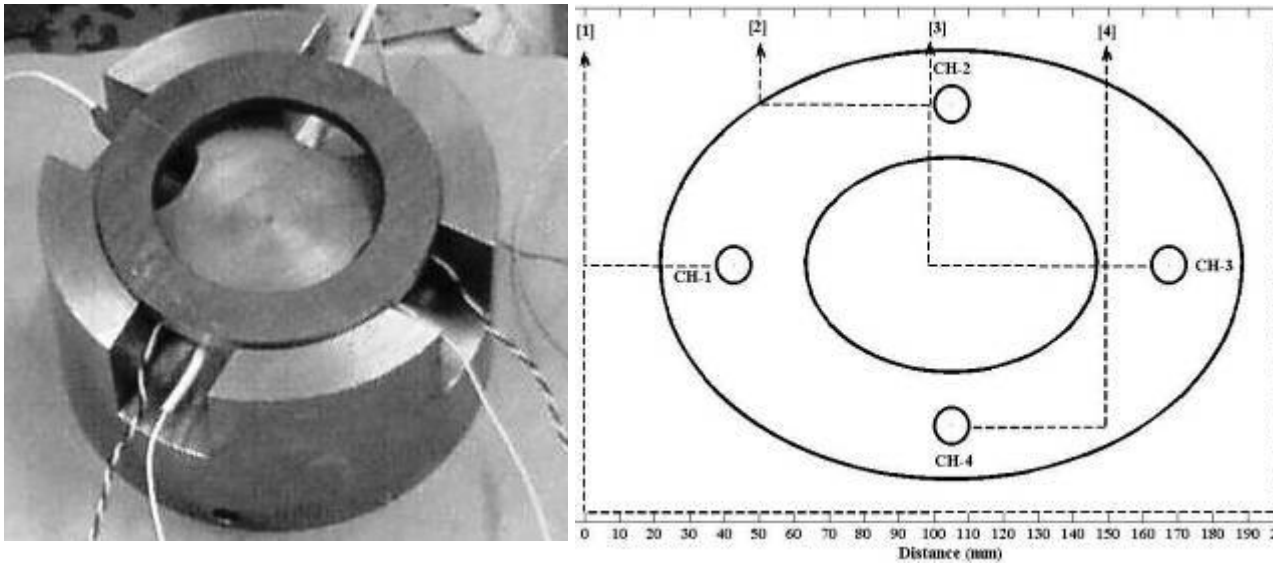

Figure 28 Sensor arrangement on the flat race showing the circumferential distances between sensors.

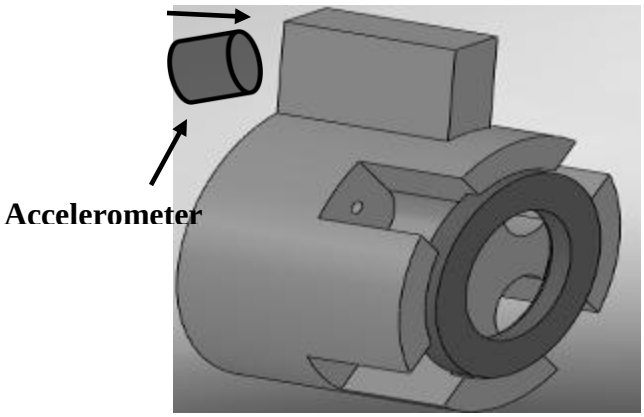

Figure 29 Accelerometer on the housing

4.1.4 Test procedures

4.1.4.1 Helical gear diagnosis

4.1.4.1.1 Seeded defect test

The seeded defect test is performed to assess the effectiveness of AE monitoring techniques for the identification of seeded defects on helical gears. In addition, the effect of gradual defect growth was explored. Prior to the testing, the gearbox was run for 3-h at 380 Nm so as to allow the gearbox to dynamically settle and reach a stabilised temperature – in this instance 60^{o}C. It was essential to capture AE and vibration data that included the defective tooth and for this purpose an acquisition time frame, or window, of 16 teeth was set whereby the trigger mechanism ensured an acquisition duration of 0.0256-s, corresponding to 16 teeth at 690 rpm for each set of data, Figure 30. To begin the tests, a defect free recording of AE and vibration was undertaken. The gearbox was then stopped and the torque set to 250 Nm and run for 5-min to accommodate the new dynamic condition. Again, defect free AE and vibration data were captured for the same acquisition window. The same procedure was repeated at 180 Nm. The defect free condition will be referred to defect-0, see Table 6. In order to carry out the seeded defect test, the test rig was stopped and the first defect introduced on the seventh tooth using a

drill, see Figure 31. The gearbox was then started, and vibration and AE data for the time frame encompassing the damaged tooth were acquired instantly. The significance of the instantaneous recording was to allow the author to explore the influence of surface/material deformation on the levels of AE and vibration as some investigators had suggested [94, 155]. The gearbox was allowed to operate until the temperature reached 60^{o}C after which AE and vibration signals were again recorded for the specific defect condition. The same procedure was repeated at 250 Nm and 180 Nm. The test sequence continued for six more defect conditions, as detailed in Table 6. Eventually, four sets of data for each defect were produced. The first was associated with data at 380 Nm torque, captured immediately after the defects were generated, and referred to as 'D' throughout this report. Other sets of data corresponded to the data at 380 Nm, 250 Nm and 180 Nm for constant temperature (60^{o}C) and are labelled as 'A', 'B' and 'C', respectively. Twenty sets of AE data were recorded for every defect and load condition. Similarly, vibration data were captured at a 10 kHz sampling rate over a time window of 0.0256 s. The vibration data were averaged.

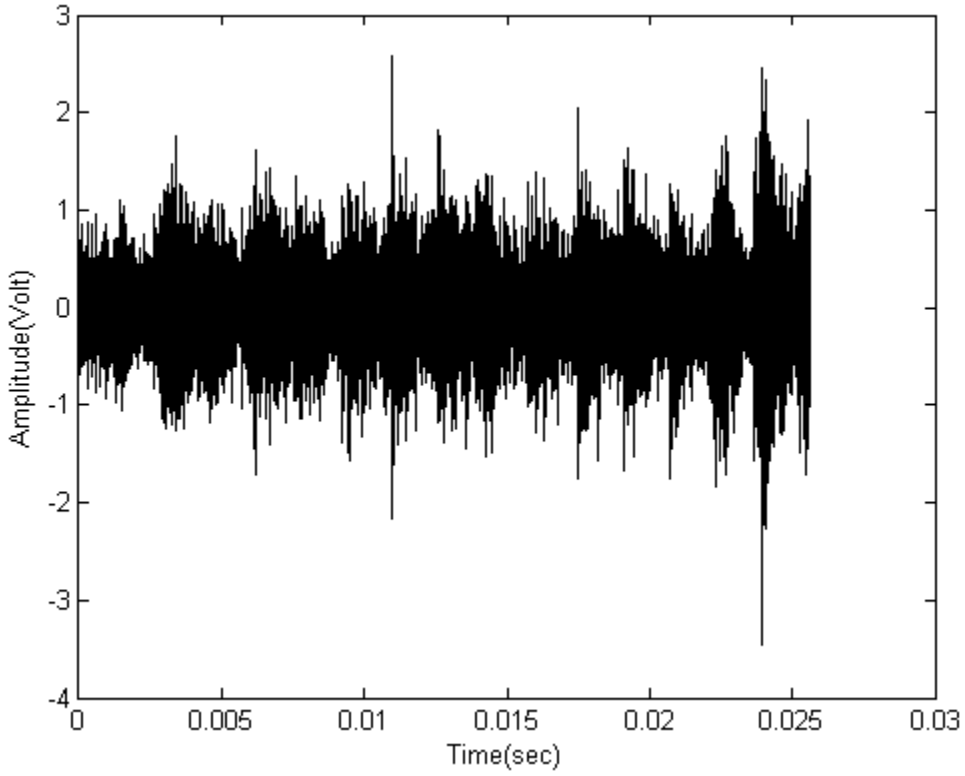

Figure 30 Mixed modes AE waveform associated with a defect free condition.

Figure 31 Seeded defect on the tooth

Table 6 Details of seeded defects

Defect type	Size(mm^2)	Depth (mm)	Removed volume (mm^3)
Defect-0	0	0	0
Defect-1	18.88	0.1	1.888
Defect-2	28.71	0.2	5.742
Defect-3	41.22	0.5	20.61
Defect-4	17.5	1	17.5
Defect-5	15	0.8	12
Defect-6	158.75	0.2	31.75
Defect-7	163.5	0.2	32.7

4.1.4.1.2 Accelerated fatigue test

This test was conducted to build further insight on the work of Tan et al. [13] on spur gears by investigating the applicability of both vibration and AE technologies in monitoring the natural pitting on helical gears. Throughout the test, the back to back gearbox was run continuously for a period of several weeks. Two tests were performed at a speed of 690 r.p.m. and the gear oil employed was Mobilegear 632, see Table 4. The first test duration was over 330 hrs at the end of which the pinion teeth face was covered by 25% pitting; prolonged running of the gearbox over 330 hrs resulted in the unexpected fracture of the test gear pinion shaft. Throughout the first test, the operational torque was maintained at 170 Nm. The second test was terminated after 778 hrs of operation at 50% pitted surface area. For the second test the operational torque was changed during the test. The load was initially set to 170 Nm but at 345 hrs and 460 hrs into operation the load was increased to 270 and 290 Nm respectively. The reason for this change of load was to accelerate the pitting progression on the tooth surface as the rate of pitting progression for test-2 was markedly slower than test-1. Therefore this variation in load provided an opportunity to accelerate the fatigue process on the pinion gears while assessing the effectiveness of AE and vibration in monitoring the pitting progress on the teeth. At regular intervals the gearbox was stopped and the pinion visually inspected; the maximum pitted area on several teeth was then registered. Figure 32 presents the pitting progress on the pinion gear teeth surface as a function of time. For the purpose of visual inspection, the pinion tooth surface was divided into eight sections, each representing 12.5% of the surface area. At a defined inspection interval, the pitted locations were sketched onto the relevant marked sections so that the total amount of surface deterioration could be estimated. The maximum pitted area on any teeth was recorded. Appendix A lists the extent of damage at each inspection period and also provides details of defect progression on the teeth's surface. The pitting initially occurred at the dedendum and moved towards the addendum. This was in agreement with that noted for the spur gears by Tan et al. [13].

Unfortunately, during this experiment the AE and vibration sensors from the gearbox casing malfunctioned so that the readings from those sensors has not been presented in this research.

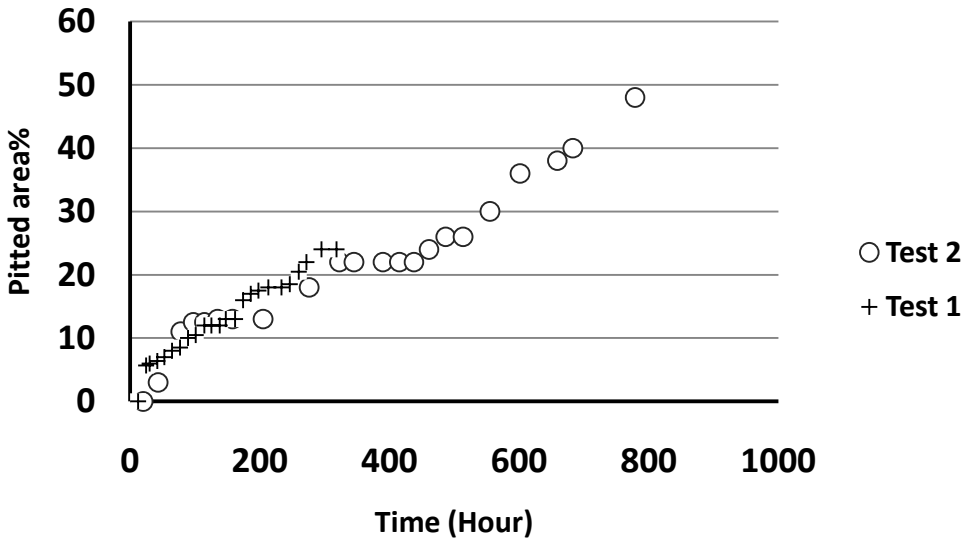

Figure 32 The pitting rate for test-1 and test-2

4.1.4.2 Fatigued shaft diagnosis

The original purpose of the experimental test was to perform an accelerated fatigue test on the pair of helical gears. During the test the transmission shaft fatigued unexpectedly. This naturally fatigued shaft offered an excellent opportunity to assess the potential of the three different measuring technologies to identify the fatigued shaft using vibration and Acoustic Emission. The results of the pitting progress on the gear teeth prior to the loss of the shaft's mechanical integrity has been presented as test-1 in section 4.1.4.1.2.

4.1.4.3 Accelerated fatigue test on bearing

This test aims to complement the work of Elforjani [17] by experimentally investigating the use of AE for detecting natural degradation of a bearing at a rotational speed of 1500 r.p.m. using a bearing fatigue machine. The test rig was allowed to operate until vibration levels far exceeded typical operating levels at which point the test was terminated. An axial load of approximately 50000N was applied on the bearing throughout the test and a total of three tests were performed.

Two tests are presented in this research with quite distinct signal-to-noise ratios; Test 2 was significantly noisier for both vibration and AE measurements. This was attributed to the variation in test rig assembly, such as adjustments and sensor attachments; therefore it offered a good opportunity to assess the methods for diagnosis. Such challenges with AE sensor attachments and noise interference have been discussed recently by Sikorska and Mba [145]. They argue that one the major sources of noise in machinery can be due to low frequency modulation of the continuous AE signal as a result of misalignment.

CHAPTER 5

5 Helical gear diagnosis

5.1 Seeded defect detection

5.1.1 Applicability of AE in monitoring seeded defects

5.1.1.1 Observation of the signals in time and frequency domains

A typical waveform associated with the defect free condition at 380 Nm is presented in Figure 30. A continuous type AE waveform is dominant, although there also exist transient AE bursts whose amplitude exceeds the underlying continuous wave; the frequency of the periodicity of the AE bursts represented the number of meshing teeth within the acquisition window. This is similar to observations of AE waveforms associated with spur gear mesh in which both continuous and transient forms of AE activity were apparent [101]. Tan et al. [101] concluded that rolling contact on the pitch line of the spur gear mesh was responsible for generating high amplitude AE transient bursts, whilst sliding contact was attributed to the generation of a large portion of the continuous waveform. In relation to helical gears, contact between a specific gear pair begins as a minute contact point which increases in contact length on the engaging pair whilst decreasing in contact length on the disengaging pair of gears. As such, the contact length varies along the pitch line of the helical gears, whereas in spur gears the contact length remains constant. In addition, the continued variation in the contact length during meshing of helical gears [156], which directly influences the load conditions experienced by the gear, will lead to instantaneous changes in oil film thickness. Therefore, AE waveforms associated with the helical gear mesh were expected to be of the continuous type with amplitude variations attributed to the gear mesh, see Figure 30. Figure 33 shows typical AE waveforms associated with each defect condition which showed relatively large transient AE bursts over continuous operational AE levels. The transient AE bursts were noted to occur at the exact tooth where the defect was seeded, see Figure 33. Such observations were not noted in a similar test with spur gears, i.e., the seeded defects were not evident in the waveforms [14, 94].

Figure 34 presents the frequency spectrum associated with AE generated from the defect-free and defect-5 conditions, showing that the frequency spectrum of AE was concentrated between 100 kHz and 300 kHz with no distinct feature between the defect free and defective condition. This applied to all AE data for every test condition. A frequency spectrum taken from a Hsu-Nielsen[4] source, undertaken during system calibration, is presented in the top of Figure 34. Interestingly, the spectrum of the Hsu-Nielsen source ranged from 100 kHz to 300 kHz with dominant peaks between 200 kHz and 230 kHz and between 250 kHz and 280 kHz. However, during gear operation, the defect-free and defective conditions showed dominance in the range of between 100 kHz and 150 kHz, see Figure 34. This meant that the frequency content measured was not a direct consequence of the detection system.

[4] This test involves breaking a pencil lead at several positions of the test rig in order to determine the optimum sensor location based on minimum signal attenuation.

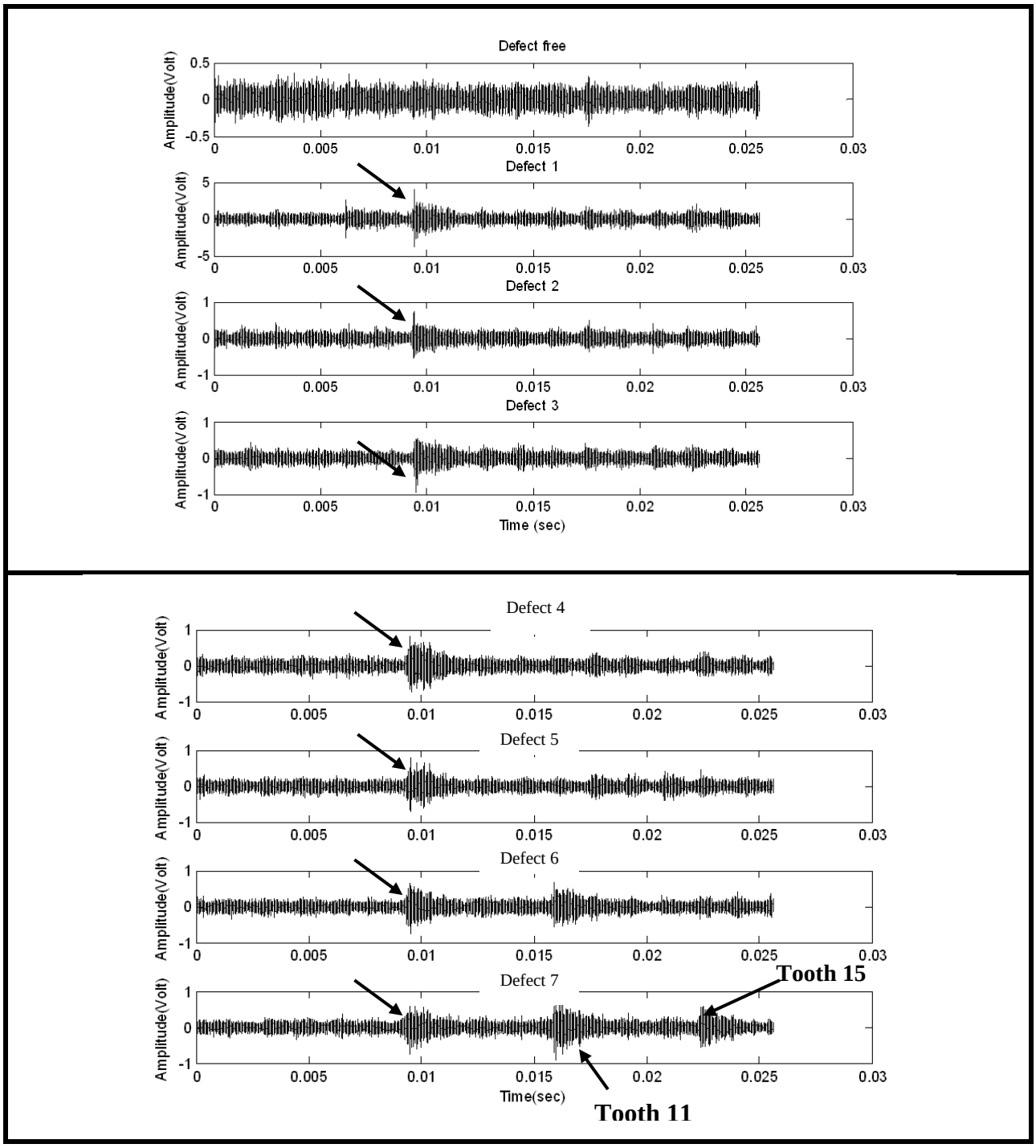

Figure 33 Waveforms associated with each defect for 'A' condition

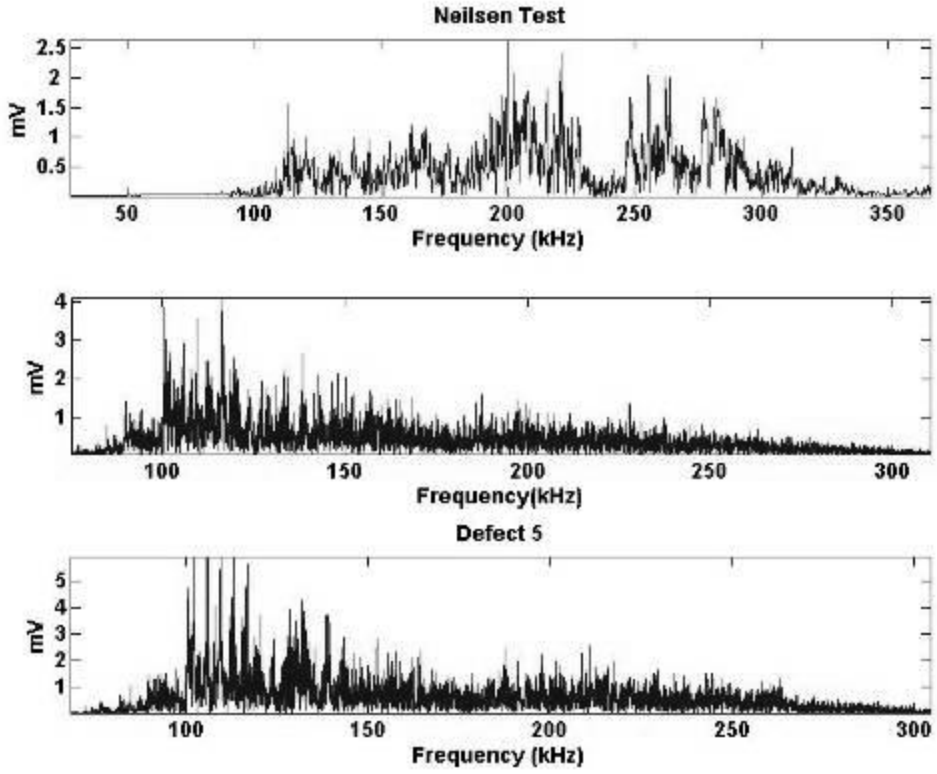

Figure 34 Frequency spectrum associated with Hsu-Neilsen source, defect-free and defect-5 conditions

Discrete wavelet analysis was undertaken to ascertain if the AE associated with the defect condition contained a unique frequency content as a function of time not evident on the defect-free AE data. The AE signatures were decomposed to eight levels using a 5^{th} order Daubechies wavelet. Table 7 shows the decomposition level and associated frequency range. Signatures associated with three defect conditions (defect-free, defect-5, defect-7) are presented in Figure 35, Figure 36 and Figure 37. These figures suggest that the frequency content does not change as a function of time, irrespective of the presence of defective teeth. This conclusion is reached because the transient AE bursts associated with the defect were evident at every frequency band. This finding was not surprising as the source of AE has been shown to include asperity contact [101] and also, as the meshing of the defective tooth involves the interaction between the geometric discontinuities of the defective tooth with another tooth, asperity interactions will be

involved which will generate a broadband frequency source. A CWT, using a Morlet wavelet[5], of defect-5 is presented in Figure 38; this served to reaffirm the view held by the author that no distinct frequency was evident as a function of time but rather the frequency content generated from defective meshing gears was broadband.

Table 7 Frequency range associated with each level of decomposition

Decomposition level	Frequency range
1	[2.5MHz-5MHz]
2	[1250 kHz-2500 kHz]
3	[625 kHz-1250 kHz]
4	[312 kHz-625 kHz]
5	[156 kHz-312 kHz]
6	[78 kHz-156 kHz]
7	[39 kHz-20 kHz]
8	[10 kHz-20 kHz]

[5] Morlet wavelet was chosen since its shape is very close to the mechanical impulse [161].

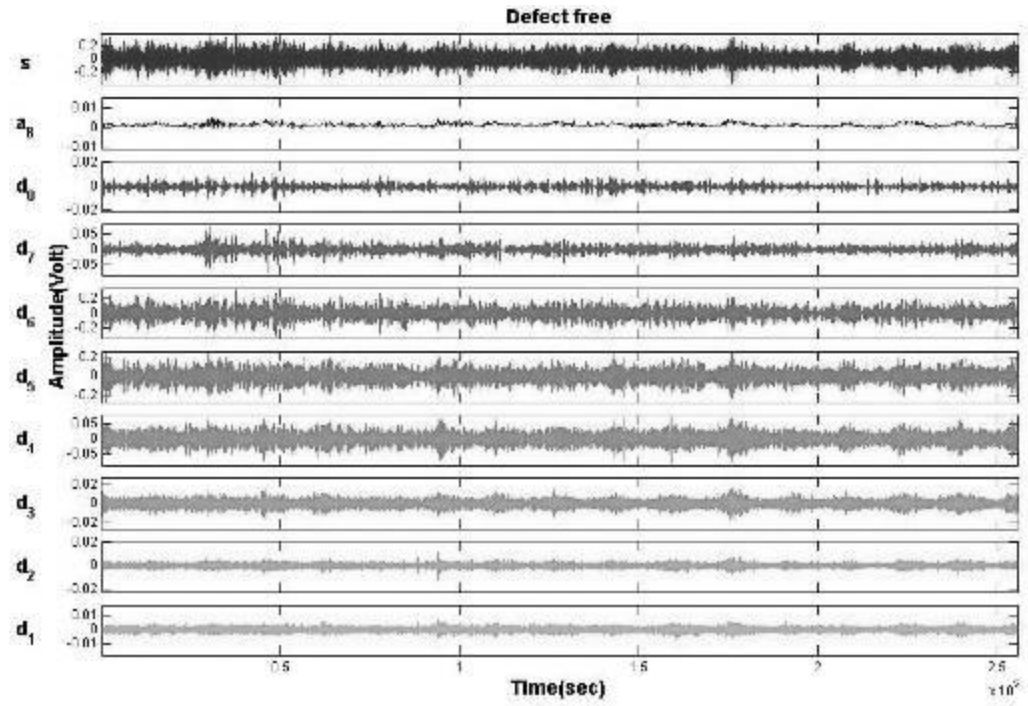

Figure 35 Decomposition of the AE signal for defect-free condition

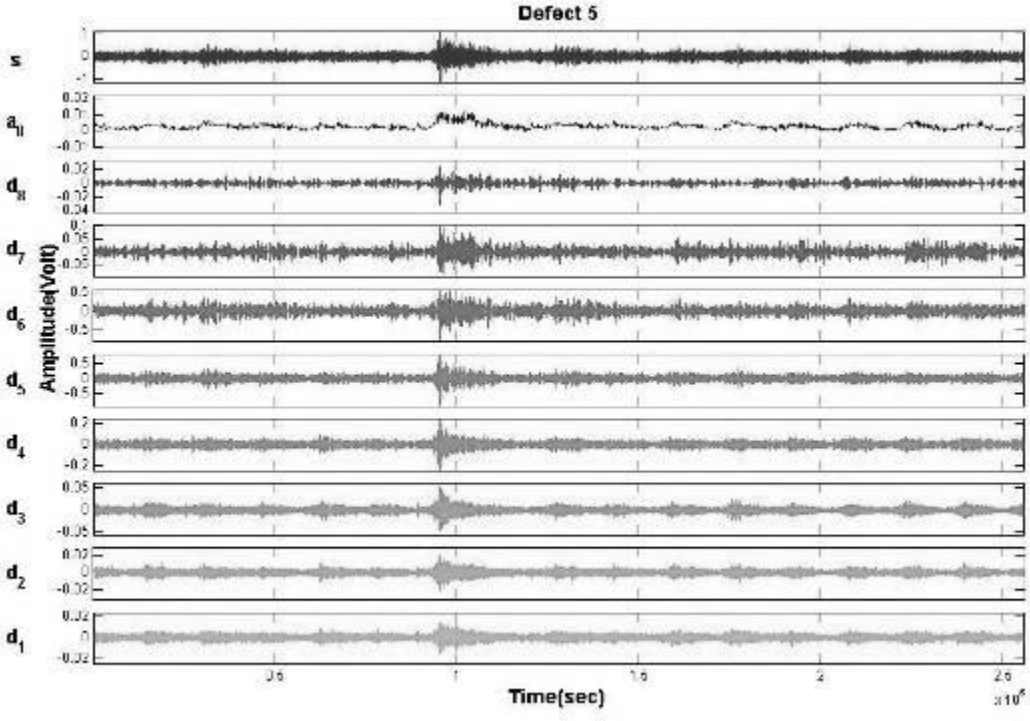

Figure 36 Decomposition of the AE signal for defect-5 condition

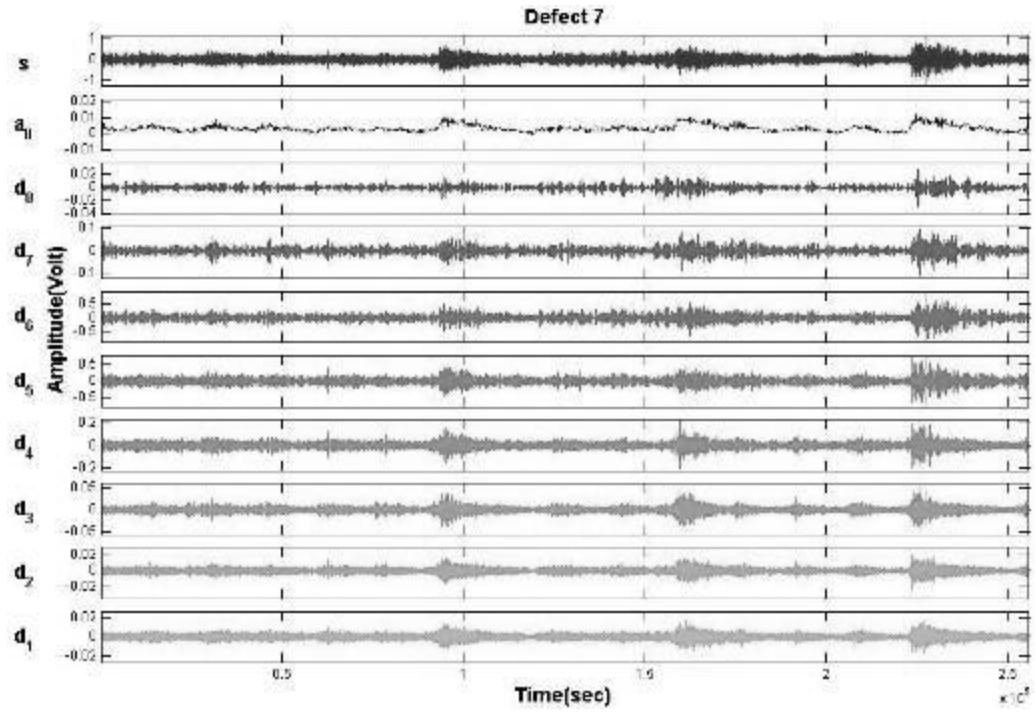

Figure 37 Decomposition of the AE signal for defect-9 condition

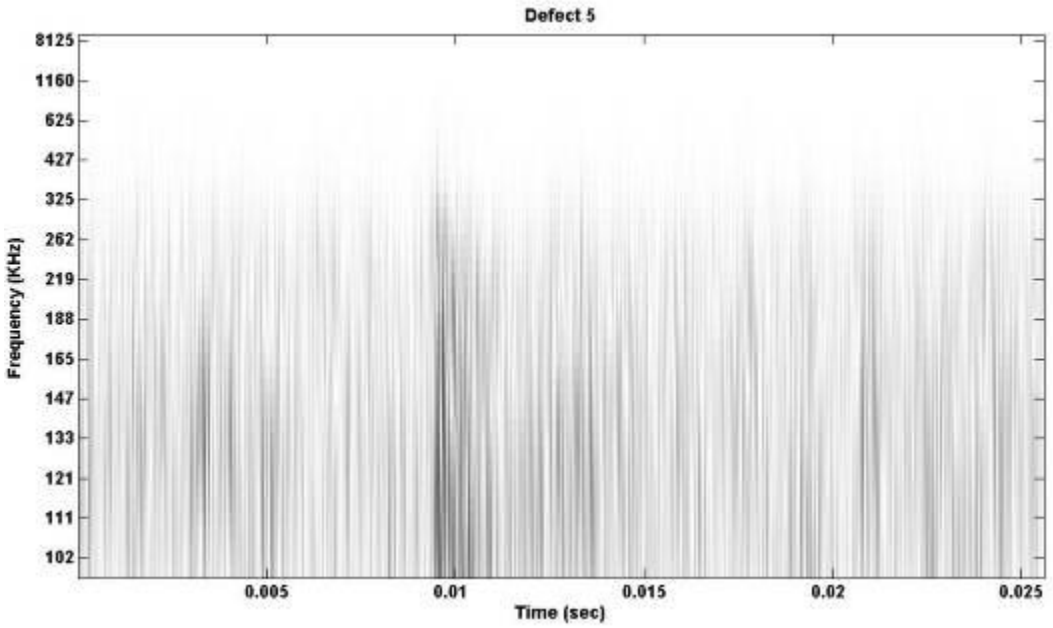

Figure 38 Scalogram plot of continuous wavelet coefficients associated with defect-5

5.1.1.2 Correlation between AE and damage area

AE r.m.s. values for all test conditions for every fault and load condition are shown in Figure 39, and figure A1 and table A1 in Appendix B. In general an increase in AE r.m.s. levels for increasing defect size for all test load conditions was noted, see Figure 39. For load conditions B (250 Nm) and C (180 Nm) an increase in AE r.m.s. levels with increasing defect width and number of defective teeth was evident, though for test conditions A (380 Nm) and D (380 Nm) a similar trend was observed between 'defect free' and defect-3 conditions after which r.m.s. values decreased slightly from defect-3 to defect-5; AE r.m.s. levels increased again from defect-5 to defect-7. The exact reason for this observation is addressed in 5.1.1.3. It was noted that the increased load condition did not necessarily always imply increased AE levels. This was noted for load condition 'A' (380 Nm) after defect-4. The exact reason for this decrease is still unclear. Of interest is that the AE r.m.s. levels of the initial defect condition (D) were relatively higher than all other test conditions but for one test condition (Defect-6, 250 Nm). This was not surprising, given that asperity contact has been shown to be a major source of AE generation during gear mesh [101-103]. Also, as noted by others [14, 94, 119] the influence of material protrusions around the edge of a seeded defect cavity which are relatively higher than the rest of the gear surface roughness, and caused as a direct result of generating seeded faults, will generate AE activity. Given that after several thousand revolutions (1,300,000) the protrusions will be progressively flattened, resulting in a relative reduction in AE levels as noted in Figure 39, this confirms the postulations of Tan et al.[14] and Al-Dossary et al. [119]. Figure 40 schematically presents the process of AE generation due to the presence of protrusions.

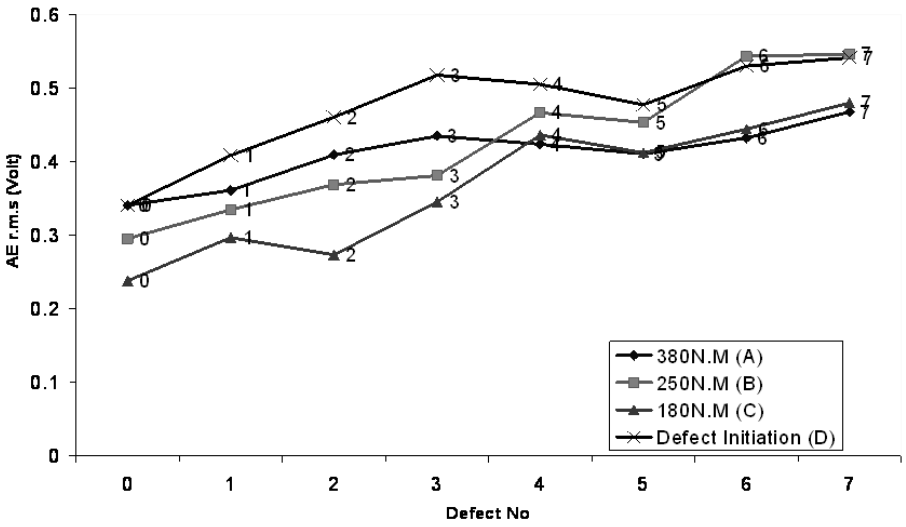

Figure 39 AE r.m.s. values for each defect condition

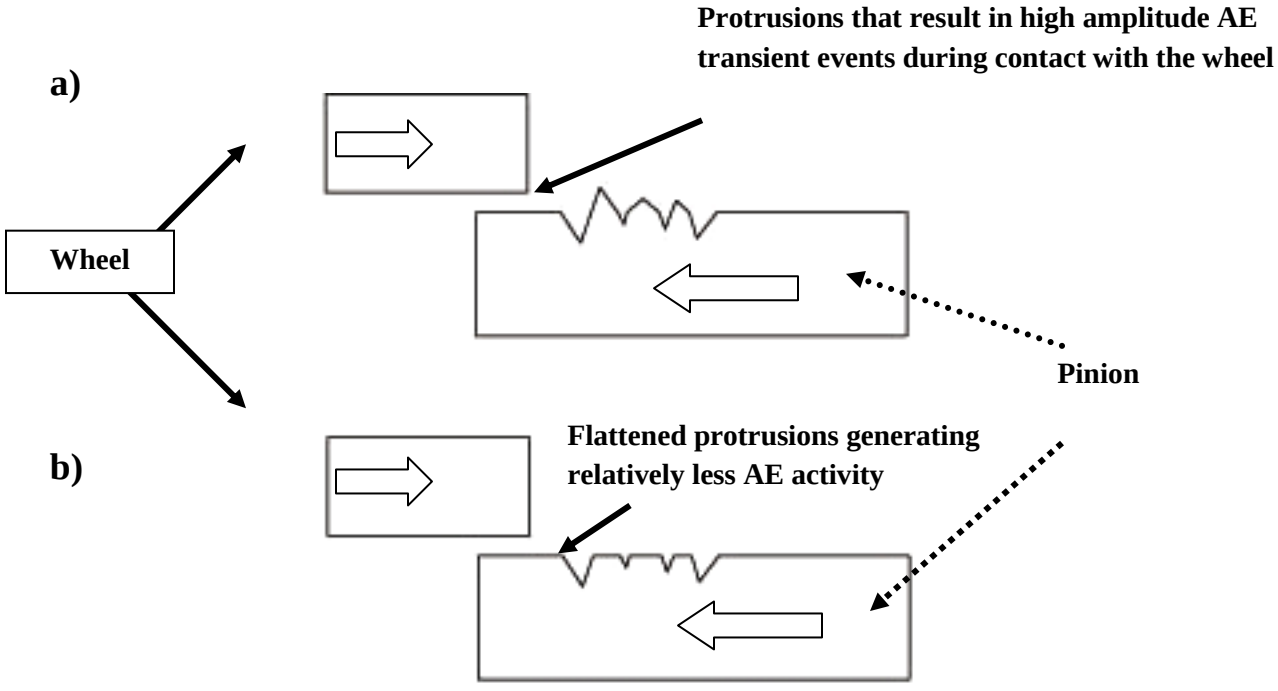

Figure 40 Schematic of the effect of protrusions on AE activity

5.1.1.3 Correlation between AE and defect volume

To address the reason for the decrease in AE levels with increasing defect size, as noted for test conditions A and D (defect-3 and defect-5), the approximate volume of each defect was calculated following casting of the defect onto 'plaster' so as to obtain a three-dimensional profile. The plaster was made of Calcium Alginate used in dental applications, see Figure 41. Plotting the volume removed against AE r.m.s. yielded an interesting observation, see Figure 42. A direct relationship between the defect volume and AE was noted for test conditions 'A' and 'D'; in some cases, where the defect width was relatively wide but the volume removed relatively less (e.g., defect-5 was wider than defect-3 but the volume removed in defect-3 was more than defect-5), the AE r.m.s. levels were higher for the case of the larger volume removed. For cases B and C, the observation was not similar, particularly at defect-3. This has some implications, particularly in understanding other influencing sources of AE during meshing. This suggested the influence of the mechanism of interaction of the fluid within the defect cavity would appear to offer a source of AE activity. This particular observation was investigated further. To this end further tests were undertaken. A gear tooth was selected and holes of varying depth (volume) and a fixed diameter (2.5 mm) were drilled into the tooth, see Table 8 and Figure 42. After each depth was seeded, the rig was operated for 45 min (3,000,000 revolutions) before any AE data was recorded. This was to ensure the temperature remained constant throughout the tests. Results, presented in Figure 45, showed that an increase in AE r.m.s. was a direct consequence of increased cavity volume, strongly supporting the notion that the entrapped lubricant within a cavity (pit, spall, etc.) will also contribute to the level of AE measured. The sampling rate applied for these particular tests was 4 MHz and a total of 65,536 data points were recorded per file, of which over 25-data files were acquired for each volume condition. This is the first known attempt at investigating this phenomenon and will, in the fullness of time, lead to future investigations. A typical waveform associated with these volumetric tests is presented in Figure 45 which shows that the holes did not cause any material protrusions nor did they result in the generation of an AE waveform typical of the presence of a defect, as shown in Figure 33.

Figure 41 Surface replica from gear tooth

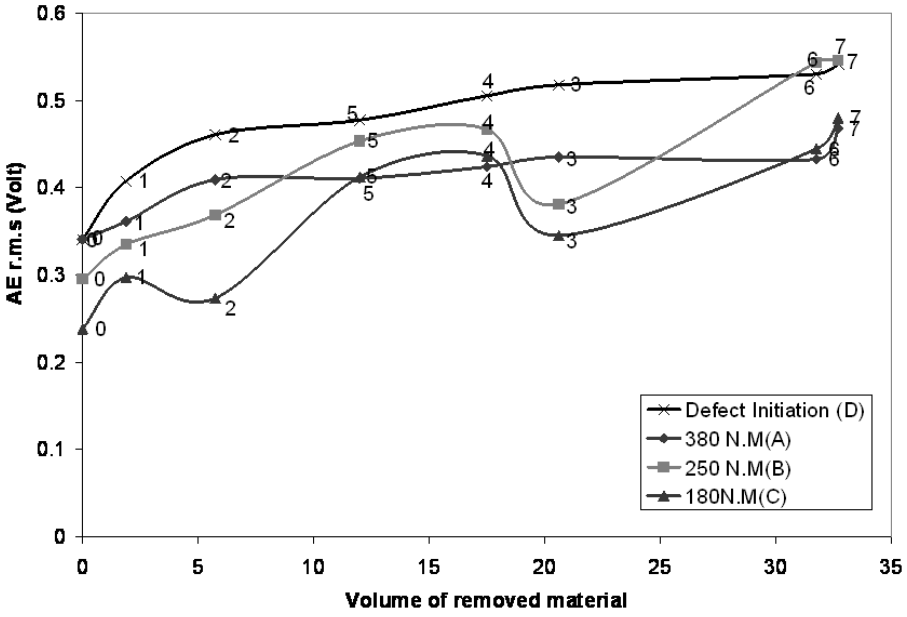

Figure 42 AE r.m.s. against volume of removed material for all conditions

Table 8 Specification of increasing defects volume on a fixed tooth at 380Nm

Defect No	Depth
0	Defect free
1	1mm
2	3mm
3	5mm
4	7mm
5 (Second hole)	7mm
6 (Third hole)	7mm

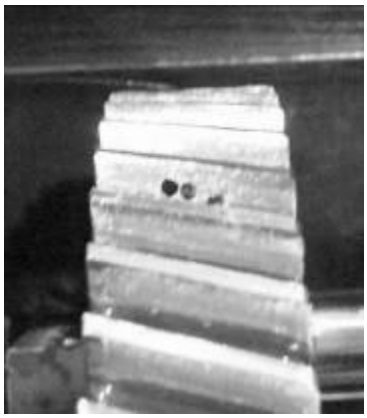

Figure 43 Holes drilled on the tooth surface

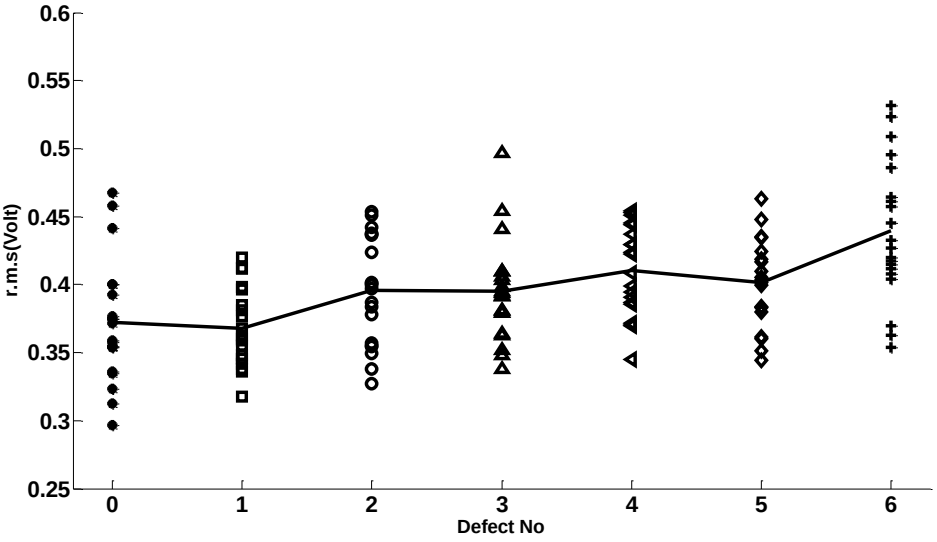

Figure 44 AE r.m.s. level against depth of the drilled hole

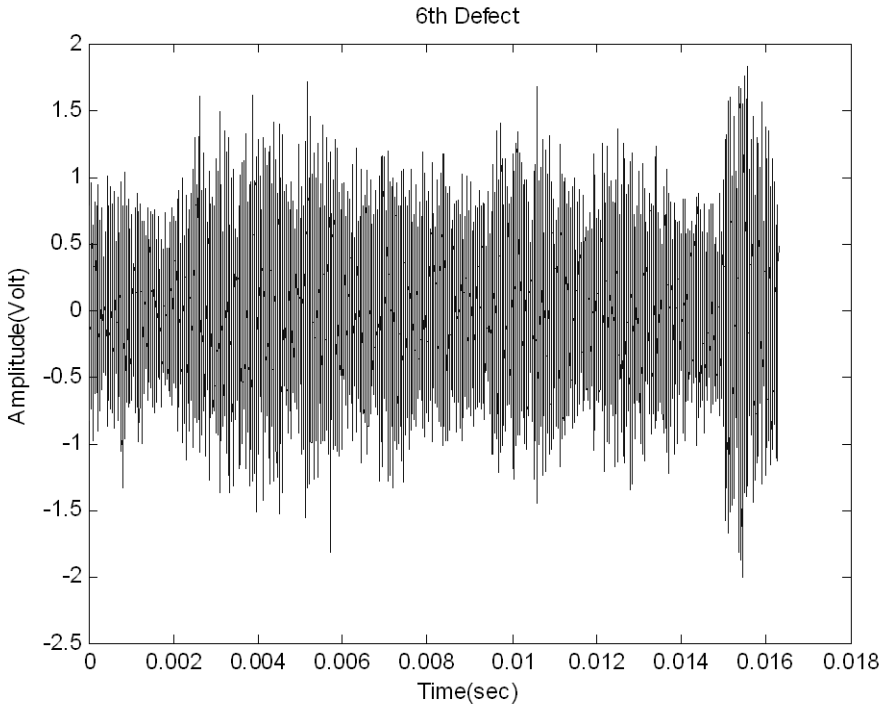

Figure 45 Typical waveform for volumetric defect

5.1.2 Vibration monitoring of seeded defects

Twenty sets of data for each defect at different conditions based on a 10 KHz sampling rate were captured and synchronously averaged. Each data set acquired was associated with a time window encompassing 16 teeth. Vibration r.m.s. values for each test condition are illustrated in Figure 46. The vibration r.m.s. level at D-condition was relatively higher than for all other conditions for the reasons discussed earlier. In addition, the plastic deformation of protrusions around the defect will lead to alteration in stiffness and consequently growth in vibration [10]. In comparison to AE r.m.s. levels, the vibration r.m.s. levels remained relatively constant, irrespective of defect condition, though it should be noted that the AE and vibration were not at identical positions. Figure 47 illustrates the vibration energy values for each defect condition calculated by integrating the frequency spectrum of the signal condition over the frequency range, encompassing meshing frequency and its side bands and the harmonics of the side bands (350 to 850 Hz). It was noted that as the defect extended along the face width, an increase in energy value was noted at 'D' and 'A' conditions but vibration energy levels remained constant at test conditions 'B' and 'C'. Furthermore, it was also noticed that as the torque level reduced, energy value associated with each defect decreased.

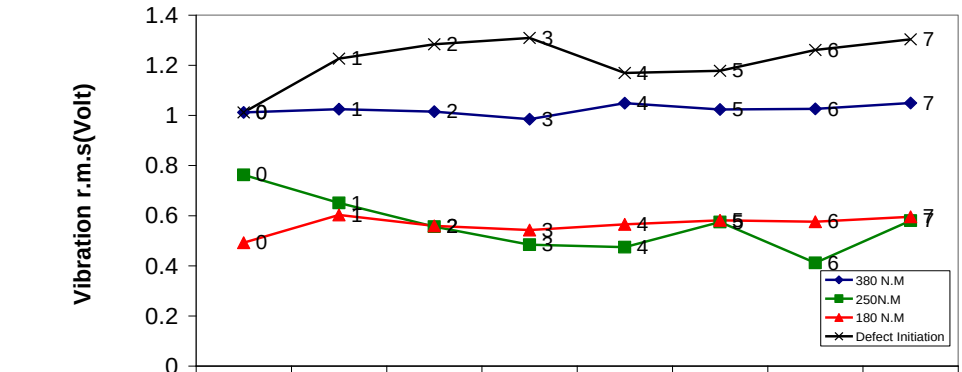

	0	1	2	3	4	5	6	7
380 N.M	1.0118	1.0249	1.0147	0.9848	1.049	1.0234	1.0263	1.0496
250N.M	0.7629	0.651	0.5561	0.4839	0.4743	0.5747	0.4115	0.5798
180 N.M	0.4923	0.6027	0.5593	0.5428	0.565	0.5815	0.5758	0.5954
Defect Initiation	1.0118	1.2265	1.2839	1.3087	1.1691	1.1779	1.2608	1.3036

Defect No

Figure 46 Vibration RMS level for each defect at different loading conditions

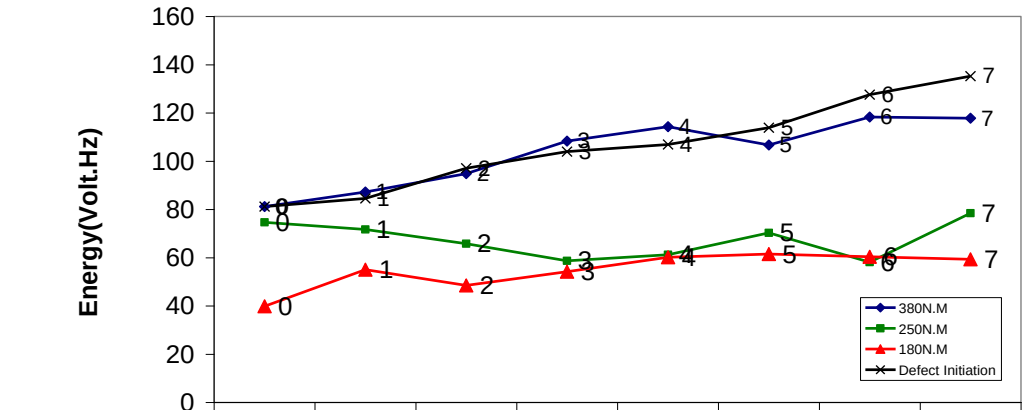

	0	1	2	3	4	5	6	7
380N.M	81.2055	87.2107	94.8485	108.363	114.296	106.722	118.3	117.843
250N.M	74.6677	71.6865	65.8258	58.7336	61.2024	70.277	58.139	78.4266
180N.M	39.8246	55.0714	48.478	54.1707	60.2082	61.5084	60.4043	59.3424
Defect Initiation	81.2055	84.5838	97.0683	103.948	106.892	113.859	127.575	135.222

Defect No

Figure 47 Energy values for sidebands around gear meshing frequency

5.2 Monitoring natural pitting progress

5.2.1 General observation

The overall trends of AE and vibration levels are presented in Figure 48. During the first test, the vibration r.m.s. levels increased for approximately 41-hrs after which they continued to increase at a lesser rate of 0.0007 $V_{r.m.s}$/*hrs*. The AE levels from the slip ring increased at a constant rate of 0.003 $V_{r.m.s}$/*hrs*. For the second test, the AE increased at a slower rate of 0.001 $V_{r.m.s}$/*hrs* for 134 hrs, as compared to Test-1, and remained almost constant for the rest of the test. On the other hand, vibration levels continually decreased with time. It was this unusual observation that resulted in the author increasing the load on the gears at 345 hrs and 460 hrs into the operation; however, this made no difference to the overall vibration and AE levels. This unusual variation in behaviour of vibration and AE with increasing pitted areas offers a good opportunity to investigate different signal processing techniques in order to improve the sensitivity of these measuring technologies. The exact reason why vibration and AE levels reduced and remained

unchanged with increasing pitted areas is unclear. The author can only attribute this to variations in assembly of the test gears; however, it highlights the vulnerability of these measurement technologies to the prevailing dynamic characteristics of the machine under investigation. The source of AE in gears is friction at the mating faces. The presence of pits on the contacting surfaces will result in an increase in surface roughness and consequently the level of friction at the mating surfaces. An increase in fiction can be directory correlated with an increase in AE levels. Furthermore, the accumulation of pits on the teeth surfaces will alter the gear mesh stiffness which will result in an increase in vibration levels.

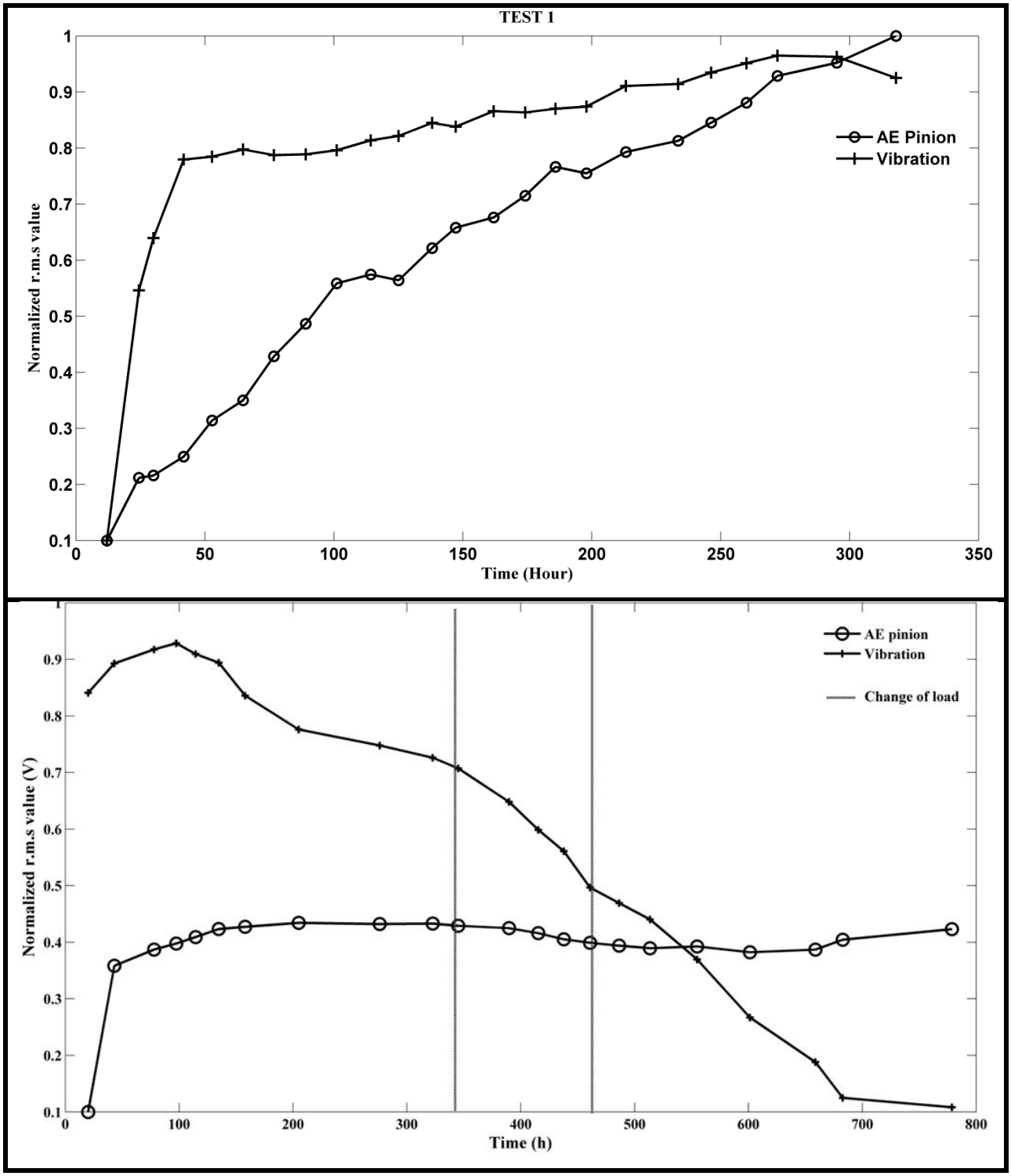

Figure 48 Observation of AE and Vibration levels for Tests 1 and 2

5.2.2 AE monitoring

Figure 49 highlights acquired AE waveforms at different time intervals from both tests. From the waveforms, it was observed that AE bursts, superimposed onto continuous AE type waveforms, were noted from the sensor response in Test-2. In contrast, the AE associated with test-1 were continuous in nature, see Figure 49.

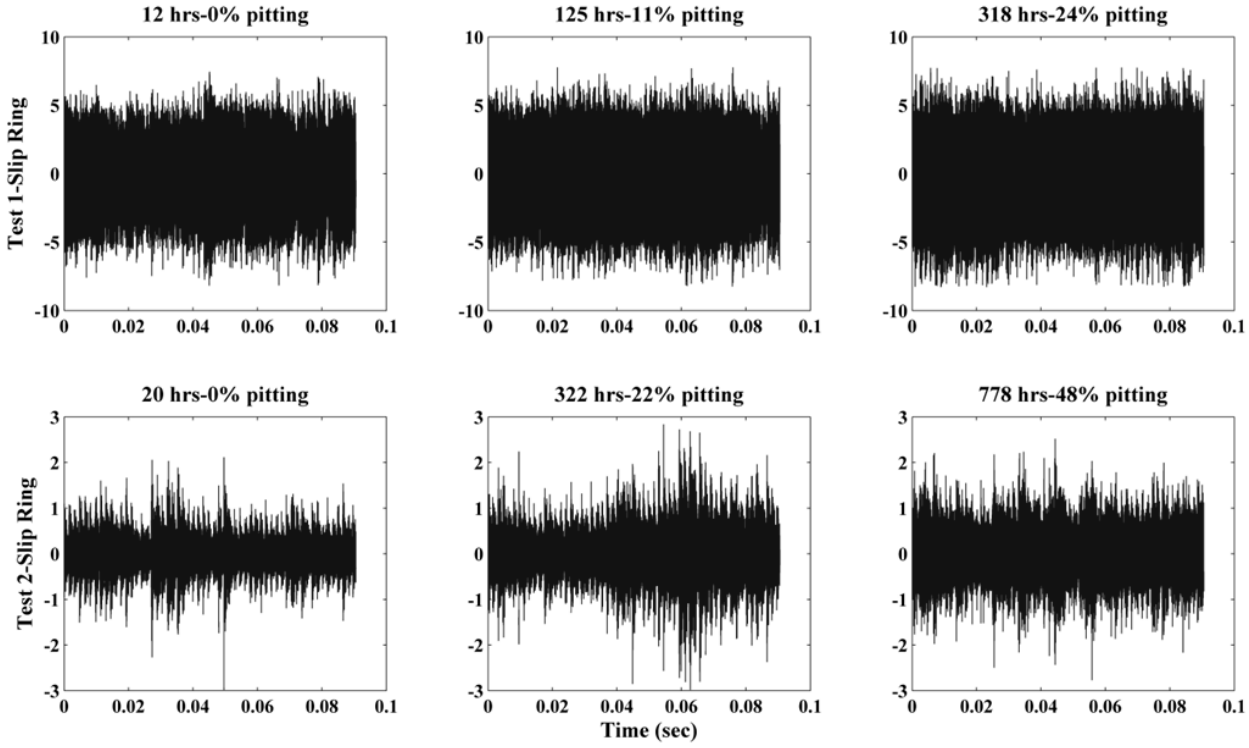

Figure 49 The AE waveforms taken at different intervals

A frequency spectrum of a typical AE signal acquired is presented in Figure 50, which highlights strong energy content between 100 kHz to 300 kHz. As the frequency spectrum offered no diagnostic information, the author decomposed the AE responses using Daubechies wavelet of order 8 (db8), see Table 7. The r.m.s. levels of AE waveforms decomposed between 500 kHz and 1000 kHz (D1) was re-plotted, Figure 51, as a function of time, and in this instance it was noted that AE levels for Test-2 increased with time and % pitted area in complete contradiction to the broadband r.m.s. levels noted in Figure 48. This would imply that the AE response to pitting was more sensitive at the frequency range between 500 kHz and 1MHz as other

decomposed levels did not show an increasing AE level with increased pitting, see Figure 51, but rather mirrored the broadband trend. The envelope spectrum of the first level of decomposition (D1), together with the envelope spectrum of the original AE signals prior to decomposition, are presented in Figure 52. The gear mesh frequency (GMF) and its harmonics are clearly evident across the envelope spectrum. The observation confirms that the decomposed AE signatures contain the meshing features at such high frequencies (500-1000 kHz).

Table 9 Decomposed levels the associated frequency range

Decomposition Level	Frequency Range (kHz)
1	[500-1000]
2	[250-500]
3	[125-250]
4	[62-125]
5	[31-62]
6	[15-31]
7	[7-15]
8	[3-7]
9	[1.5-3]

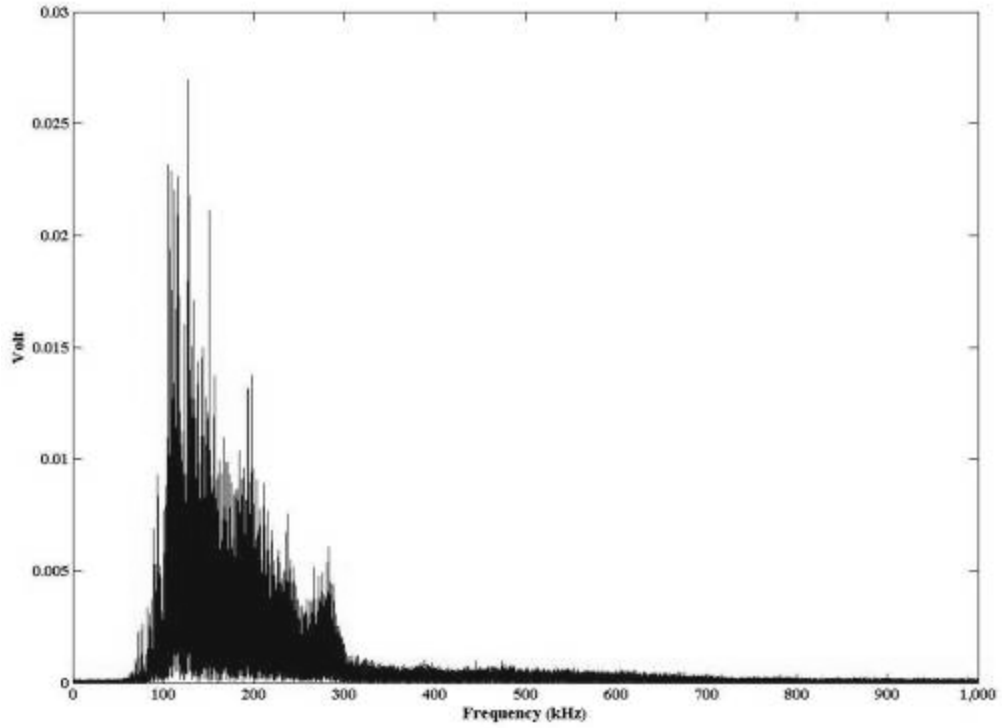

Figure 50 The frequency spectrum of a AE signal from TEST-2 showing concentration of energy between 100 and 300kHz

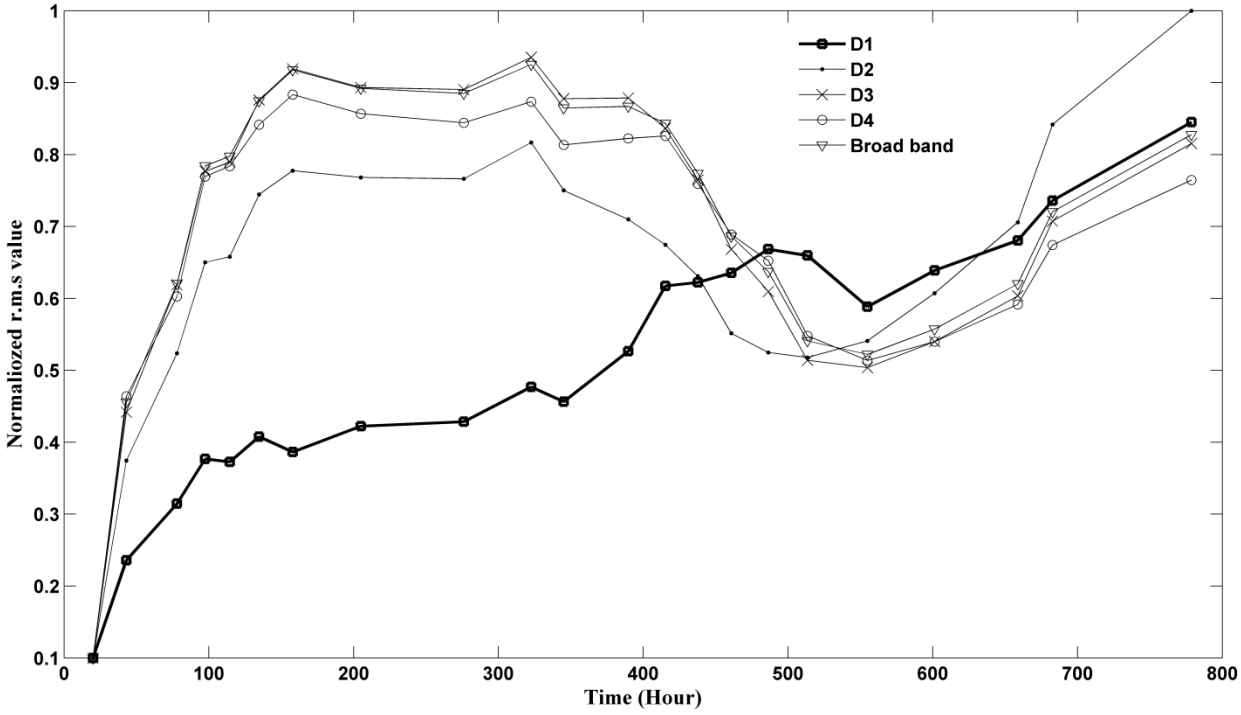

Figure 51 Figure 7 A.E levels for test-2 (broadband and decomposed levels)

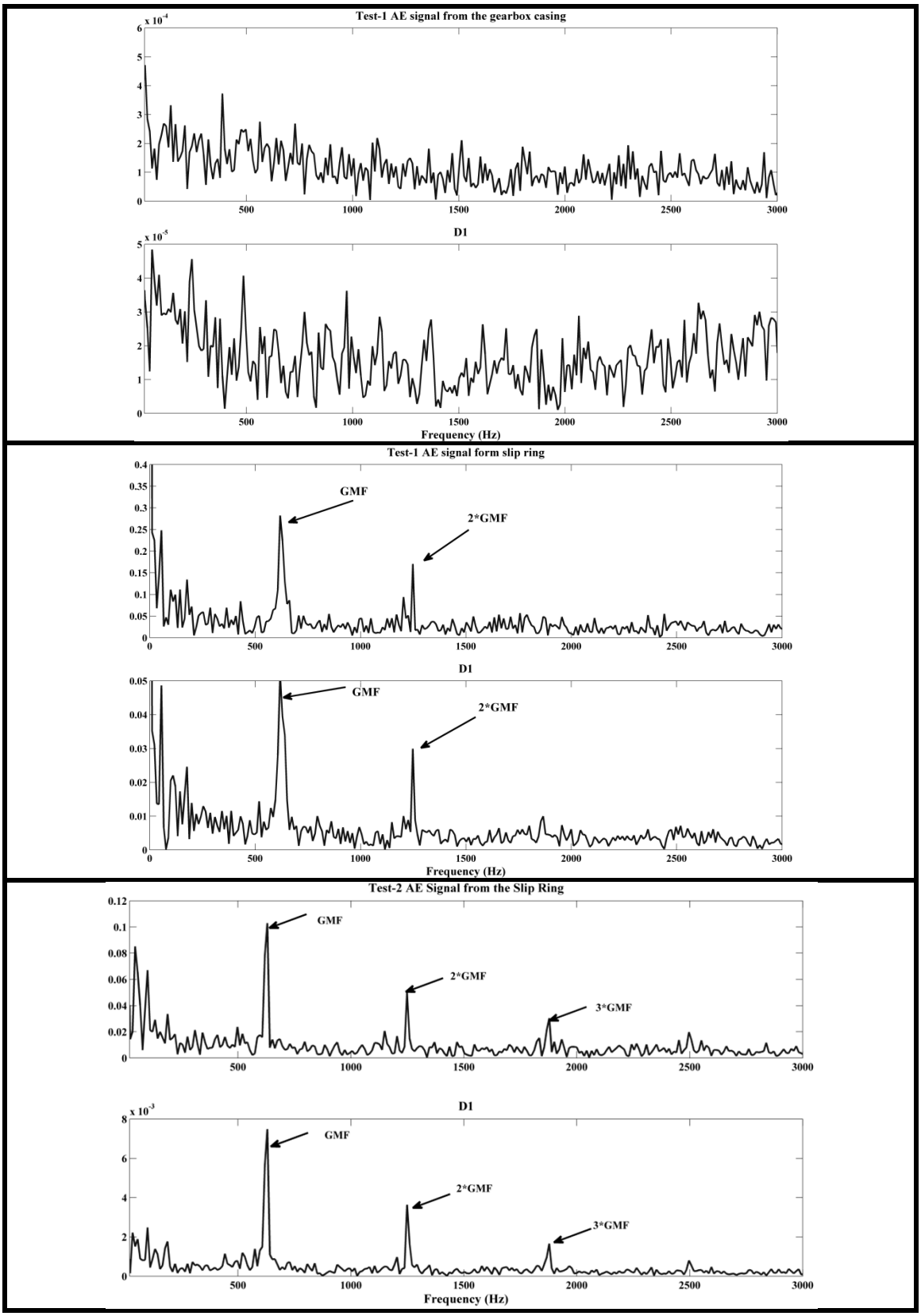

Figure 52 The envelope spectrum of the original and decomposed signal (D1) for the AE measurement from the pinion gear.

The author explored the suitability of spectral kurtosis for providing additional capability. Spectral kurtosis (SK) is a great measure of spikiness of data over different frequency bands. It was applied to AE signatures associated with both tests. From Figure 53, it can be seen that no distinct difference on the SK spectrum was evident, suggesting that for all AE signatures measured from the start to the end of both tests, the SK value did not show any peculiarities. The relative stability in the values of SK over the test duration is related to the mechanism of AE generation in gearboxes. The source of AE activity from meshing gears is asperity contact and, given the increase in pitted area, the changes of the asperities across the gear face will continually evolve and the corresponding AE generated will be somewhat continuous in nature and the generation of AE transient events, associated with asperity interactions, will be closely spaced. As such it was not expected that the spectral kurtosis would show or highlight any specific frequency sensitive to transient events under the conditions as experienced in these tests.

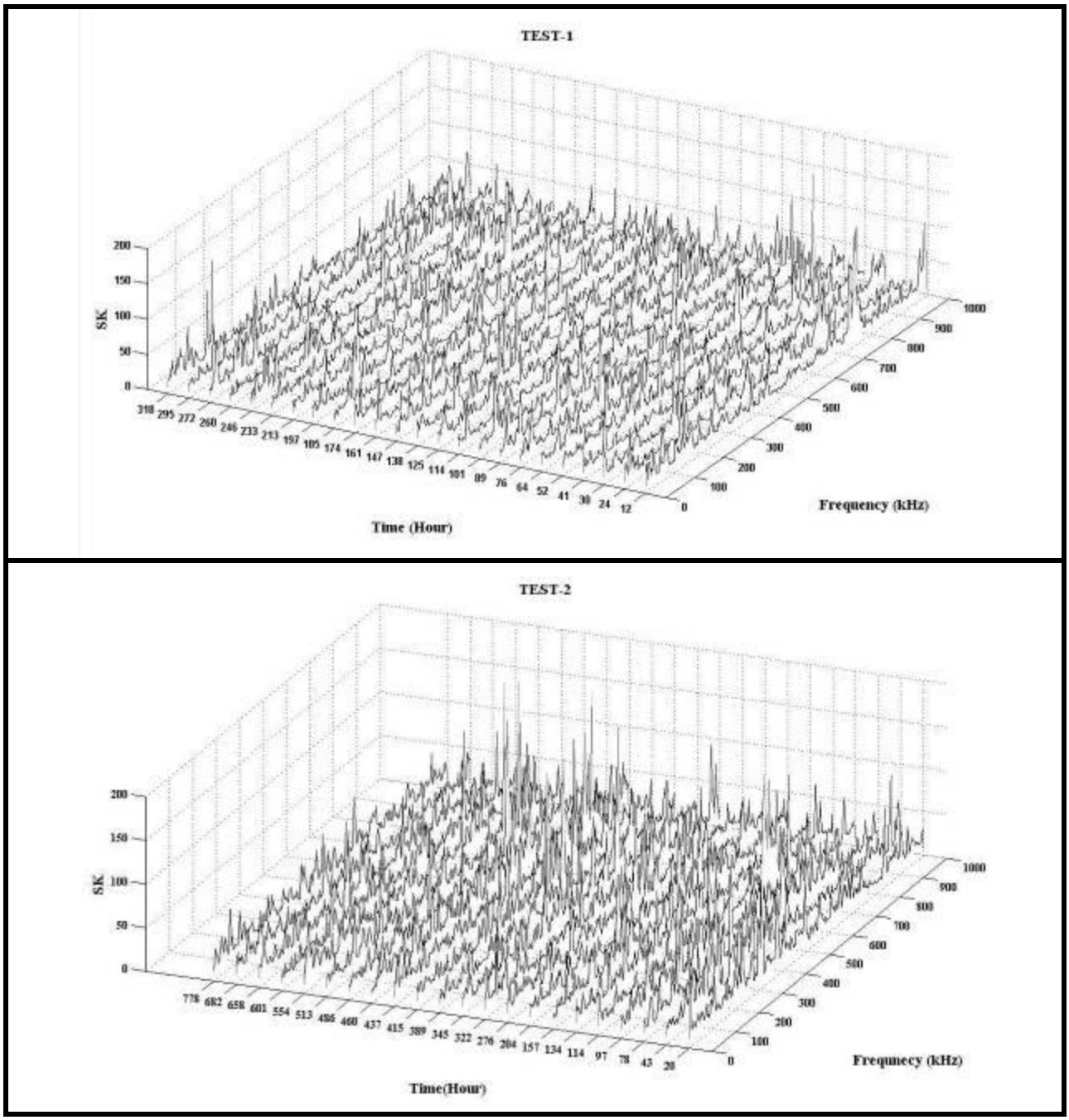

Figure 53 Spectral Kurtosis measurements of the AE signals at different inspection intervals

5.2.3 Vibration diagnostic of natural pitting

For the first test, the vibration r.m.s. steadily increased over the test duration, showing an adequate sensitivity to pitting progression, whilst for the second test, the trend of vibration continually decreased in duration, even though the surface pitted area increased. The frequency spectra of the vibration signals at defined time intervals are detailed in Table 10 and Figure 54. The gear mesh frequency and its harmonics were evident throughout the test. The observation of the frequency spectrum for the second test confirmed that, despite the gradual reduction in the vibration r.m.s. value, gear mesh frequency and its harmonics were also evident.

Table 10 Defined time intervals

	Test 1 (Hours)	**Test 2** (Hours)
A	12	20
B	64	134
C	125	276
D	213	486
E	260	601
F	318	778

Again, a wavelet analysis (db wavelet), was undertaken on the vibration data. The signals were decomposed into nine levels, see Table 7. The vibration r.m.s. values for five decomposed levels (D1 to D5) were calculated and plotted in Figure 55. From the first test, the highest rate of increase (0.0008 $\boldsymbol{V_{r.m.s}/hrs}$) was associated with the first level of decomposition (D1) showing that this level was more sensitive to the development of surface pitting in comparison to other levels. Whilst for the second test, the vibration r.m.s. values for all decomposed levels did not show an increasing trend with increased pitted area.

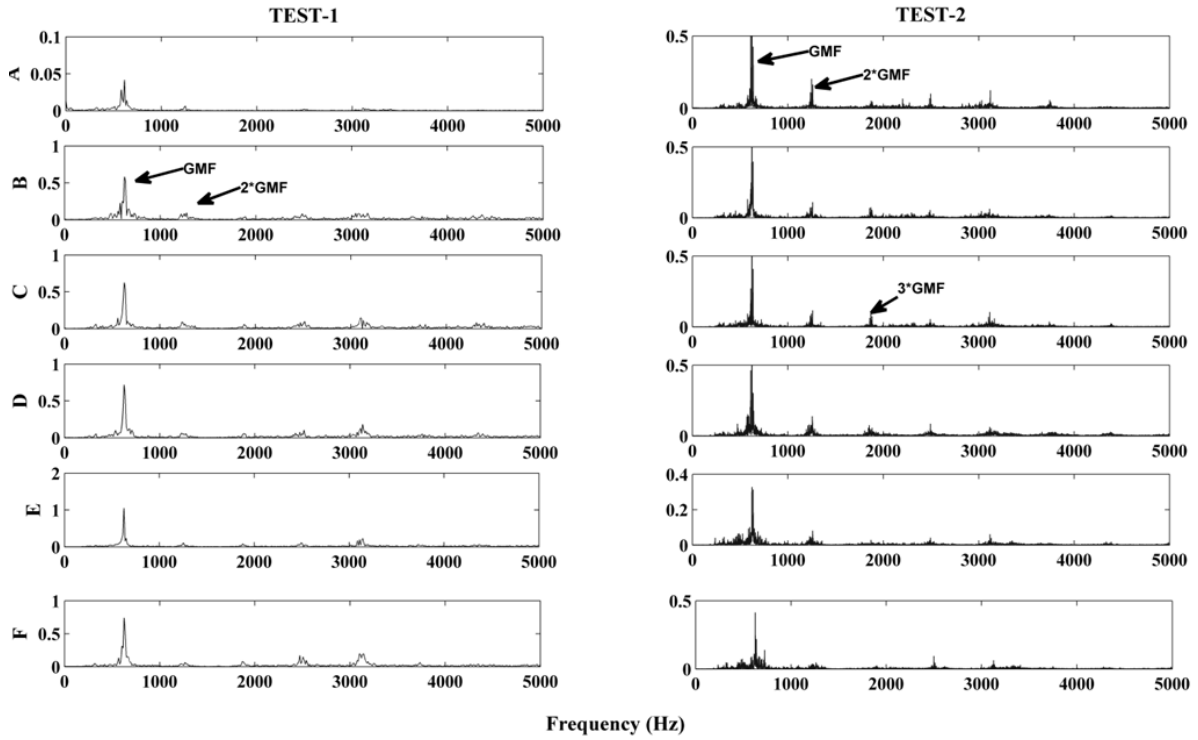

Figure 54 Frequency spectrum of the vibration signals at different intervals

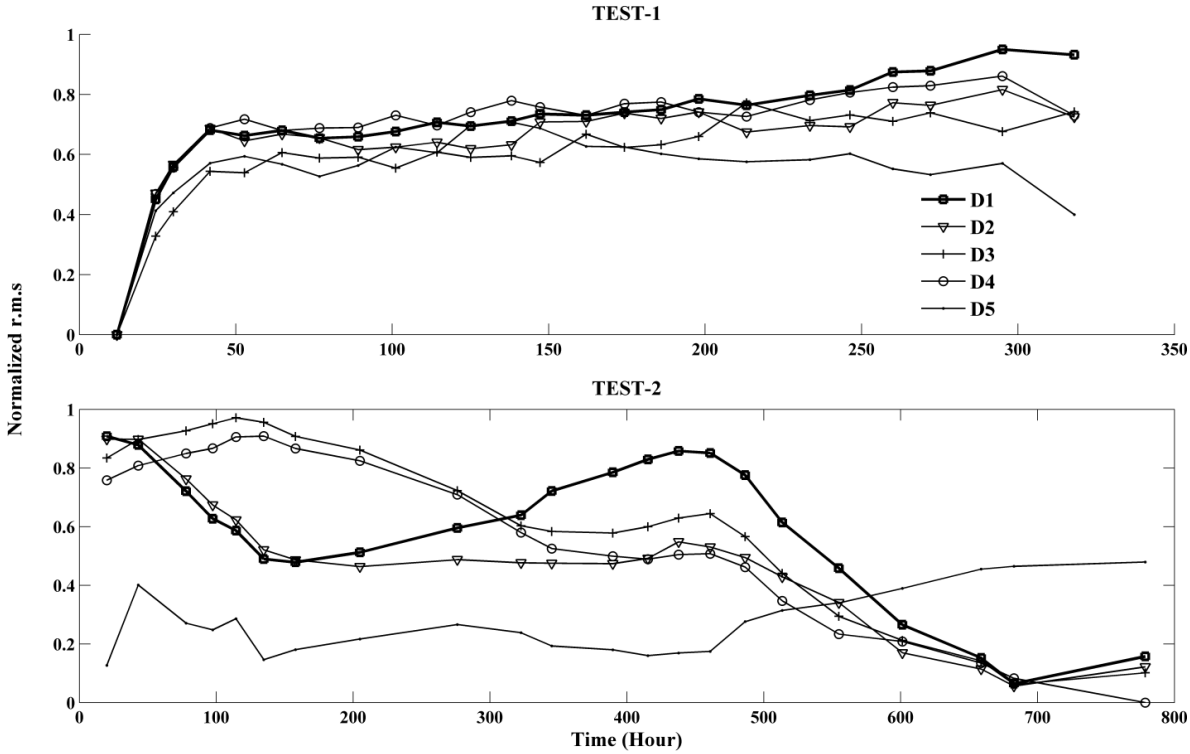

Figure 55 The r.m.s. values for decomposed levels D1-5

The spectral kurtosis analysis was applied to the vibration signatures and the results are presented in Figure 56. Results of the analysis presented quite distinct SK features (see Figure 56). Although the value of SK did not increase upon the termination of the first test, it showed an increased level across all frequencies from 322 hrs of operation for Test-2. This was attributed to the severity of damage upon the termination of the second test (50%) which was much higher than the first test (24%). The increased pitting area will generate higher vibration impulses during gear mesh, hence it was not surprising to see the SK values increase. Such observation was also noted by Antoni [72]. Figure 57 [72] shows the vibration waveform for Test-2. This figure also shows how the vibration waveform evolved from being continuous to spiky at the end of the test. The presence of spikes spaced at the shaft frequency are apparent.

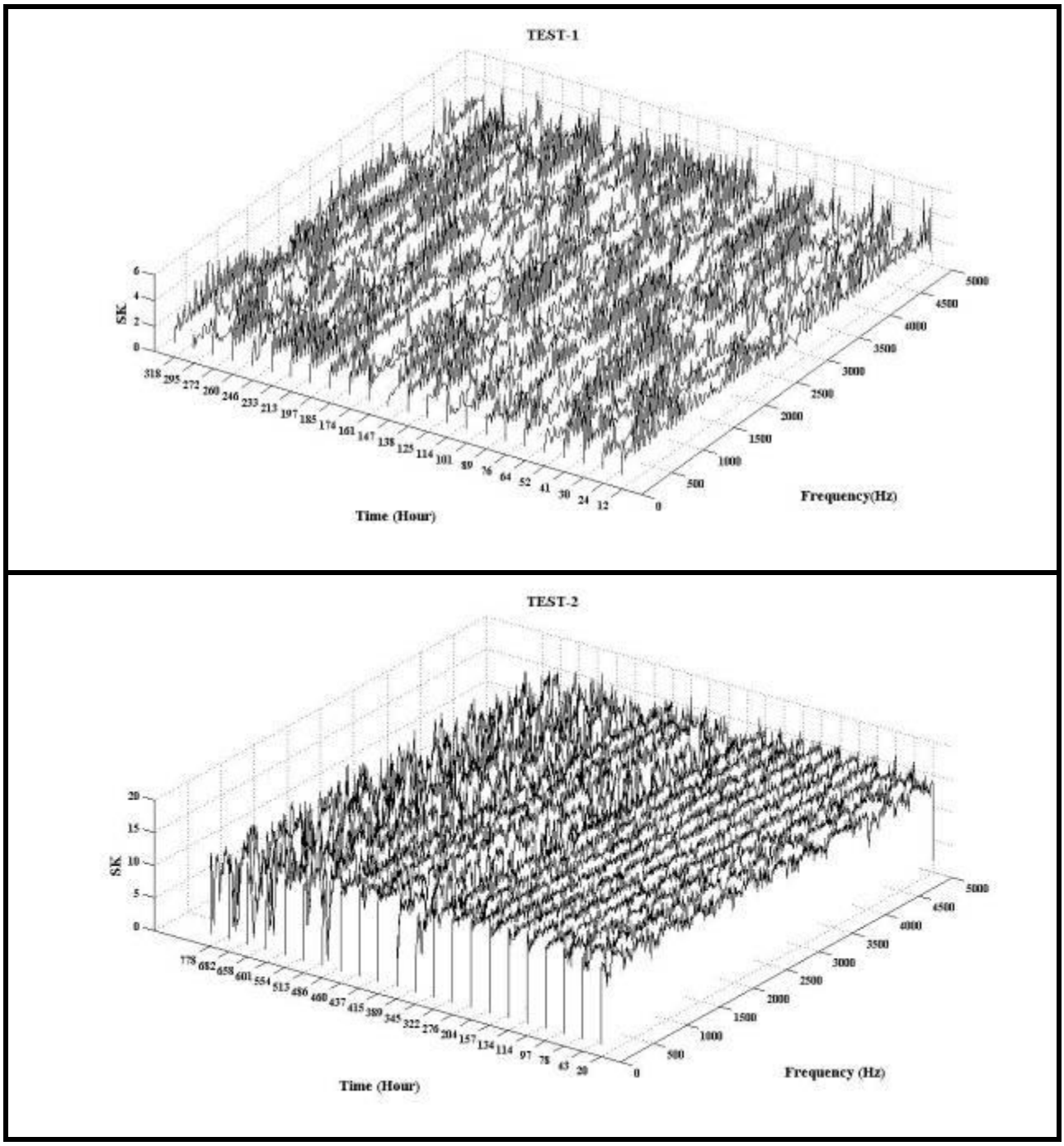

Figure 56 SK measurements of the vibration signals at different inspection intervals

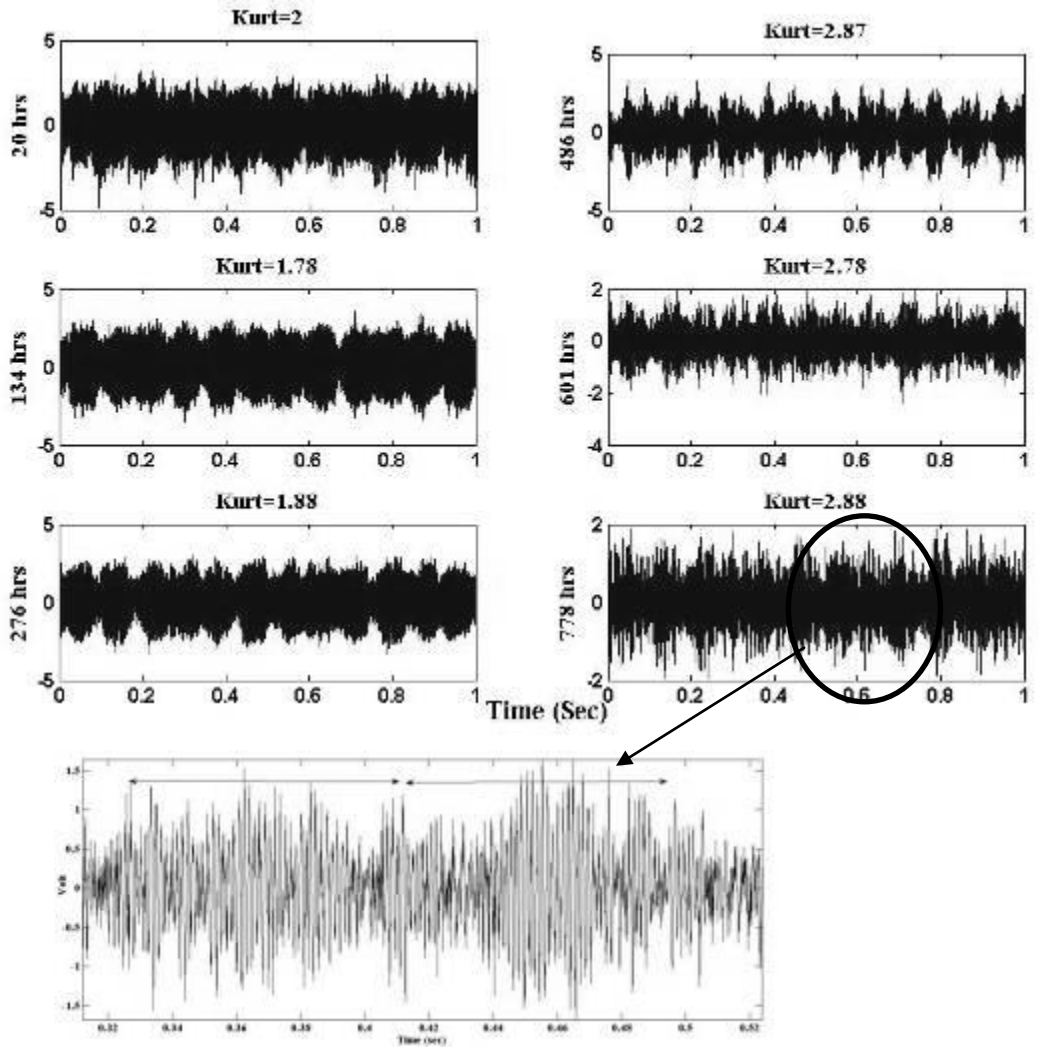

Figure 57 Vibration waveforms for different operational periods (Test-2)

5.3 Conclusions

The author applied AE and vibration technologies to diagnose both the seeded and natural defects on helical gear surfaces. Unlike spur gears, AE exhibited rather different diagnosis behaviour in relation to the helical gears. This was expected due the difference in the meshing mechanism of spur and helical gears. Seeded defects in helical gears are evident in the AE waveform. Such observation was not noted by Toutountzakis et al. [94] using a similar test procedure on spur gears. Furthermore, previous investigation into applying AE to spur gears

showed that overall r.m.s. levels were sufficient for correlating increased natural pitting with AE and vibration [13]; however, the two cases presented in section 5.2 have shown quite conflicting trends for helical gears. In summary the following has been concluded:

- There is a direct relation between volume of removed material and AE r.m.s.; this is the first observation of its kind.
- Measurement of AE r.m.s. levels from the rotating gear have been shown to be more sensitive to identification of seeded defects on helical gears than vibration measurement from the sensor placed on the bearing pedestal. However, the author suggests further experiment of that kind with an AE and vibration sensor both being placed on the bearing pedestal in order to achieve a comprehensive comparison between the vibration and AE methods.
- Condition monitoring of the helical gears may demand the application of the advanced signal processing methods to effectively monitor the natural pitting progress with AE and vibration. It was found that the application of Wavelet analysis significantly improved the diagnostic capability of AE signals under conditions that otherwise would not have offered any diagnostic information. On the other hand, the SK analysis on vibration data was successful in detecting severe pitting; however, it did not offer any diagnostic advantage for the AE measurement on the specific case presented using helical gears.

CHAPTER 6

6 Shaft crack diagnostics

6.1 Observations

Observations of measurements of vibration, AE and motor current recorded over 400 hrs of operation are presented in Figure 60. It should be noted that the test gears suffered from natural pitting wear over the duration of the test, which at termination was approximately 25% pitting across the contact area of the helical test gears, see Figure 58. Increases in vibration (S3) and AE (S1) from 25 hrs of operation to approximately 350 hrs were noted – a direct consequence of the increased pitted area over the test duration, see Figure 59 and Figure 60. At about 345 hrs of operation, a sudden loss in the torque transmitted through the gearbox was noted; this was caused by an unplanned shaft breakage which was not seeded. The shaft fracture was due to a crack which had initially developed in the vicinity of the key way slot in the shaft. Even after breakage, the cracked shaft faces remained in contact because the cracked region of the shaft was within the gear bore region, see Figure 61.

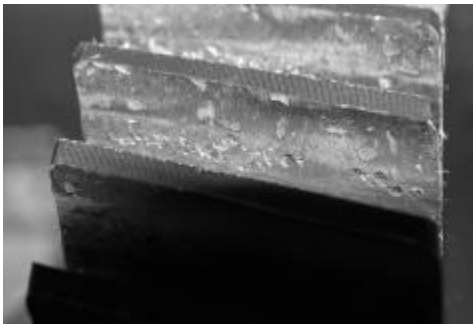

Figure 58 Pitted area at 400 hrs of operation

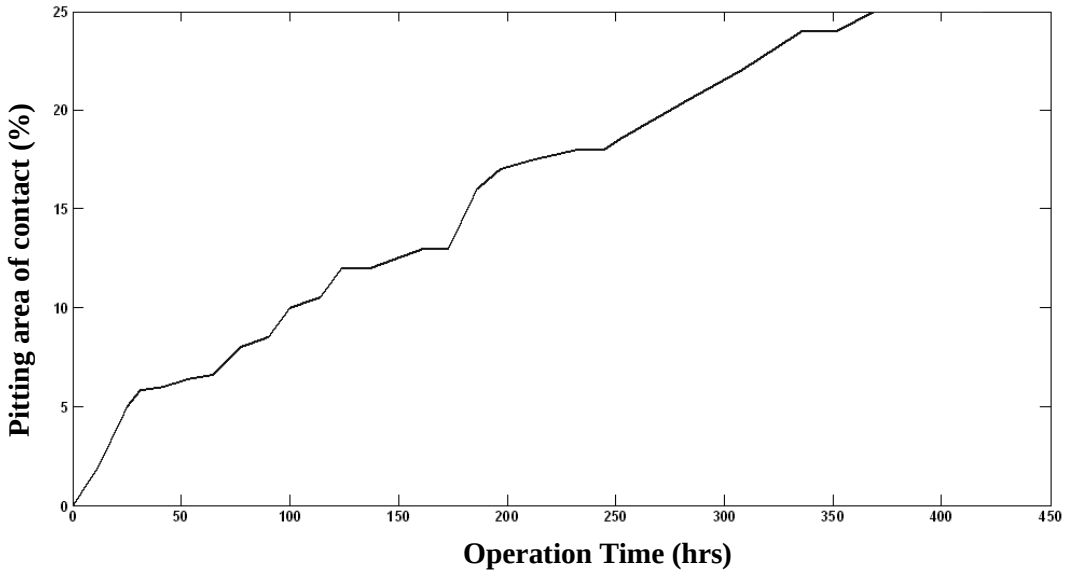

Figure 59 Pitted area progression during testing

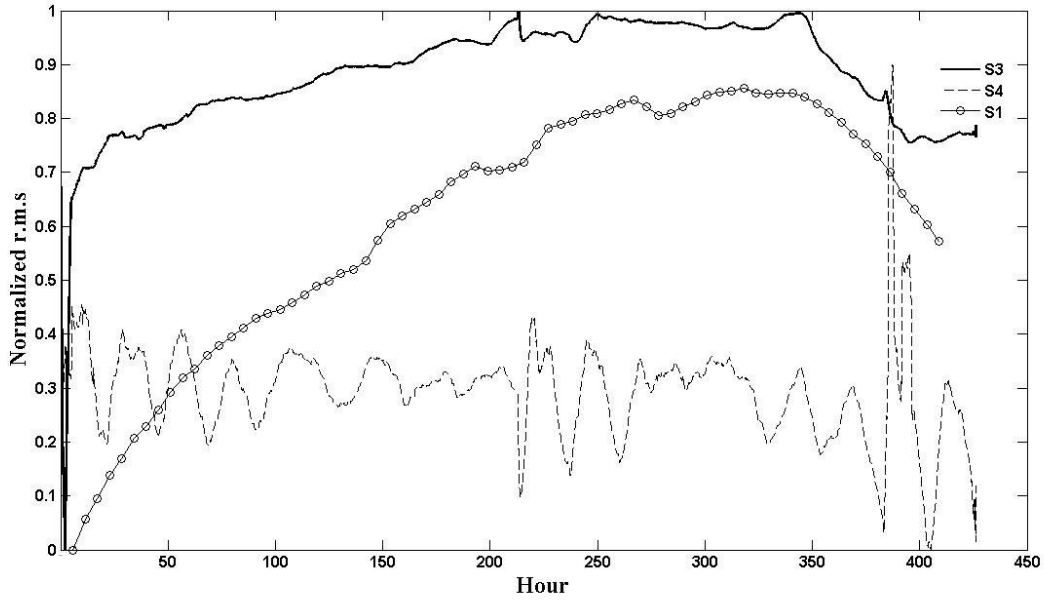

Figure 60 Normalized r.m.s. trend from sensors over the entire test duration

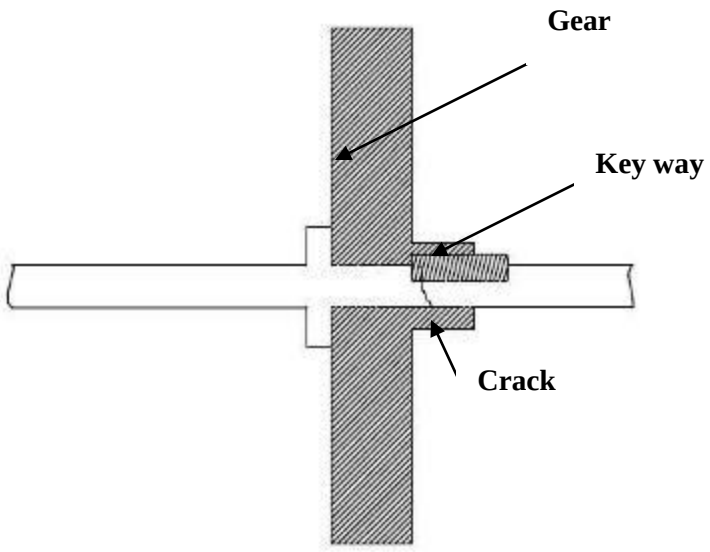

Figure 61 Location of cracked shaft restrained within the gear bore

Figure 60 presents normalized r.m.s levels from sensors over the entire test duration. At 345 hrs into operation sensor S3 (vibration bearing) showed a marked reduction in levels, Sensor S4 (motor current) showed a large increase between 385 and 395 hours into operation, whilst sensor S1 (AE gear) showed a gradual reduction in levels from 345 hrs into operation. After 426 hours of continuous running, the gearbox test was terminated and the gearbox inspected. The shaft fracture was evident and the cause, based on visible features, was attributed to bending fatigue, see Figure 62. The source of the crack growth was in the vicinity where the key way was cut into the shaft. The angle (15^{o}) between the shaft vertical axis and fatigued zone implies that the resulting fatigue was single origin. The fact that the ruptured shaft was still able to rotate due to being constrained within the gear bore made diagnosis a particularly difficult task.

Figure 62 Fractured shaft

The next parts of this chapter explore the use of three monitoring technologies to identify the presence of such loss of mechanical integrity. To accomplish this, data sets from all three technologies at defined intervals, see Table 11, were used for analysis. Investigations undertaken on all data sets involved spectral analysis in an attempt to relate the cracked shaft to specific machine related frequencies. In addition, discrete wavelet transform was applied to all data sets; acquired signals were decomposed into nine levels using an 8^{th} order Daubechies wavelet (Db8). This wavelet was chosen as it was as the shape of the mother wavelet has been shown to be a good approximation of a transient response in the measured motor current [154, 157]. Table 12 shows the decomposition level and associated frequency range.

Table 11 Selected data at defined operational time intervals

	Time (Hour)	Shaft Physical state
A	100	Healthy shaft
B	200	Healthy shaft
C	300	Healthy shaft
D	360	Loss of transmitted torque
E	385	Fractured shaft
F	400	Fractured shaft

Table 12 Frequency bands associated with each decomposition level

Decomposition level	Frequency Range (Hz)
1	[2500-5000]
2	[1250-2500]
3	[625-1250]
4	[312-625]
5	[156-312]
6	[78-156]
7	[39-78]
8	[20-39]
9	[10-20]

6.2 Data analysis and signal processing

6.2.1 Motor current signal analysis

Figure 63 presents the FFT of the acquired motor signal which was dominated by the line frequency (50 Hz) thereby masking all other frequencies; this was typical of all current data. As such the original signal was decomposed using wavelets to offer further insight into the frequency content. Kar and Mohanty [157] have reported the difficulties in diagnosis of the higher frequency content of the current signature through conventional FFT analysis.

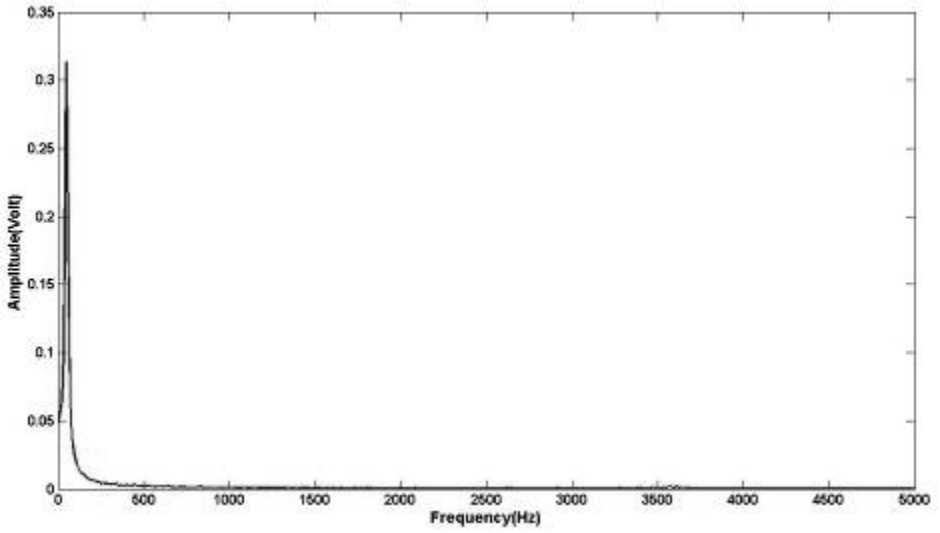

Figure 63 Frequency spectrum of motor current signature (100 hrs of operation)

Once the original signal was decomposed with wavelets, a Fourier transform was applied on each decomposed level, see Figure 64. Important frequency features such as gear mesh frequency (GMF) and its second harmonics were identified for levels D2 and D3. It was noted that for the decomposed level D3 (625 to 1250 Hz), the Fourier analysis offered some important diagnostic information. At time interval B, for decomposed level D3, the gear mesh frequency and side bands spaced at twice the pinion rotational speed (2X) were present, see Figure 65. After the shaft fracture (time interval D) it was noted that the side bands increased in amplitude relative to the gear mesh; this suggests an increase in amplitude of the modulating frequency

which points to increased misalignment [1]. At time interval F, prior to stopping the tests, the relative amplitude of the side bands to the gear mesh had increased even further, see Figure 65. This is indicative of the presence of frequency modulation as well as amplitude modulation. The variation in modulation frequency and consequently the modulation index, influences the strength of the carrier and modulating frequencies. In this particular instance the cracked shaft's inability to transmit the torque uniformly resulted in a variation of modulating frequency. Interestingly this observation was only noted at decomposition level D3. All other decomposed levels of measuring current signatures did not offer any unique diagnostic information in the frequency spectrum.

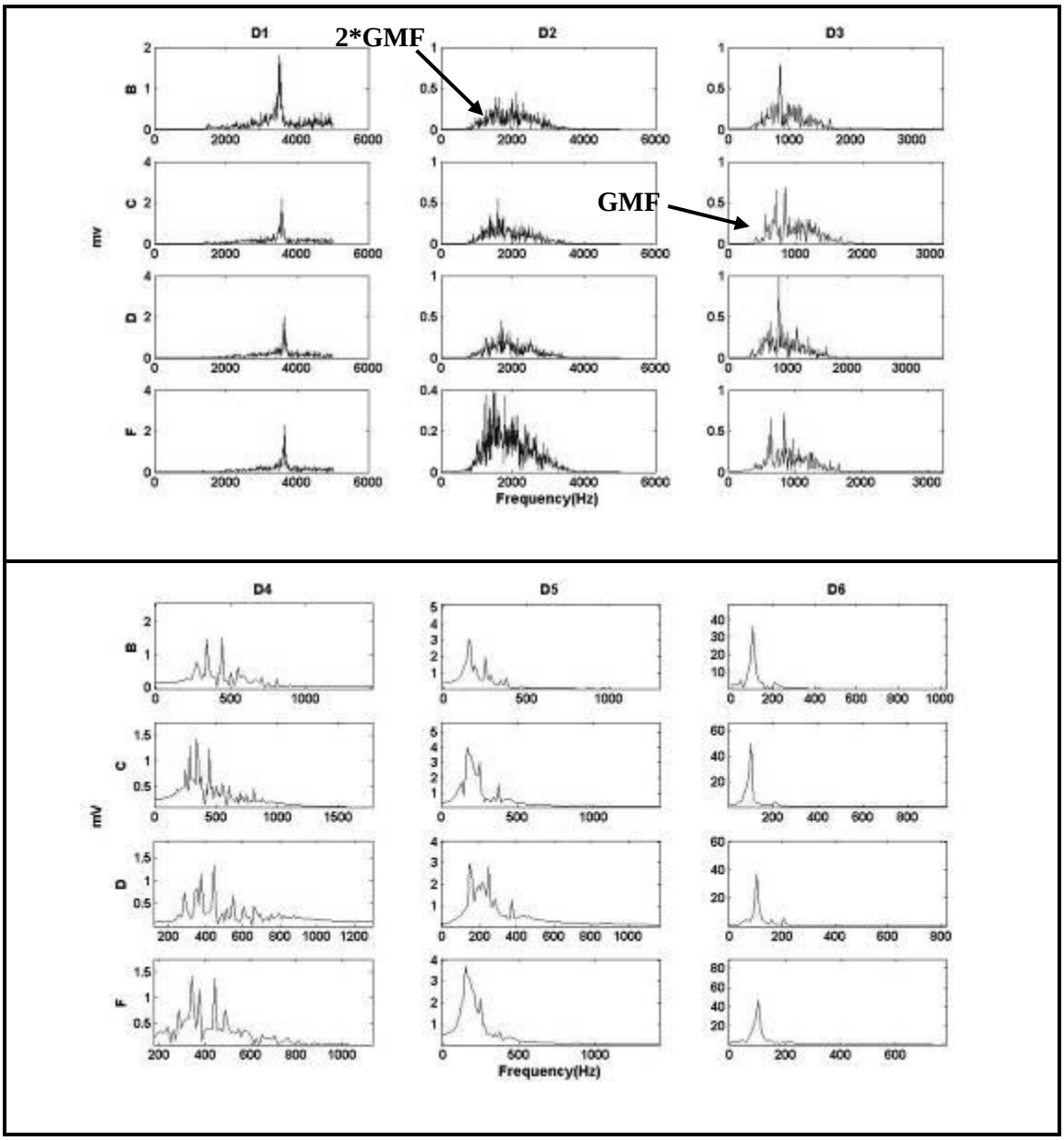

Figure 64 Frequency spectrum of the decomposed signals for various operational times

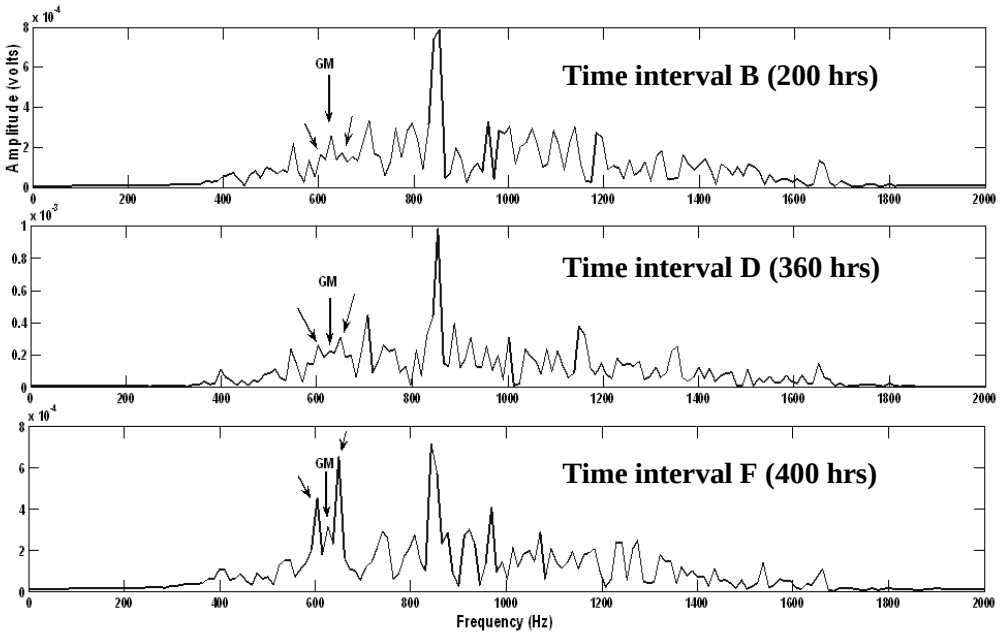

Figure 65 Fourier transform of decomposed signature at various time intervals (level D3)

The root mean square (r.m.s.) associated with each decomposed level (D1-9) was calculated and this revealed an interesting observation as a relatively large transient increase in motor current drawn was evident at levels D1 to D3 only, see Figure 66. The frequency range within these three bands (D1 to D3) included the gear mesh frequency and its harmonics. The exact reason for the observation of the large transient current level, seen 40 hrs (385hrs) after the initial loss of torque, is not known although the author attributes it to a dynamic system response whereby the gearbox components, shafts and gears, find a dynamic equilibrium after the cracked shaft.

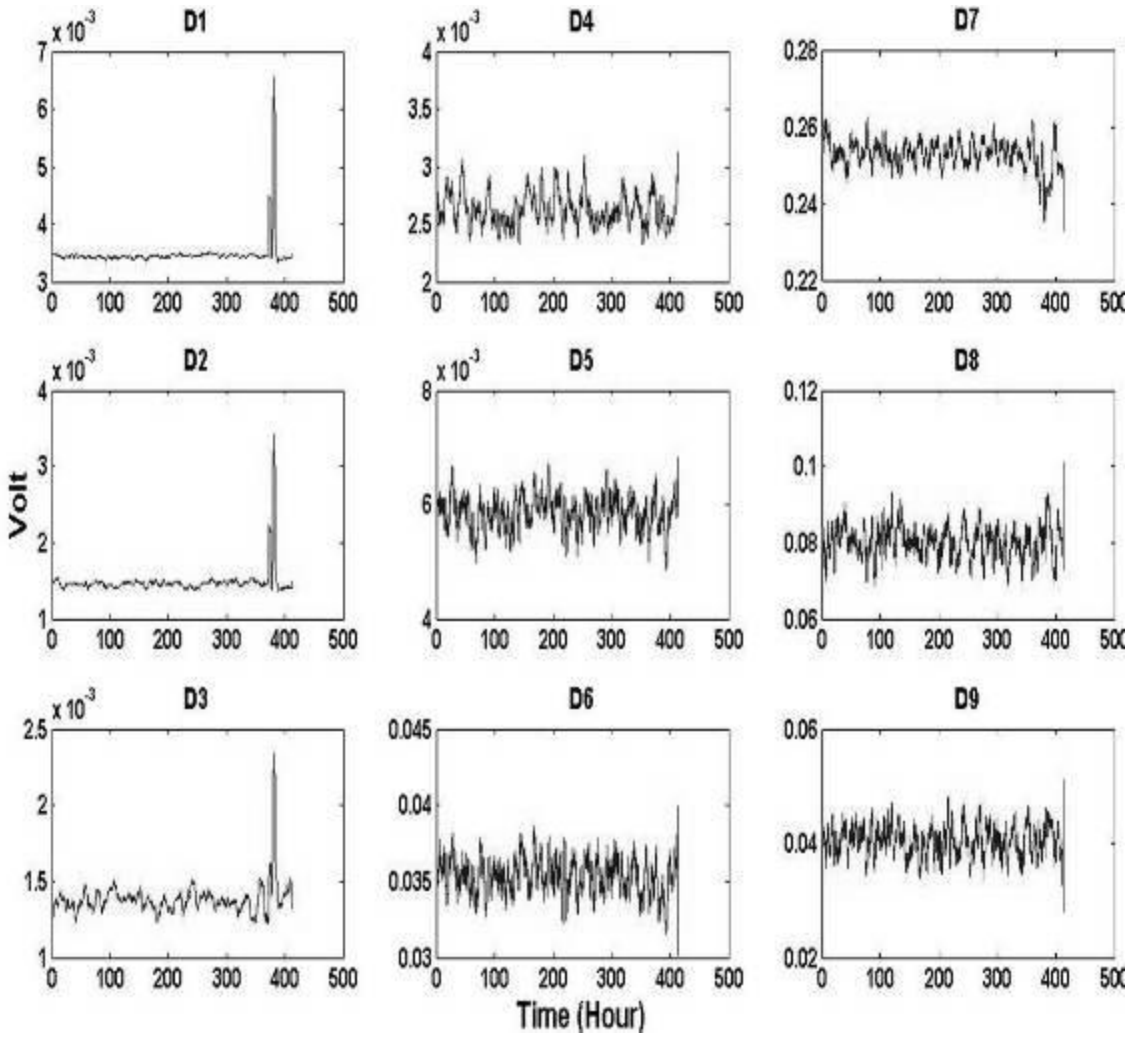

Figure 66 Electric current r.m.s. levels associated with the different decomposed levels

6.2.2 Vibration analysis

The vibration spectrum for the six time intervals (Table 11) is presented in Figure 67; the gear mesh and its harmonics are clearly dominant in the spectrum. Trends of vibration of r.m.s. levels of the shaft frequency, twice shaft frequency, the gear mesh and twice gear mesh are presented in Figure 68. The r.m.s. trends of vibration presented in Figure 68 were calculated from signals taken at 10 minute intervals. No discernable diagnostic information could be extracted from the results presented in Figure 68; however, it was noted that the trend of the gear mesh frequency closely matched the overall vibration trend shown in Figure 60 in which the gradual increase in vibration over time was attributed to increased surface pitting, and the sudden reduction in vibration was due to shaft fracture (loss of torque).

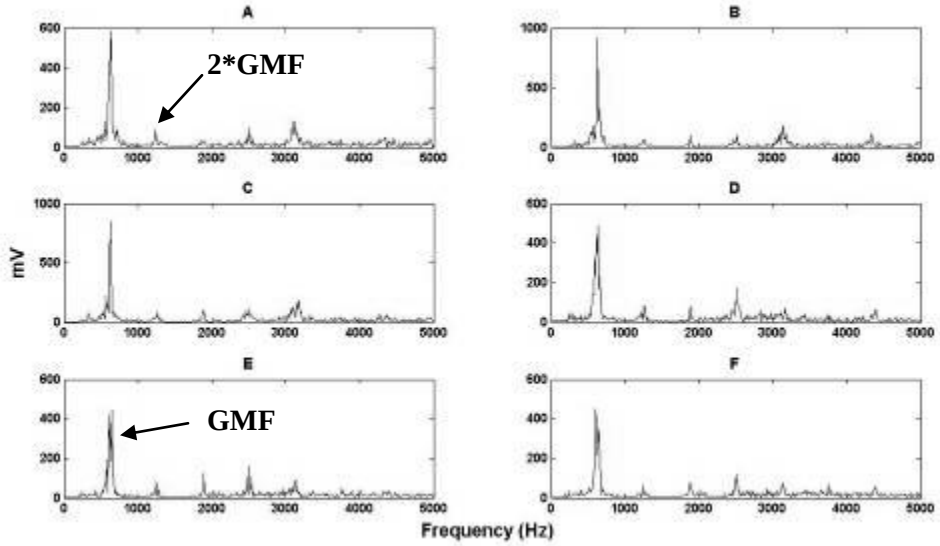

Figure 67 Frequency spectrum of vibration signatures associated with different states of shaft deterioration

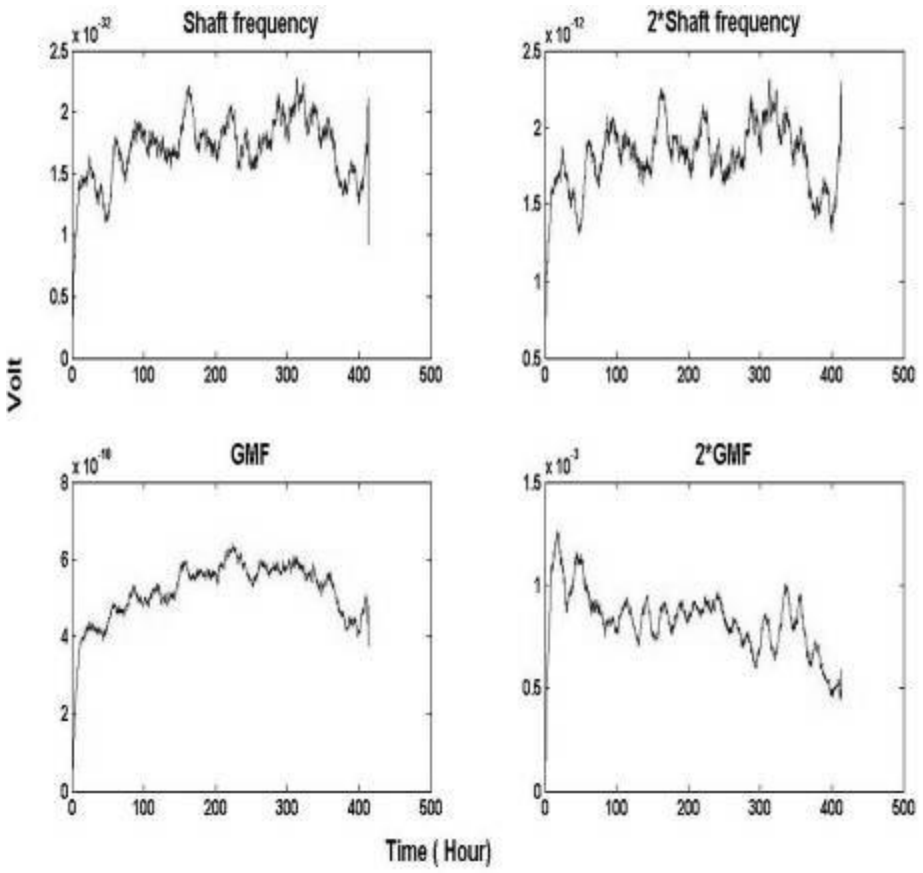

Figure 68 Vibration amplitude of selected frequency components

Closer observations of the frequency spectrum (Figure 69) showed side bands either side of the gear mesh frequency. The amplitude of the side bands increased significantly from 0.2v at 300hrs of operation (just before fracture) to 0.4v at 360hrs of operation (after fracture). The frequency difference between the side bands and the gear mesh was equivalent to two times the pinion shaft speed (2X). This matches classical gear angular misalignment symptoms of which side bands equivalent to twice the rotational speed, about twice gear mesh frequency, are to be expected. Also noted was at time interval D, 360hrs of operation, side band spacing at not only twice the pinion shaft speed but also at the wheel shaft speed (approx 9 Hz) was now evident and by 400hrs of operation the discrimination between the gear mesh and side bands was no longer evident due to the increased energy levels of the sides bands and smearing of the frequencies in

the vicinity of the gear mesh frequency. In addition, it was noted that the side bands were non-symmetric.

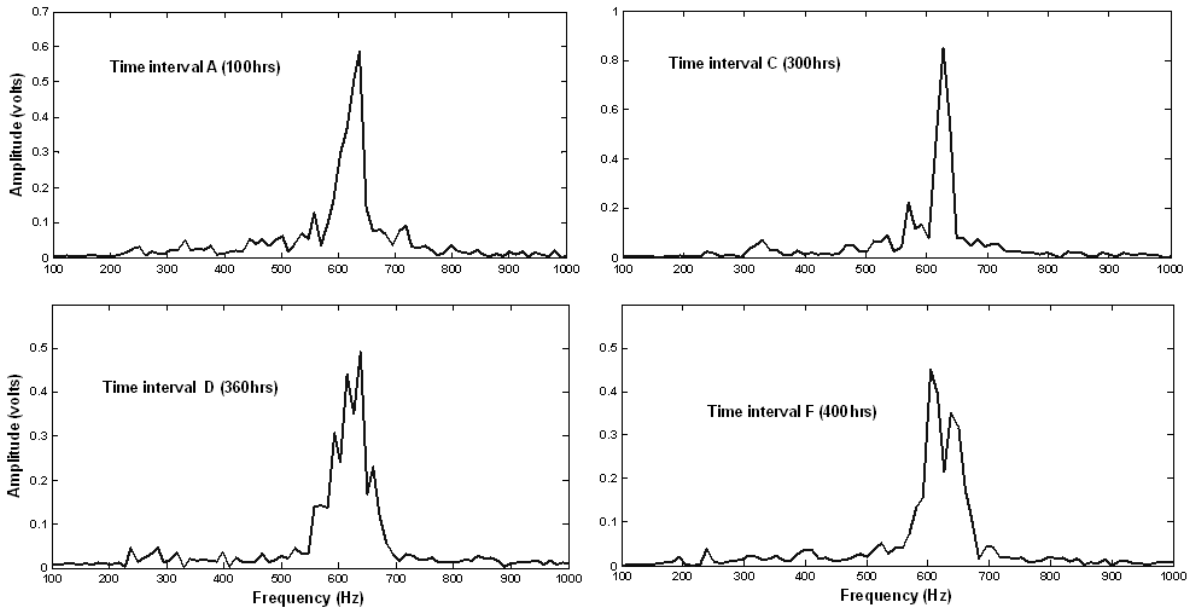

Figure 69 Spectrum of vibration signals around gear mesh frequency

6.2.3 Acoustic Emission results

The AE waveform from both sensors S1 and S2 at the time frames listed in Table 11 are shown in Figure 70. The data acquired from the signals from S1 and S2, regardless of operation time, are of a continuous nature.

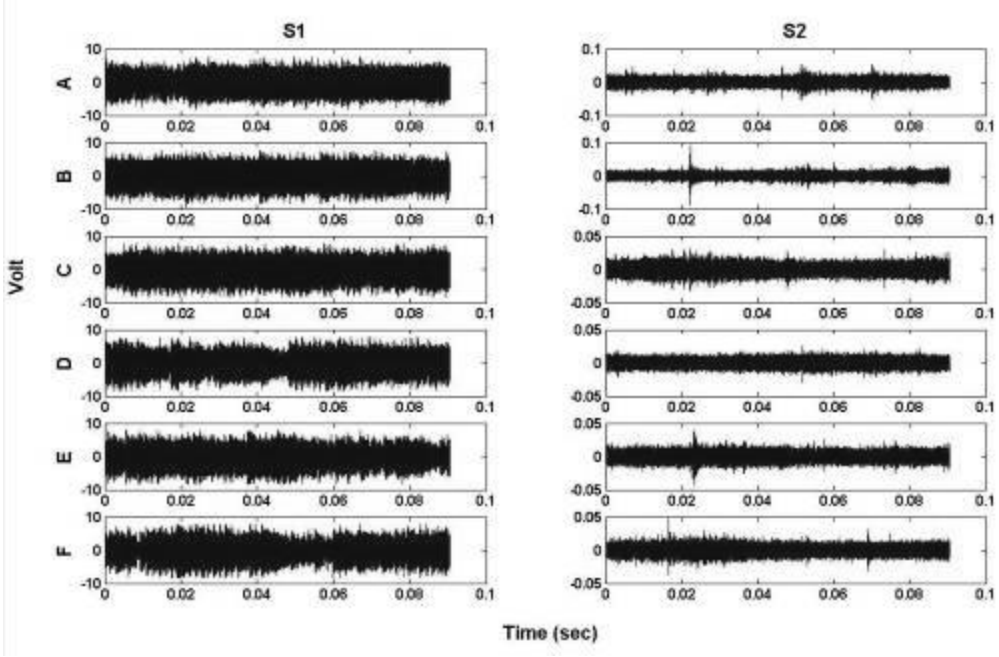

Figure 70 Waveform from S1 and S2 taken at different intervals

The frequency spectra of a sample of the AE signals from S1 and S2, associated with different stages of the shaft deterioration, are presented in Figure 71 and show that the AE activity is concentrated between 100 kHz and 300 kHz with no distinct features evident between the healthy and damaged shaft. This applied to all acquired AE signatures and agrees well with observations from section 5.1.1.1 in which the AE signals associated with the presence of seeded surface defects on the gear tooth face exhibited no change in frequency content.

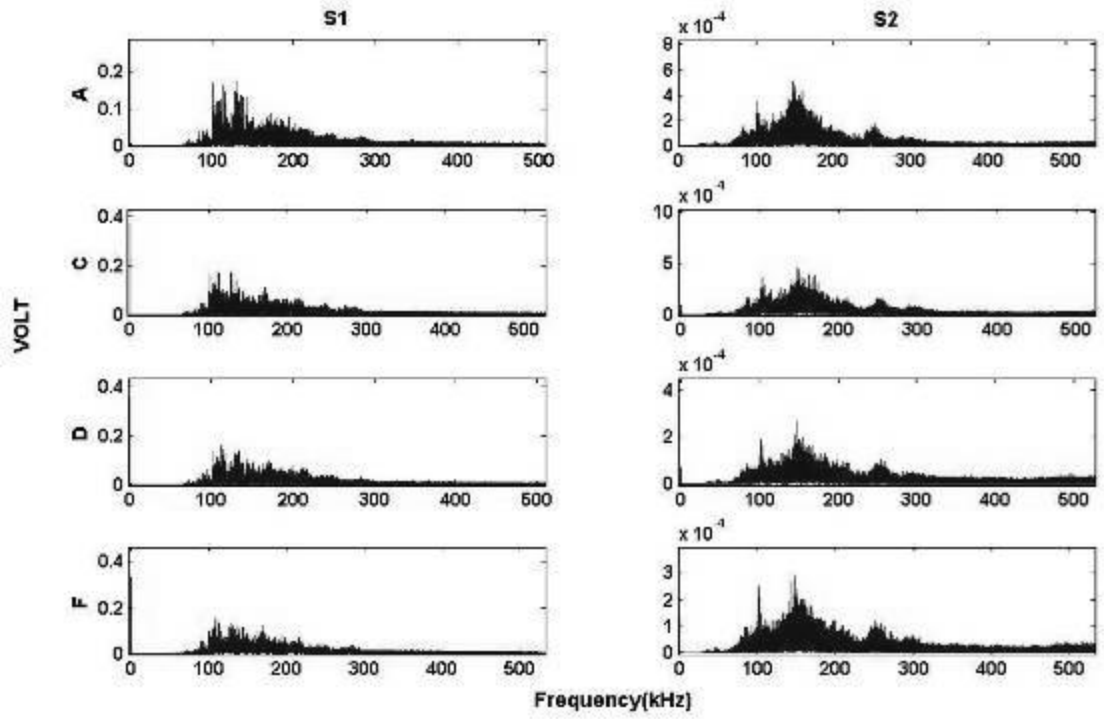

Figure 71 Frequency spectrum of AE signal from S1 and S2

Further investigation involved decomposing the AE signatures with wavelets so that specific frequencies could be investigated. As such, the acquired AE signatures were decomposed with an 8th order Daubechies wavelet. The frequency spectrum of the decomposed AE signatures offered no distinct features between the healthy and damaged shaft, evident at the frequency ranges encompassed by D1-4, see Figure 72 .These frequencies fall within the AE frequency range.

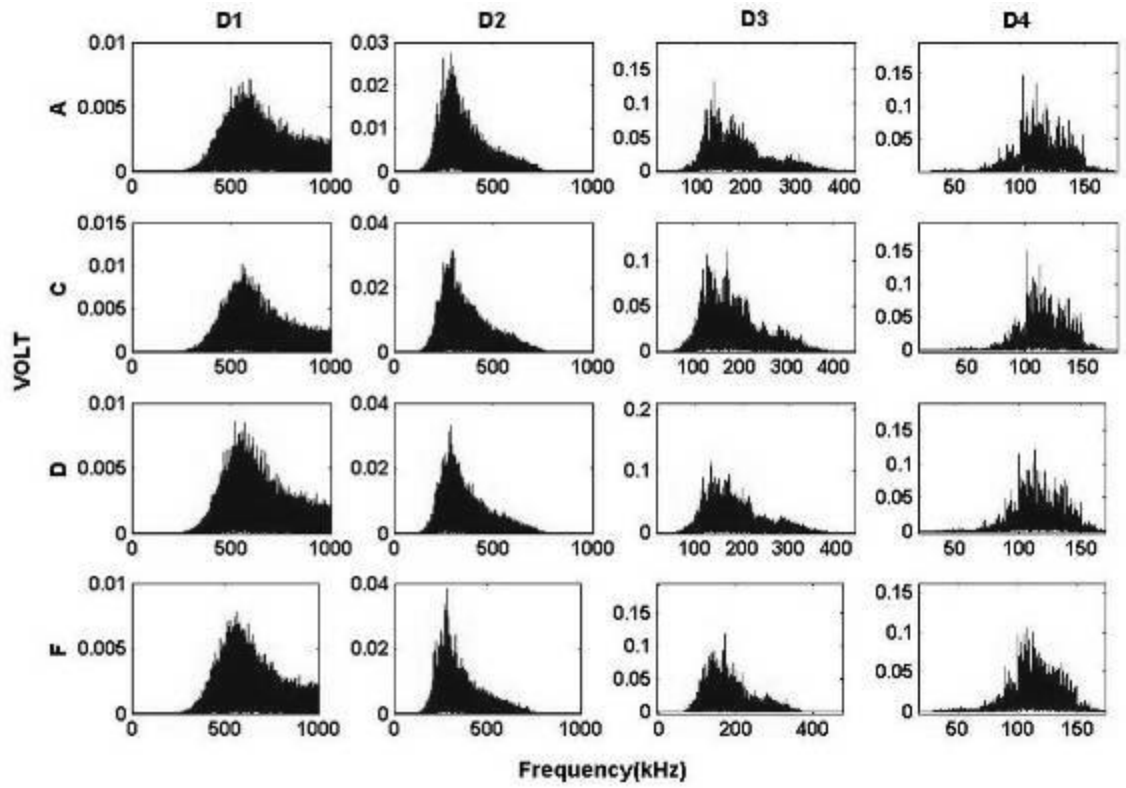

Figure 72 Frequency spectra of the decomposed signals for AE sensor S1

The AE waveforms were enveloped and the spectrum of a selected range of the enveloped AE signature is presented in Figure 73. Surprisingly there was a distinct difference in the envelope spectrum prior to, and after, the shaft breakage. Prior to shaft breakage the frequency spectrum of the modulated AE signatures taken from AE sensor S1, contained the gear mesh frequency and twice the gear mesh frequency; however, after shaft breakage harmonics of up to four times the gear mesh were evident. Interestingly, the frequency spectrum of modulated decomposed AE signatures, at level D3, taken from the AE sensor on the gearbox casing (S2), showed the presence of the gear mesh and some of its harmonics prior to shaft fracture, whilst after the fracture, the harmonics were no longer evident, see Figure 74.

The reason for the presence of higher harmonics of the gear mesh, up to four times, is attributed to impacting/rattling of the gears after the shaft fracture. This rattling/impacting phenomenon is supported by the frequency modulation evident on the motor current signature analysis noted earlier. Also, due to the loss of transmitted torque through the shaft, the bearings supporting the gears will experience less dynamic loading, influencing the transmission path between the meshing gears, the bearings, the gearbox casing and the AE sensor (S2) on the gearbox – as such the spectrum of the modulated AE signature, at the decomposed level D3, did not include the gear mesh frequency after shaft fracture.

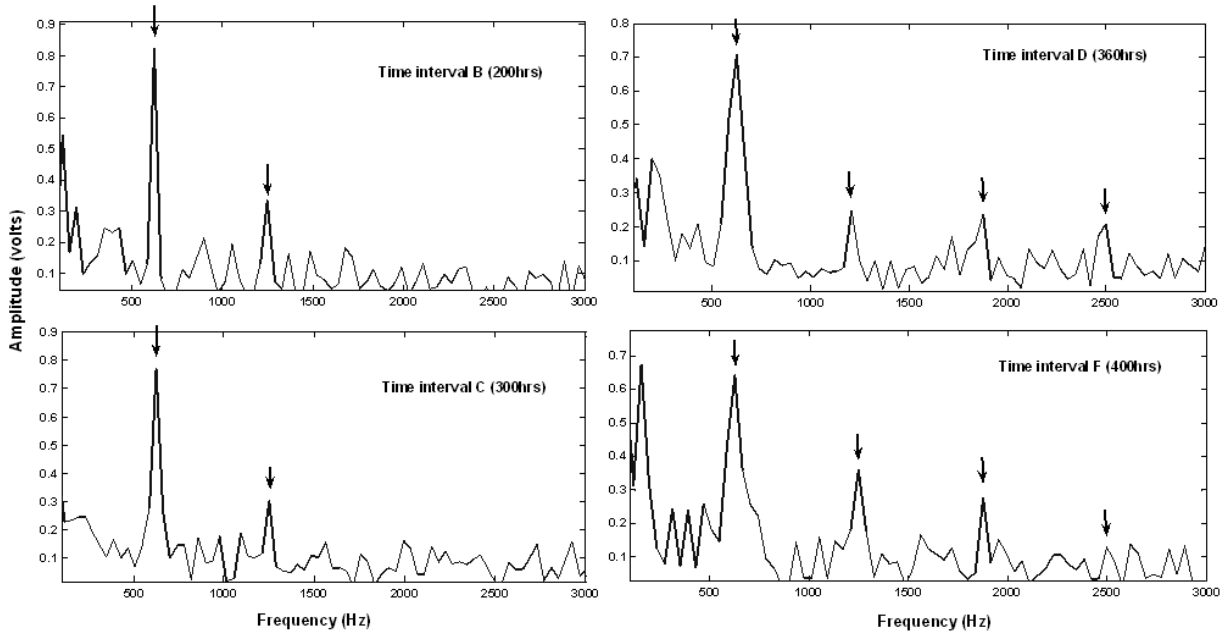

Figure 73 Frequency spectrum of the enveloped AE signals for S1

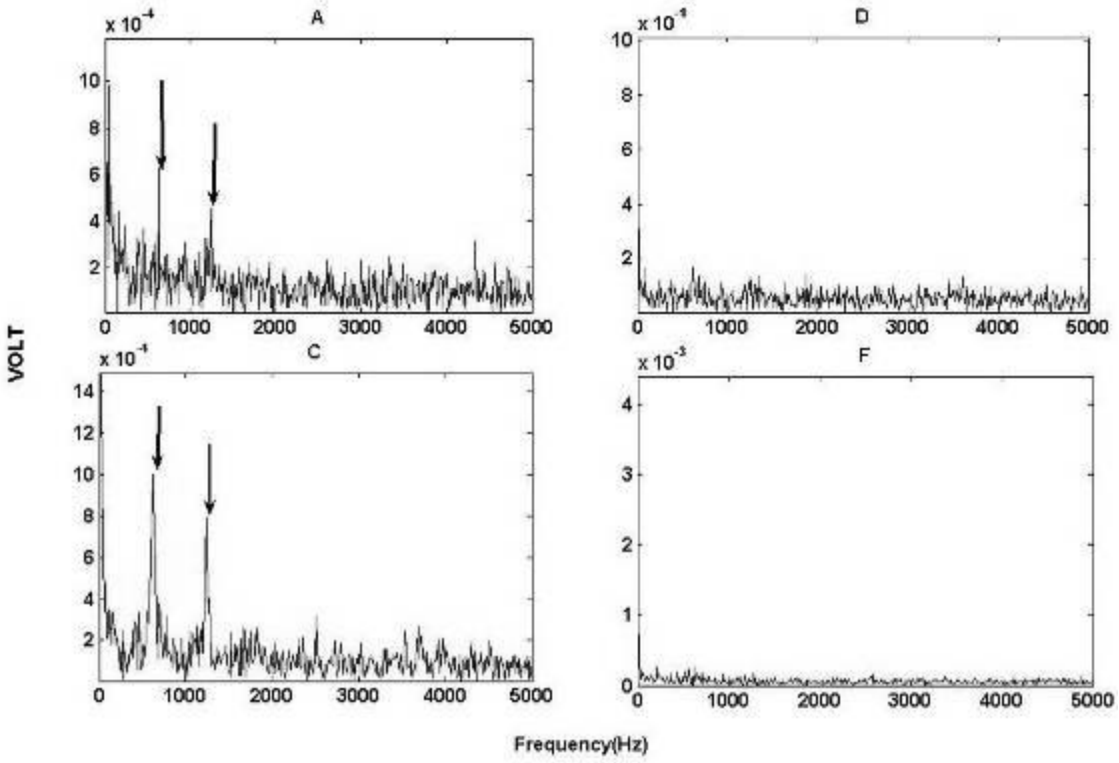

Figure 74 FFT of enveloped AE at level D3 for S2

6.2.4 Conclusions

- The wear progression on the gear teeth surface was noted from measurements of AE (S1 only) and vibration (S3 only) whilst measurement of the motor current did not show any correlation with increasing surface damage.
- Observation of the vibration frequency spectrum showed an increase in side band energy centred at the gear mesh frequency after shaft fracture.
- Observations of the frequency response of AE measurements showed no changes in frequency content prior to and after shaft fracture. However, the spectrum of envelope AE showed several harmonics of the gear mesh after fracture. Conversely the frequency spectrum of the enveloped AE response from the casing (sensor S2) showed the presence of the gear mesh frequency prior to fracture only. These observations present unique diagnostic capacities of AE measurements which hitherto have not been reported.

It has been shown that the presence of a cracked shaft can be detected by all three technologies though the success of detection is dependent on the diagnostic path chosen by the investigator.

CHAPTER 7

---

7 Condition monitoring of the rolling element bearings

7.1 Defect diagnosis

The overall trends of AE and vibration levels for both tests are presented in Figure 75. Also presented in Figure 76 is the defect observed on termination of Test-1, clearly displaying a spall on the flat race.

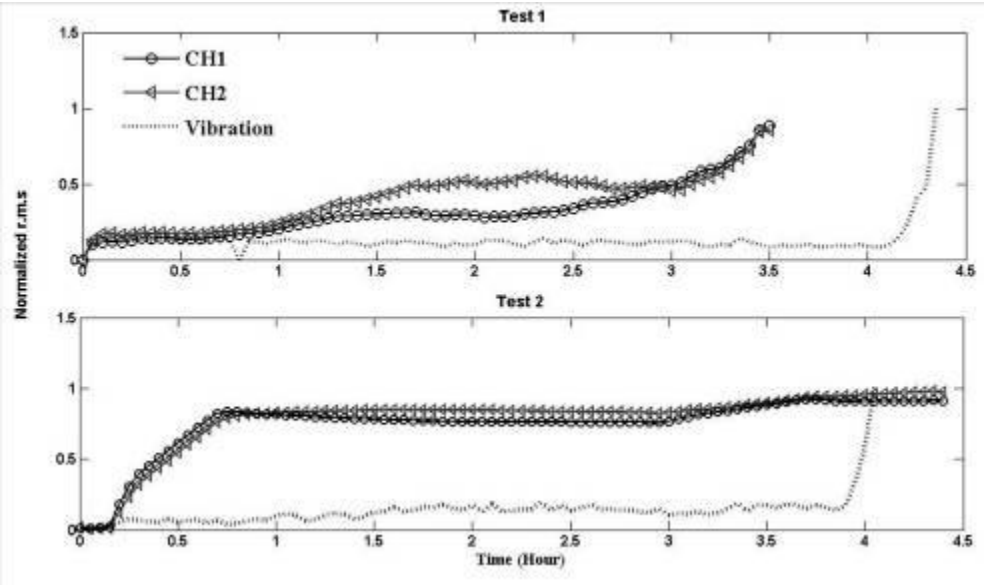

Figure 75 Overall AE and vibration r.m.s. levels

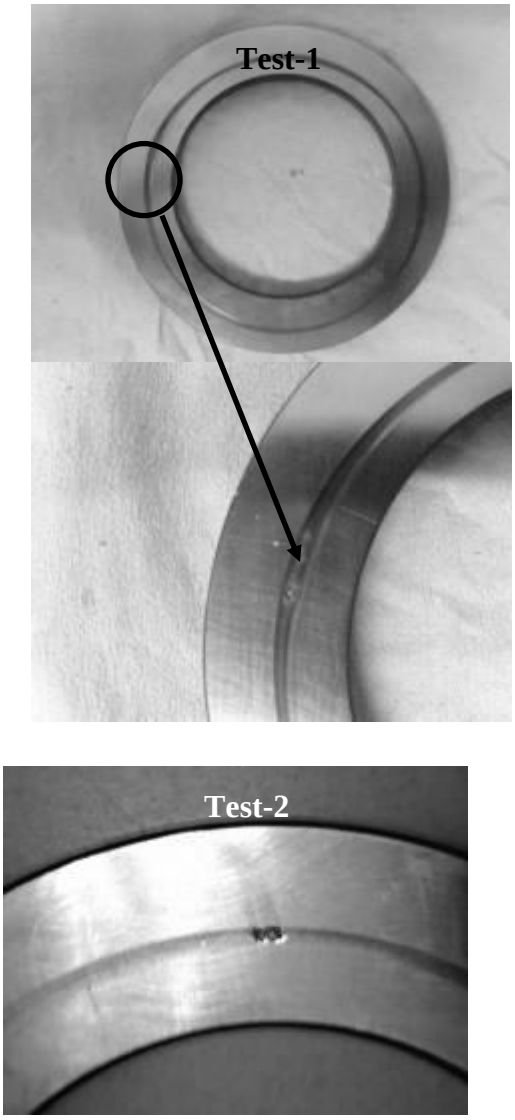

Figure 76 Defect on the outer race

7.1.1 Vibration Monitoring

The vibration waveforms for both tests at defined time intervals are detailed in Table 13 and Figure 77. Under ideal conditions it would be expected that for the particular type of defect generated during the test, large transient vibration impulses spaced at a defect frequency would be evident. This defect frequency is characteristic of the bearing elements. However, due to the high level of operational noise, resulting in a low signal to noise ratio, the presence of these

spikes was not always visually evident in the captured waveforms. The frequency spectra of the waveforms are also presented in Figure 78. The Ball Pass Frequency (BPF) was evident at stages ‘E’ and ‘F’ of Test-1 whilst this defect frequency was barely present at stages ‘E’ and ‘F’ on Test-2. In addition, several harmonics of the running speed (25 Hz) were noted with the third harmonic (75 Hz) dominant for both tests. In an attempt to achieve a better resolution in detecting the fault frequency, envelope analysis was undertaken. The signals were band-pass filtered about a centre frequency of 1570 Hz using the least-square FIR filter of order 50 with a bandwidth of 40Hz . Although is its usually recommended to chose the bandwidth a few things the higher than the defect frequency of interest, in this instance the bandwidth was kept narrow as the authors wanted to avoid interference from other frequencies close to 1570 Hz. Selection of this centre frequency was based on observation of the spectrum of the last recorded vibration stage where a large peak was evident at 1570 Hz for both tests, see Figure 79. It is believed that this frequency (1570 Hz) is associated with one of the resonance frequencies of the bearing test-rig and this frequency was excited due to the impulsive impacts of the rollers over the defective race. The filtered signals were enveloped using the Hilbert transform. Figure 80 presents the envelope spectrum of the filtered signals with the defect frequency now clearly evident at interval ‘F’ particularly for Test-2. This was to be expected given the selected frequency for filtering was chosen from the spectrum at interval ‘F’. This also shows that the selection of the filtering frequency is dependent on the dynamic characteristic of the bearing/machine at the time of vibration measurement, as seen in Figure 79, where the filtering frequency of 1570 Hz was not dominant at the earlier test intervals.

Table 13 Timing interval

	Test 1	Test 2
A	40 min	40 min
B	80 min	80 min
C	120 min	120 min
D	180 min	160 min
E	220 min	200 min
F	264 min	240 min

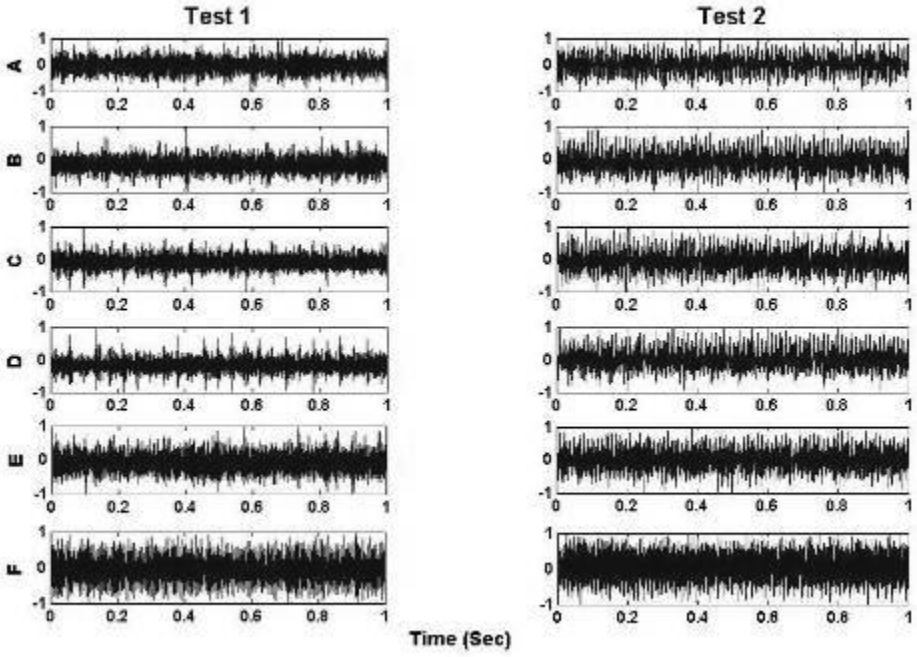

Figure 77 The vibration waveform associated with different test intervals.

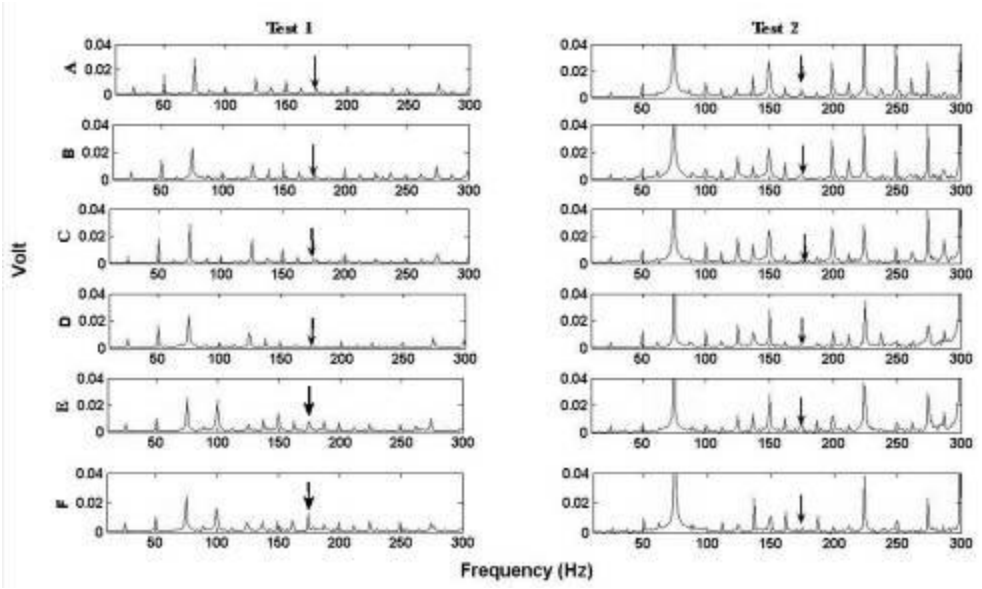

Figure 78 FFT of the signals at different intervals [10Hz-300Hz]

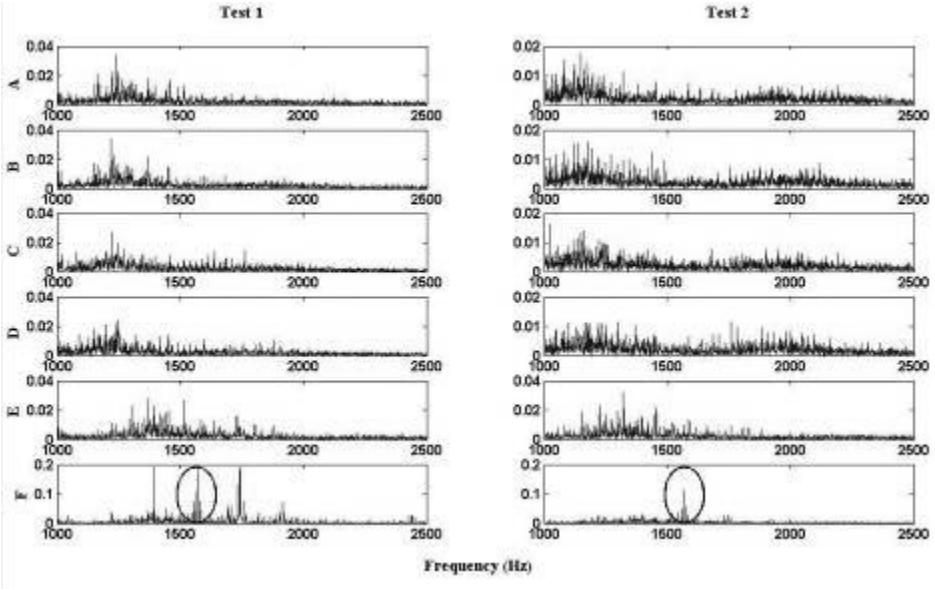

Figure 79 Vibration frequency spectrum

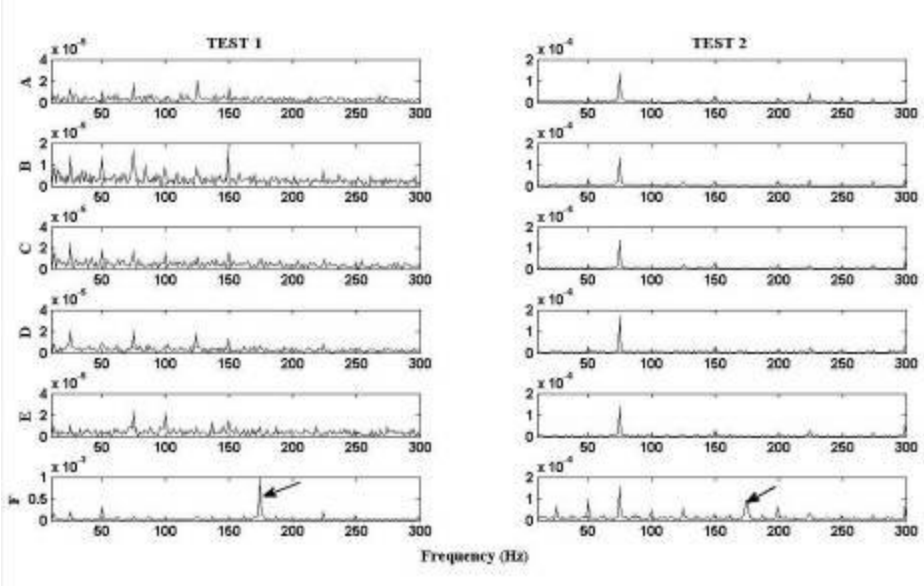

Figure 80 The envelope spectrum of the vibration signals filtered at 1570 Hz

Although performing envelope analysis in conjunction with band-pass filtering was successful in discriminating the BPF, prior knowledge of the entire frequency spectrum and location of the dominant amplitude across the spectrum is essential for selection of the most effective filter frequency. Furthermore, since the presence of random Gaussian noise can affect the resolution of the frequency spectrum, and this can vary at the different stages of mechanical integrity, the estimation of the optimum filter frequency can be challenging. This is very important when dealing with the intelligent monitoring systems, in which the automatic selection of filter frequencies can be significantly influenced by the level of signal-to-noise ratio. Indeed, the key to performing an effective envelope analysis is to choose an effective band-pass filter and since the rolling bearings in practice are operated under different working conditions (speed and load), a generic band-pass filter with fixed parameters (Centre frequency and Band width) will not be sensitive enough to perform a compelling diagnosis [162]. One such method for optimal filter selection is the spectral Kurtogram.

In order to improve the de-noising of vibration signals, the concept of Spectral Kurtosis (SK) was employed. This involves calculating the Kurtogram for each signal from which the bandwidth and centre frequency required to design a band-pass filter are determined. The

criterion was set such that the frequency and bandwidth (window size) at which the spectral kurtosis of the signal is maximum was employed to build a new band-pass filter. The determination of SK was based on the algorithm developed by Antoni [73, 163]. A sample Kurtogram of signals at an early stage (A) and upon the termination (F) of tests is presented in Figure 81. The centre frequency (Fc) at 'F' was significantly higher than at interval 'A', suggesting a change in the impulsive vibration nature as the defect matured.

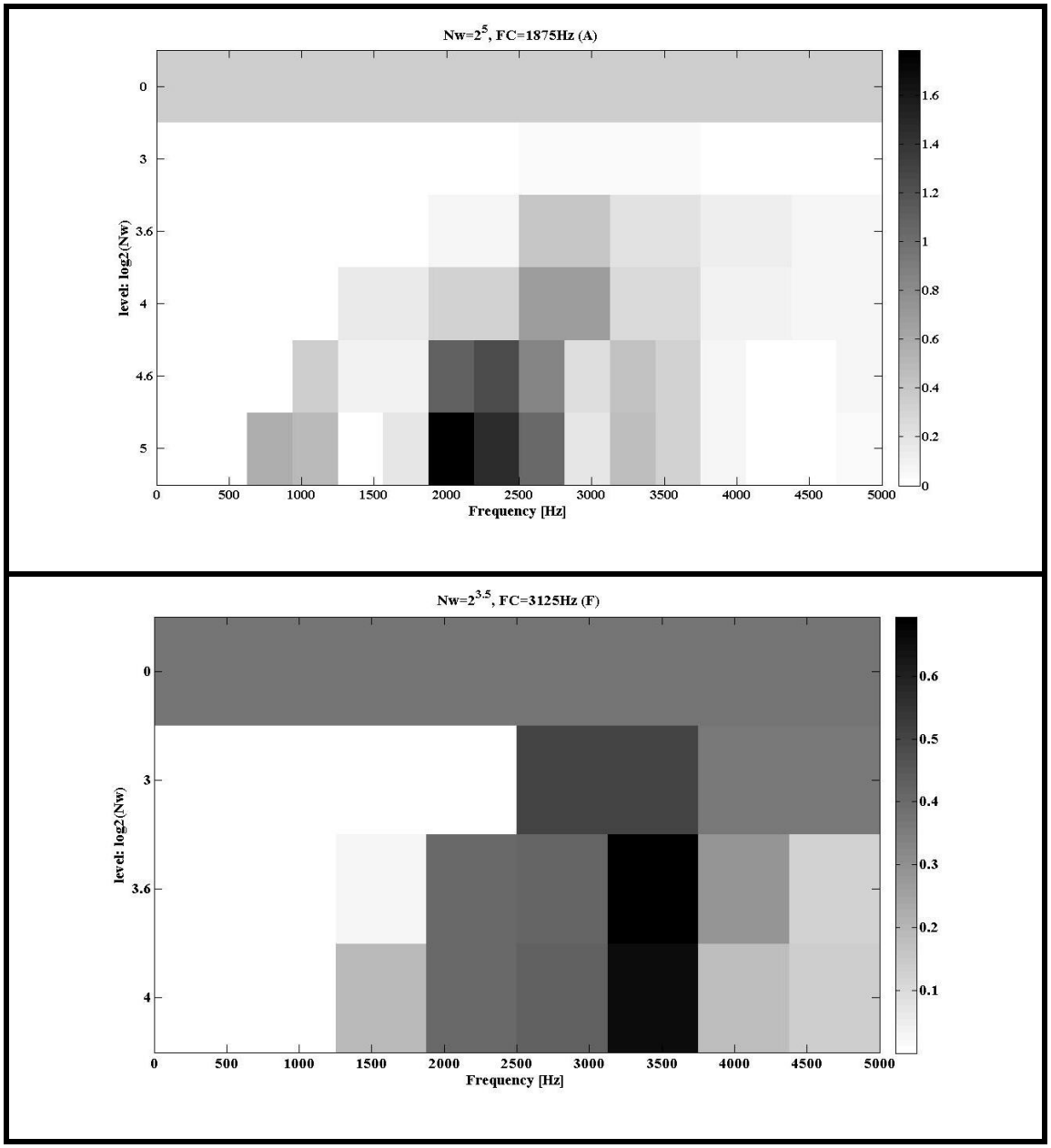

Figure 81 The Kurtogram for Test-1; time intervals 'A' and 'F'

From the SK analysis, the centre frequency, together with bandwidth for the time intervals A-F, were calculated and are listed in Table 14. In addition, the Kurtosis values associated with the centre frequencies are also presented. The window size is the length of the data points within that particular window within which the STFT of the signal and corresponding SK values were estimated (Equation 10-13), whilst the centre frequency is the frequency at which the calculated SK value, at that particular windows size, is maximised. It is believed that the higher SNR is achieved at this centre as it matches one of the system's natural frequencies [72].

Table 14 Estimated features from Kurtogram

	Test 1				***Test 2***		
	Fc(Hz)	**Nw**	**Kurt**		**Fc(Hz)**	**Nw**	**Kurt**
A	1875	32	1.8		1875	32	3.4
B	1875	32	1.7		1875	32	1.7
C	1875	32	3.4		1875	32	1.6
D	625	32	2.4		1875	32	1.9
E	2812	32	3.3		2187	32	3.7
F	3125	11	0.8		2187	32	1.9

Nw: Window size **Kurt**: Kurtosis **Fc**: Centre Frequency

The signals were band-pass filtered at the determined centre frequencies, which were based on the extracted features from the Kurtogram, and the resulting time waveforms are presented in Figure 82 and Figure 83[6]; the window size (N_w) corresponds to bandwidth (B_w) with

[6] The window-based finite impulse response filter was employed for filtering. The size of window used to design the filter was equal to that calculated from the Kurtogram of each signal.

B_w=Sampling frequency /N_W. From these figures it is evident that filtered signals offered a higher level of signal to noise ratio showing the capability of SK based filtering for de-noising. To quantify the improvements in the signal-to-noise Crest factor (CF), values were compared before and after filtering. The CF is defined as the ratio of the peak value divided by the signal r.m.s. which gives an indication of signal peak-to-average ratio. CF is a traditional method of measuring the smoothness of a signal and therefore a faulty bearing will generate a spiky signal profile resulting in an increase in CF. Figure 84 shows the values of CF for filtered and unfiltered signals in which an average increase in CF levels of approximately of 264% and 250% were noted for Test-1 and Test-2 respectively after band-pass filtering.

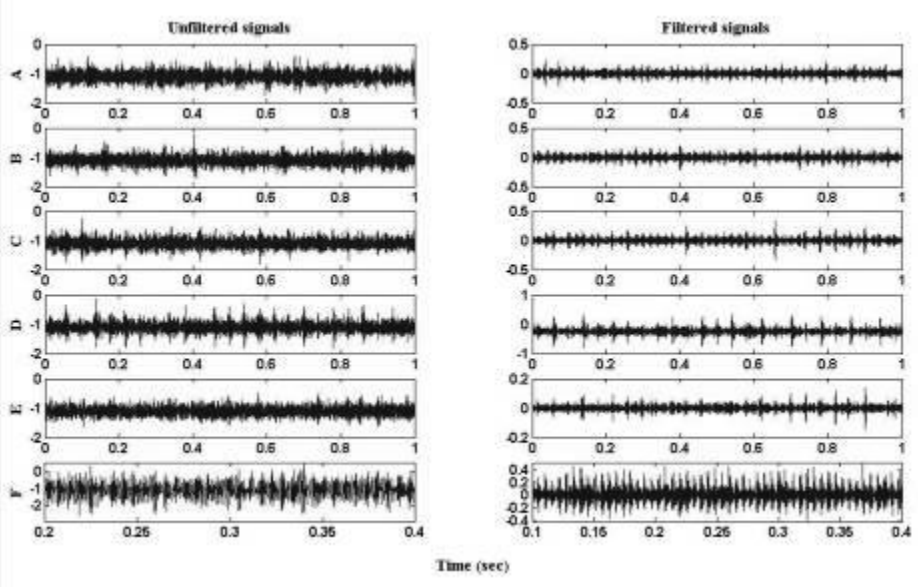

Figure 82 Vibration waveform for Test-1 (Filtered designed based on Kurtogram)

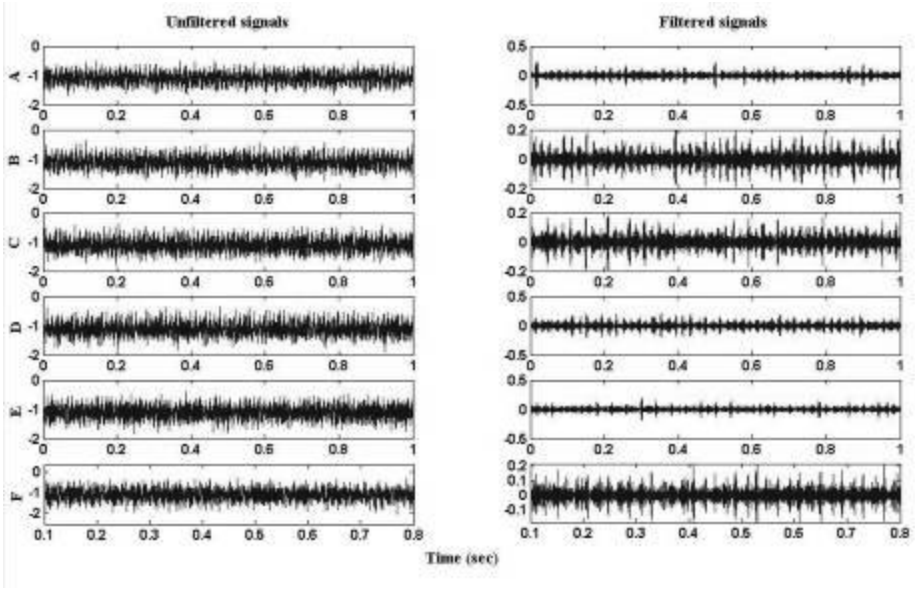

Figure 83 Vibration waveform for Test-2 (Filter designed based on Kurtogram)

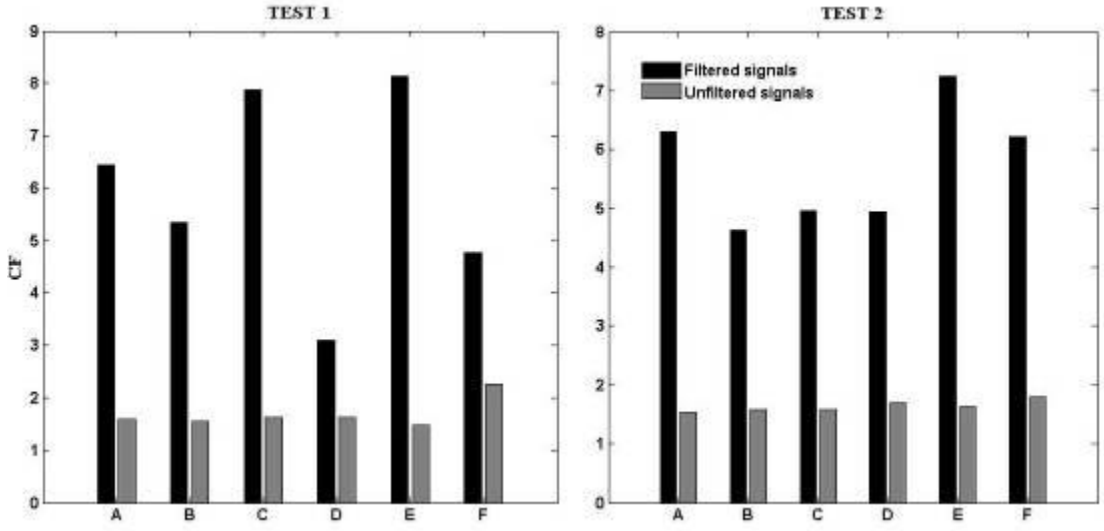

Figure 84 CF values associated with filtered and unfiltered signals

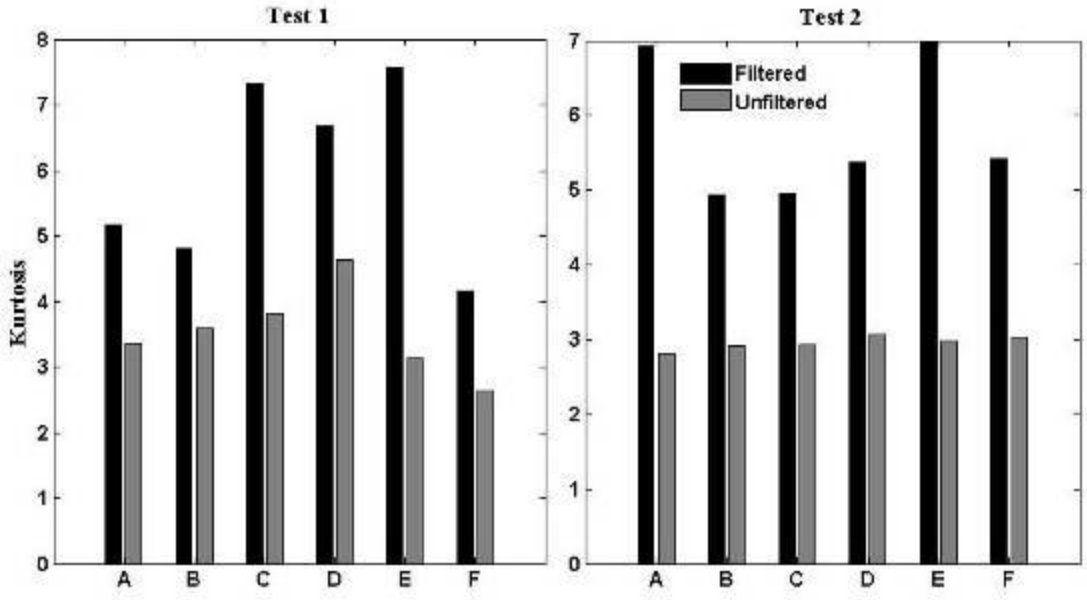

Figure 85 The relative increase in level Kurtosis values after band-pass filtering

The Kurtosis values of the signals at intervals 'A' to 'F' prior to, and after, filtering are also presented in Figure 85 showing a 70% and 95% average rise in Kurtosis values as a result of band-pass filtering for Test-1 and Test-2. This agrees with observations from Figure 82 and Figure 83 where the presences of spikes were more evident on the filtered waveforms. The squared envelope of the signals, for both tests, were calculated and the corresponding frequency spectrum of the enveloped signals are also presented in Figure 86 in which the defect frequency is clearly marked upon the termination of both tests. The capability of discriminating the BPF in the corresponding envelope spectrum clearly indicates the effectiveness of SK in diagnosing the fault frequency. In comparison to the envelope spectrum presented earlier in Figure 80, it is evident that the level filtering offered by the Kurtogram had improved the earlier detection of the defect frequency, at interval 'D' which is much earlier than noted in Figure 80. For Test-2 the SK-based filter did not offer any improvement in the earlier detection of the defect frequency, suggesting a limitation in its de-noising effectiveness.

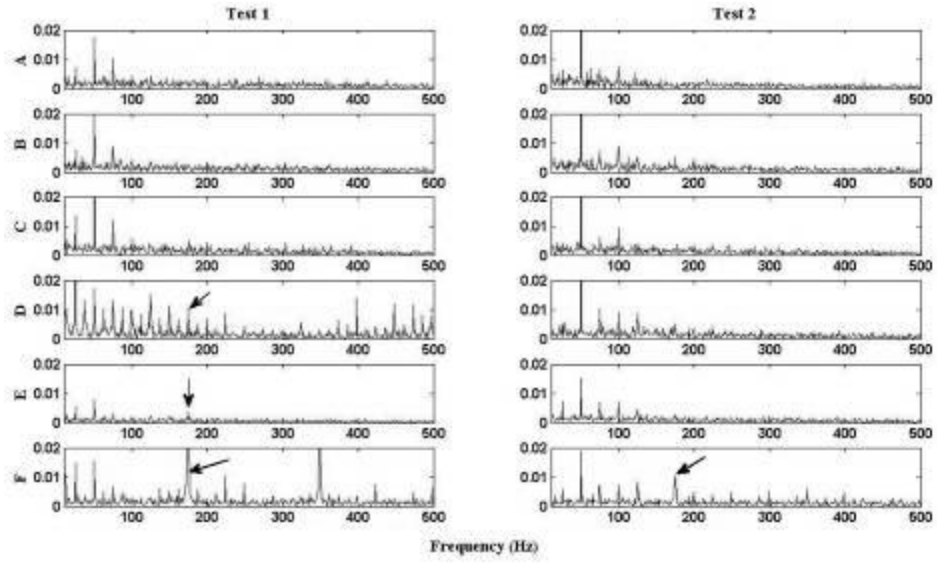

Figure 86 Envelope spectrum of the SK filtered signals

7.1.2 Acoustic emission diagnosis

In Figure 75 an initial increase in AE r.m.s. levels between 0-12min for Test-1 and 0-30 min for Test-2 was noted. The initial rise in r.m.s. values is associated with the run-in stage of the bearings after which the AE activity remained constant for period of 18mins and 2hrs for the first and second tests respectively. For the first test, the level of AE r.m.s. started to increase after approximately 1hr into operation suggesting the onset of failure. A similar observation was noted for the second test after 3hrs of continuous running. Comparing the overall trend of vibration and AE r.m.s., it is evident that the AE is more sensitive in monitoring the progression of the defect. In addition, AE levels increased approximately one hour before the vibration levels began to change. This was noted in both tests, for instance in Test-1 AE levels started to increase at 3hrs of operation whilst vibration levels increased after 4hrs at operation. It must be noted that these are accelerated failure tests and the difference in periods between these techniques (AE and vibration) in identification of the defect will most certainly be much longer for non-accelerated test conditions.

The AE signals for different intervals, as set in Table 15, were chosen for further analysis, see Figure 87. Interestingly, for Test-1 at time period 'F', the AE waveform showed large transient bursts spaced at one of the bearing defect frequencies. This is a classical AE bearing defect phenomenon as noted by several investigators [17, 118]. However, for the second test, the underlying noise level obscures any apparent high transient events in the waveform.

Table 15

	Test 1	**Test 2**
A	35 min	42 min
B	70 min	87 min
C	105 min	132 min
D	140 min	174 min
E	175 min	219 min
F	210 min	267 min

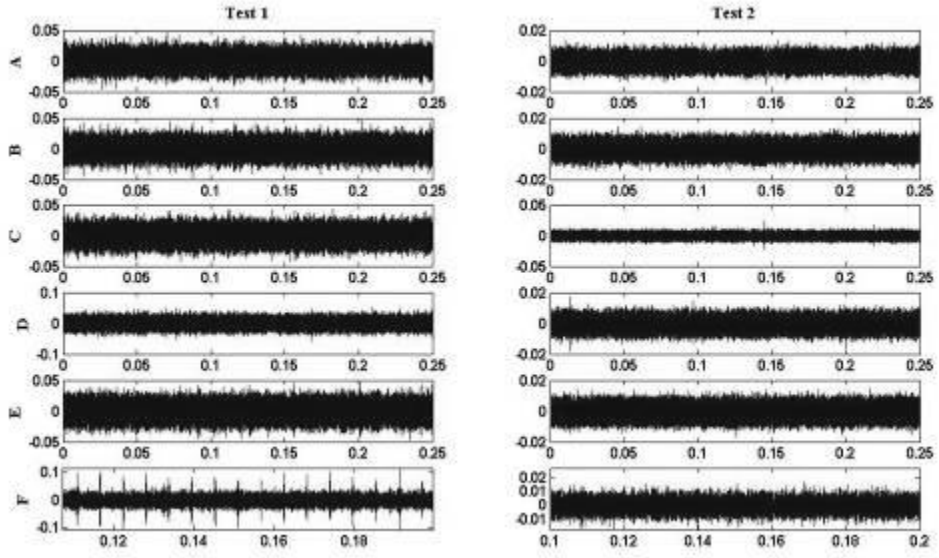

Figure 87 The AE waveform at different time intervals

The frequency spectrum of recorded AE signals shows that most AE activities are concentrated between 50 and 450 kHz, see Figure 88. Furthermore, the AE and vibration waveforms upon the termination of Test-1 are presented in Figure 89. The AE bursts spaced at 175 Hz, representing the defect frequency, are apparent in the AE waveform. Also the values of Kurtosis and the Crest Factor associated with AE signals are significantly higher. This reiterates the diagnostic advantage of the AE over vibration as it is more sensitive to damage detection [12]. A time-frequency plot of a section of AE wave associated with a surface defect showed a broad frequency range (100 to 600 kHz), see Figure 90. This shows the significant, high frequency content of AE associated with the bearing defect. A Gabor wavelet transform was employed to determine the time-frequency spectrum. For the wavelet analysis *AGU-Vallen Wavelet* software, developed by Vallen System GmbH, was employed [164].

In order to identify any modulating features, the envelope spectrum of the signals was generated using the Hilbert transform. The plots of envelope spectra for both tests are presented in Figure 91. Results from the first test show the presence of the BPF and its harmonics. Surprisingly, the presence of the defect frequency 175 Hz, was noted for all the timing intervals (A-F) although the magnitude of the peak increased with time reaching a maximum at the termination of the test. For the second test, the presence of the harmonics noted in the first test were not evident though the second and fourth harmonics were noted at the end of the test – time interval 'F'. The reason for the inadequate clarity in discriminating the harmonics and fault frequency is attributed to the presence of noise and therefore a lower signal-to-noise ratio than in Test-1. It is worth mentioning that, although the two tests were quite distinct in the level of SNR, the observation of the increase on two AE trends in Figure 75 and also the harmonics of BPF across the envelope spectrum upon the termination of both tests, clarifies the effective measurement of AE signals.

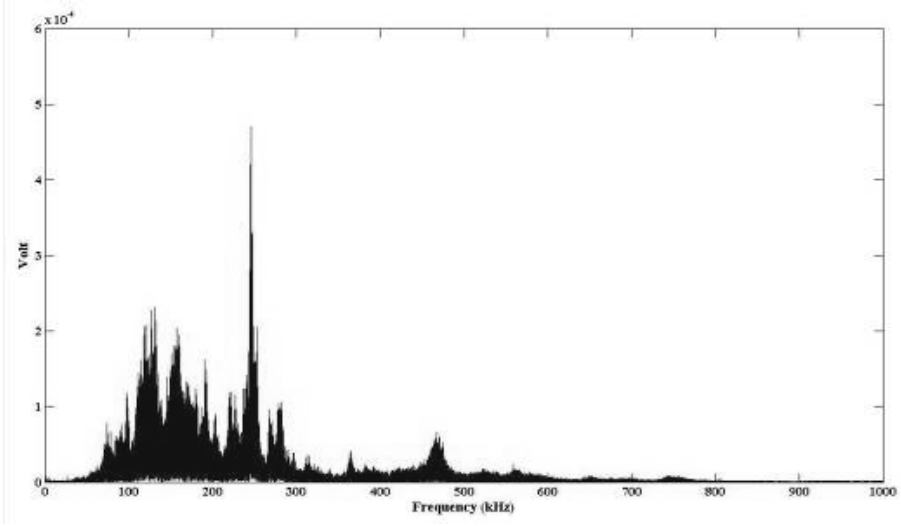

Figure 88 Frequency spectrum of the AE signal

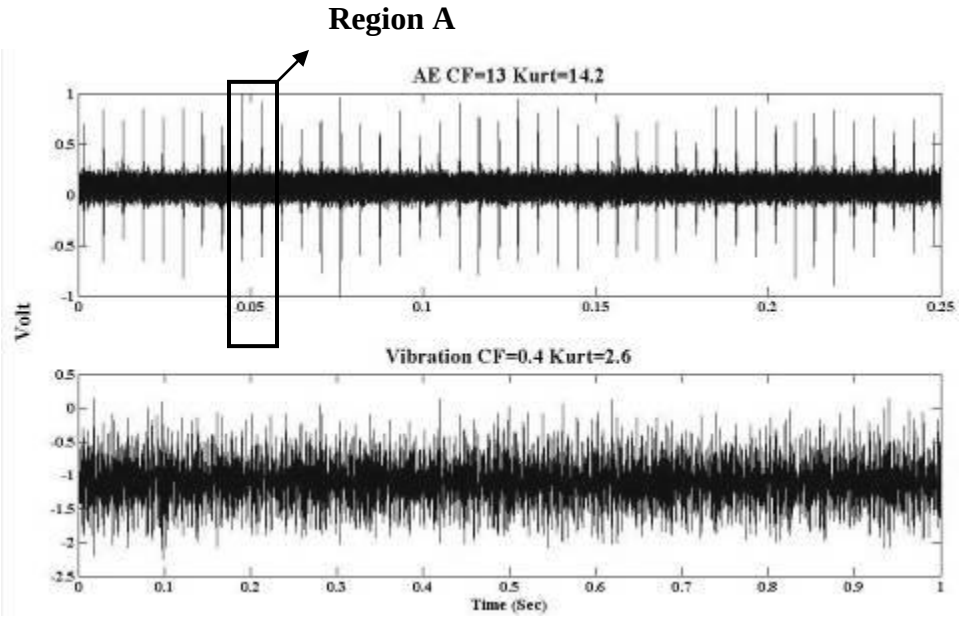

Figure 89 AE and vibration waveforms associated with Test-1

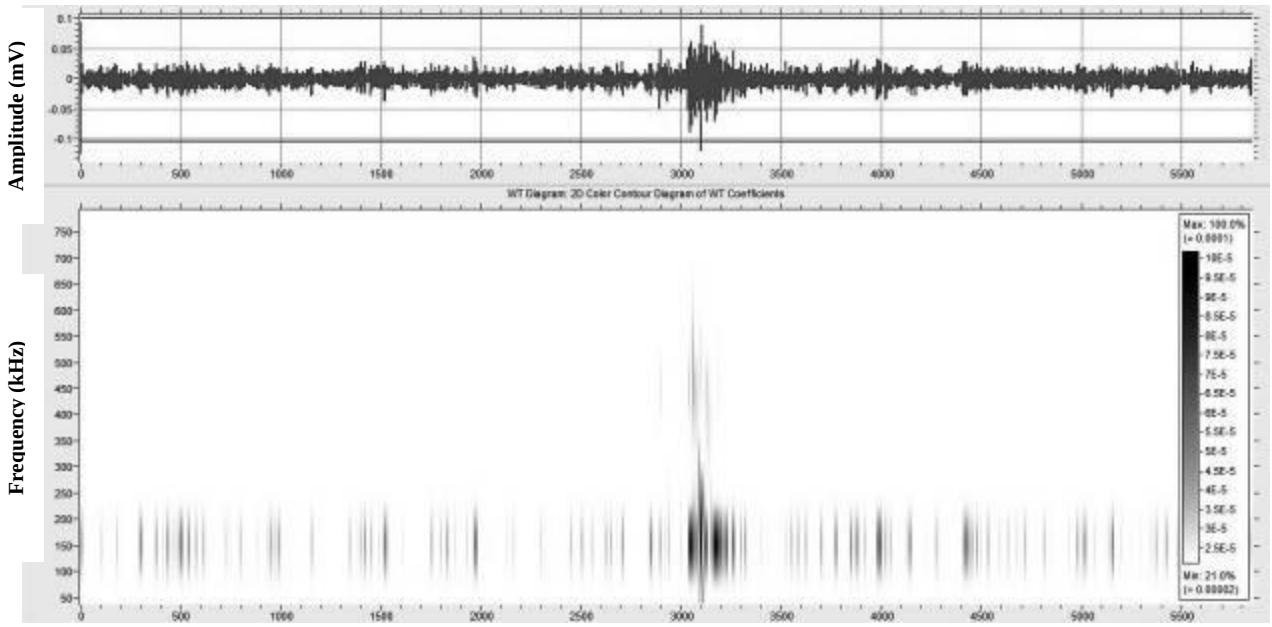

Figure 90 CWT associated with region A

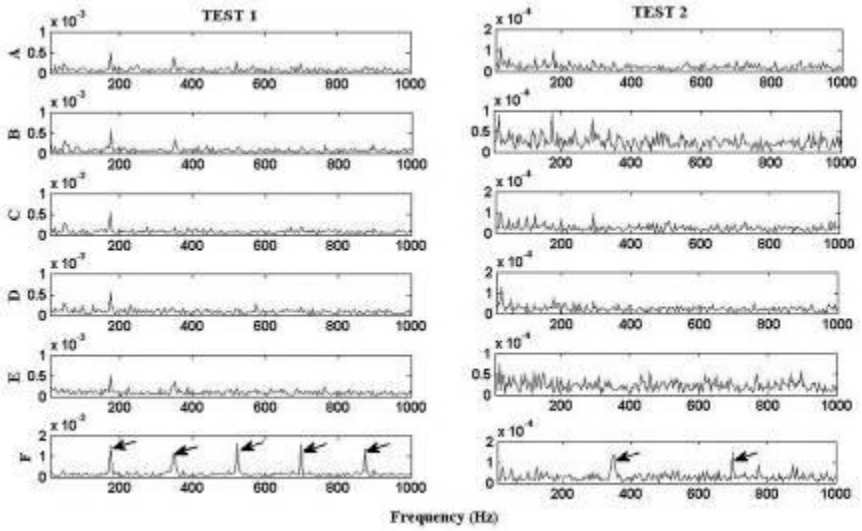

Figure 91 The AE envelope spectrum for the first and second tests

As with the vibration analysis, an SK analysis was undertaken for the AE waveforms. Table 16 shows the optimum frequency bands for time intervals 'A' to 'F'. According to this table, the optimum centre frequencies associated with the undamaged race (A-E) were outside the sensor measurement range. This is because, for the undamaged bearing, the higher frequencies within

the sensor measurement range are predominately Gaussian, so the maximum Kurtosis value occurs at the lower frequency range, below 30 kHz to 40 kHz.

Table 16 Optimum Bandwidth and Centre frequency for AE signal

	Test 1		***Test 2***	
	Fc (Hz)	$\log_2(Nw)$	Fc (Hz)	$\log_2(Nw)$
A	39062	7.5	31250	7
B	31250	7	31250	7.5
C	31250	7	65185	12.5
D	31250	7.5	31250	7.5
E	31250	7.5	15625	8
F	714843	8.5	61523	10.5

The filtered waveforms are presented in Figure 92, showing a significant improvement in the level of SNR compared with the unfiltered signals in Figure 87. This is also manifested in Figure 93 in which an average of approximately 242% and 95% increase in CF values were noted for the filtered signals on Test-1 and Test-2 respectively. Furthermore, Figure 94 illustrates the envelope spectrum of the filtered signals based on SK analysis. The BPF and its second harmonic were present across the frequency spectrum for both tests while such observations were not noted for the unfiltered envelope spectrum in Figure 91.

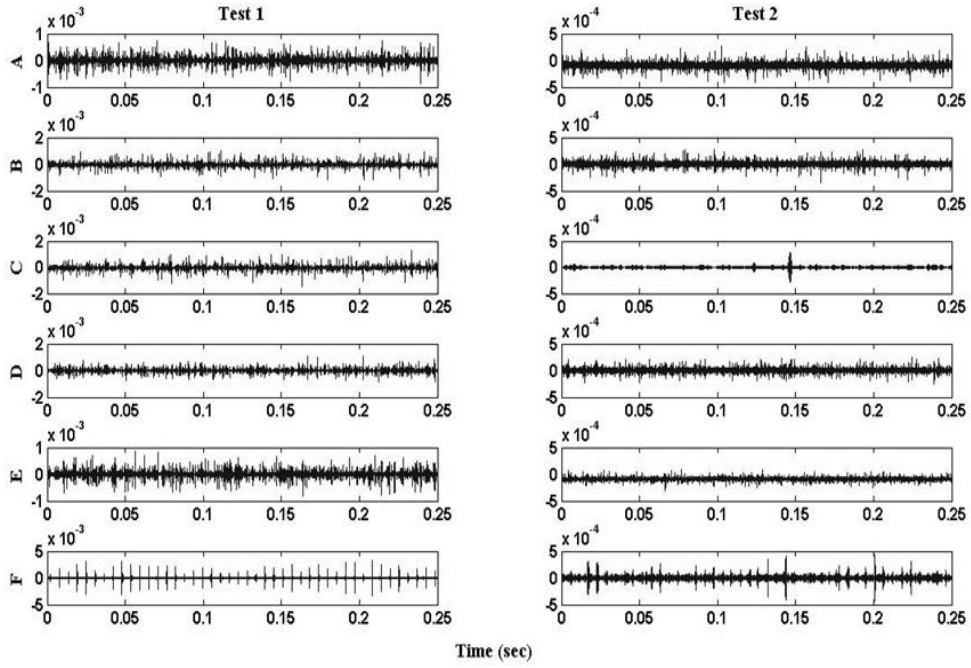

Figure 92 AE waveforms associated with filtered signals

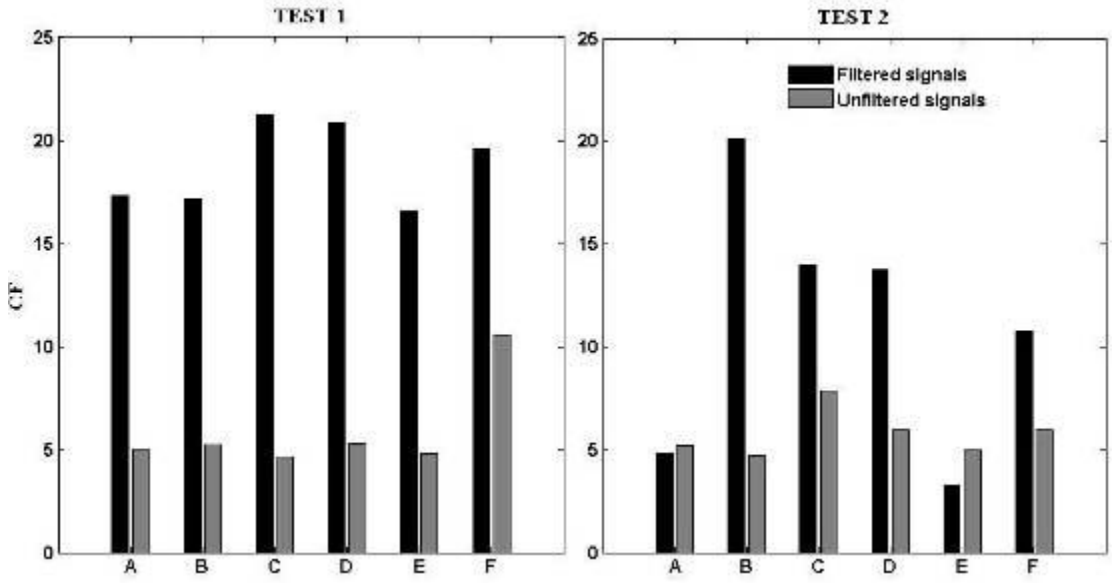

Figure 93 CF values associated with filtered and unfiltered signals

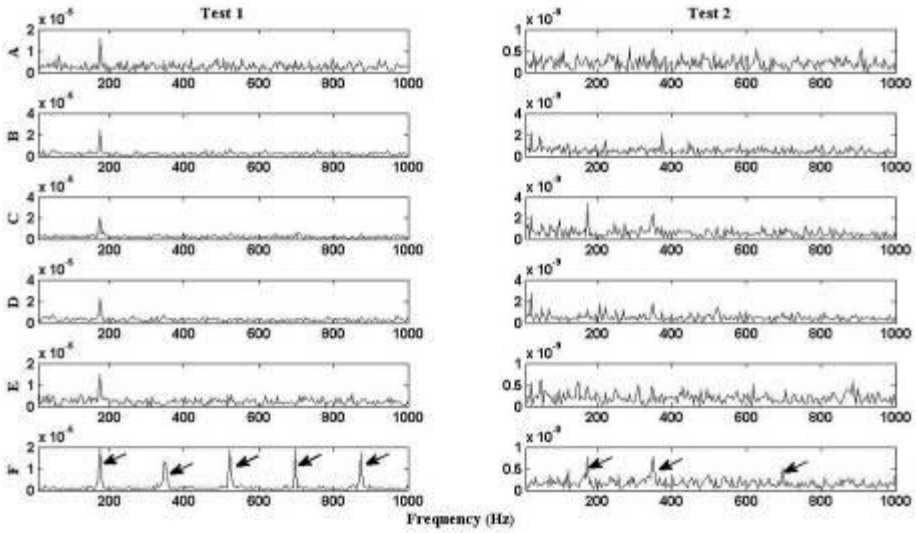

.

Figure 94 Envelope spectrum of the SK-based filtered signals

Having noted the improvement in signal-to-noise ratio, particularly for Test-2, the author compared the SK to wavelet-based filter analysis. The AE signals were decomposed using Daubechies wavelet of order 8 (db8). The envelope spectrum at each level of decomposition (D1-9) was carefully studied and level D1 (500 kHz - 1000 kHz) was found to be the most sensitive for identifying the presence of the defect. The envelope spectra of the signals at D1 are presented in Figure 95 in which BPF and its harmonics are evident upon the termination of both tests.

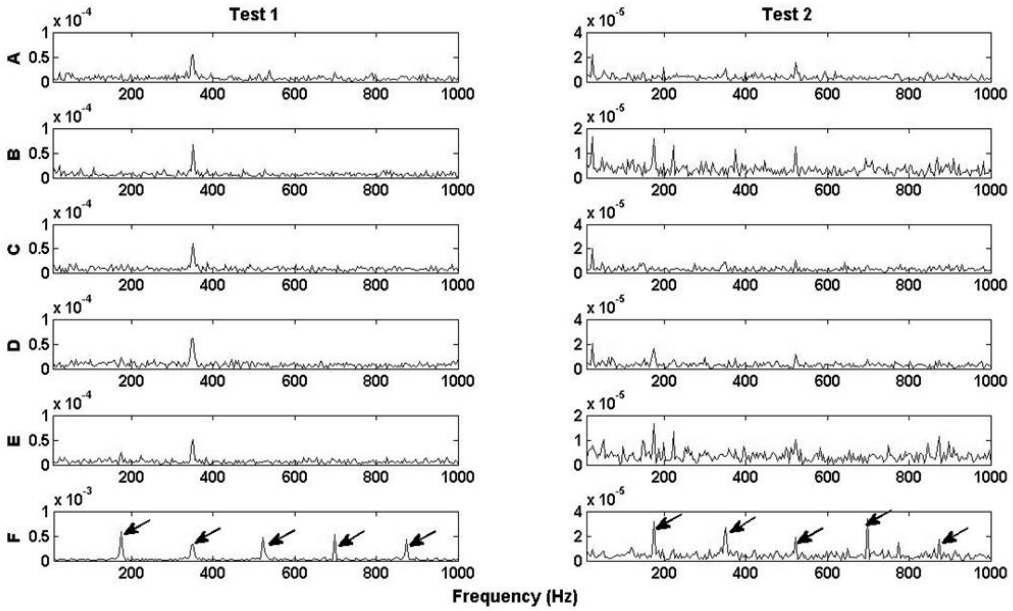

Figure 95 Envelope spectrum of the AE signals at D1

The CF values for the original filtered (SK) and decomposed (db8) signals are presented in Figure 96; this was compare the SNR ratio after band-pass filtering. In comparison to the original values of CF, the SK filtered signals showed an increase in CF of approximately 242% and 95% for Test-1 and Test-2 respectively. Crest factor values noted for decomposed signals (D1) were in the order of 18% and 70% for Test-1 and Test-2 respectively, implying that the SK offered the optimum filtered characteristics for identifying impulsive effects, which are typically associated with defective bearings. The waveforms, together with CF values at interval 'F' for D1, the original unfiltered waveform and the filtered waveform (SK), are also presented in Figure 97 in which the presence of impulsive AE events associated with the defective bearing are most evident for the SK filtered signals. There was only one instance where the wavelet based filter had a better CF than the SK filtered data (Test-1, interval 'F'). Although the defect frequency and its harmonics are clearly marked in the envelop spectrum presented in Figure 95, the level of signal to noise ratio for SK based filtering is relatively high .This observation reinforced the benefits of applying the SK for defect diagnosis for varying signal-to-noise ratios.

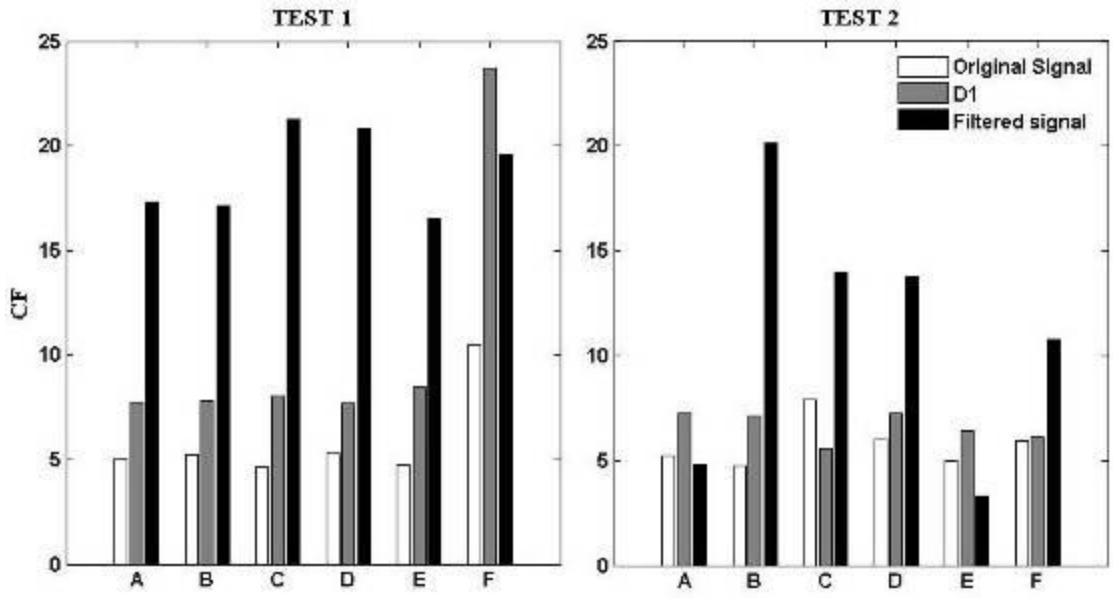

Figure 96 CF value attributed to different diagnostic methods

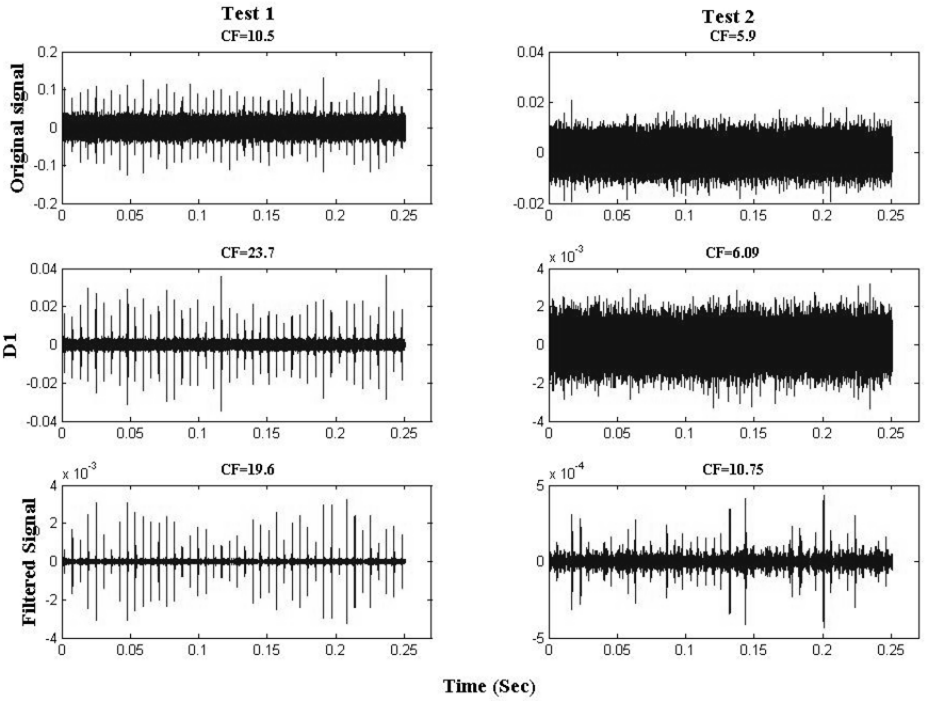

Figure 97 Comparison between D1 and filtered signals at interval 'F'

7.1.3 Bearing defect location

The most common method for source location involves employing differences in time of arrival of waves at the receiving sensor. Given the actual location of the AE sensor and the wave velocity for the bearing material, the location of the AE source can be determined. The sensor positions on the race allow linear location of the source to be calculated which involves linear interpolation between the coordinates of two adjacent sensors based on the differences in arrival time at the receiving sensors. After conducting the simulated AE source test (Hsu-Nielson) it was found that the dominant frequency of the AE signal registered to be approximately 300 kHz. This can be equivalent to a symmetric zeroth Lamb propagating with 4000 m/s on a steel surface [17]. The accuracy of this speed prediction was confirmed by performing several Hsu-Nielson tests on the different locations between each sensor. The locations of the simulated source were identified with 4% accuracy. For this investigation, a threshold of 70 dB was set and whenever the threshold was exceeded, the location of the source was computed and identified. Further, any AE event detected above this threshold was assigned to the geometric position (source); this is a cumulative process and as such a fixed source will have the largest number of contributory events in a cumulative plot. Figure 98 presents location results for Test-1 at three chosen time intervals. At 120mins and 180mins into operation the recorded events suggested activity in the vicinity of sensor 4; however, by 206mins into operation, a large number of AE events were registered between sensor-1 and sensor-2, suggesting the development of surface damage. The location of this abnormally high concentration of AE events matched the location of damage upon the termination of tests, see Figure 76 . The events noted earlier in the tests are attributed to spurious AE activity. At the start of Test-2, AE events were registered across the entire bearing circumference. This was clearly to be expected during the run-in phase as AE will be generated across the entire bearing circumference. However, by 15mins into operation, a significant increase in events, over 240 events, was noted between sensor-3 and sensor-4, see Figure 99, and by 23mins of operation a flurry of events between sensor-3 and sensor-4 were noted. This also matched the physical location of the defect upon inspection at the end of the tests. It should be noted that data for Test-2 after 23min is not available. This was due to the unexpected failure of data acquisition system.

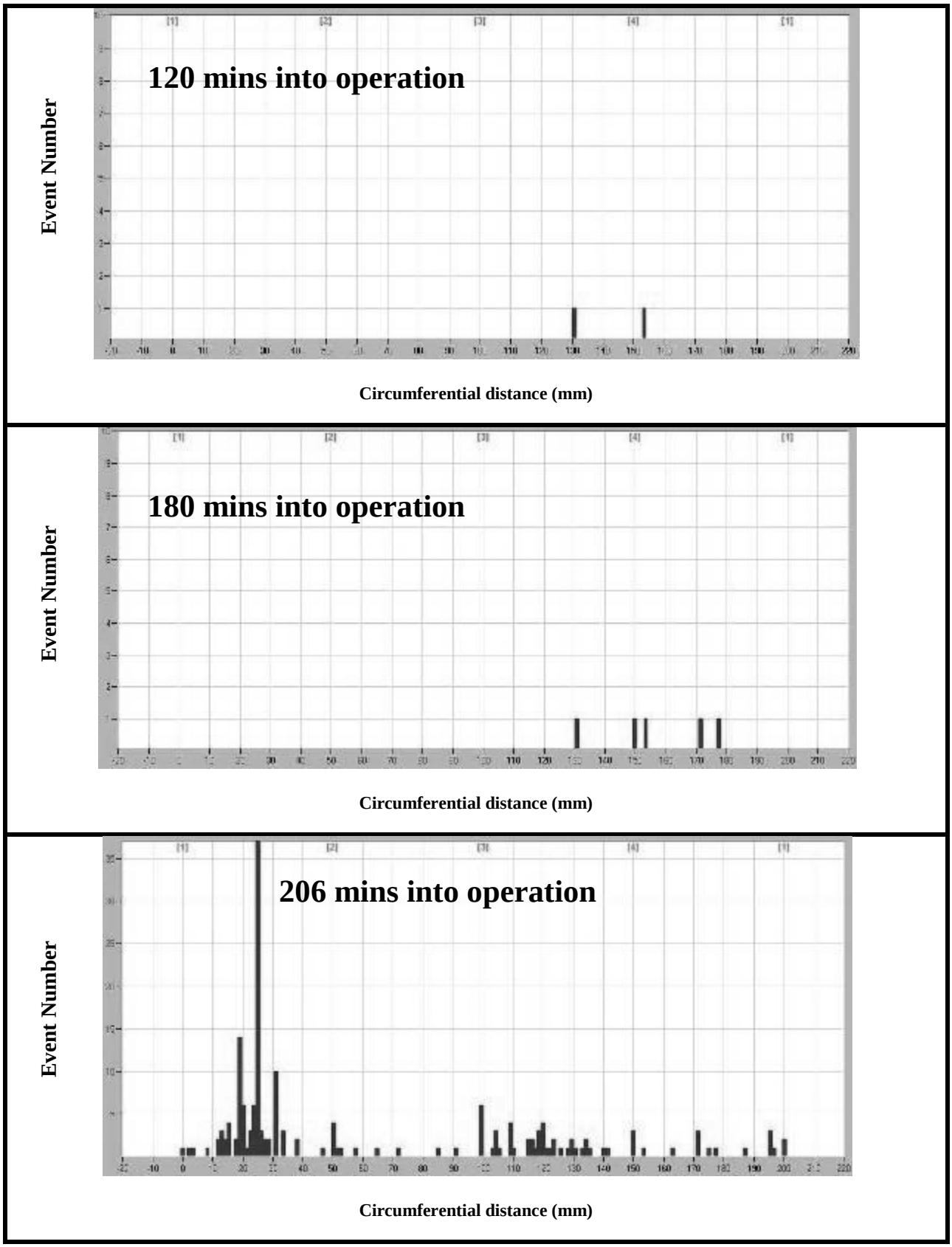

Figure 98 AE events against sensor position at different time intervals for Test-1

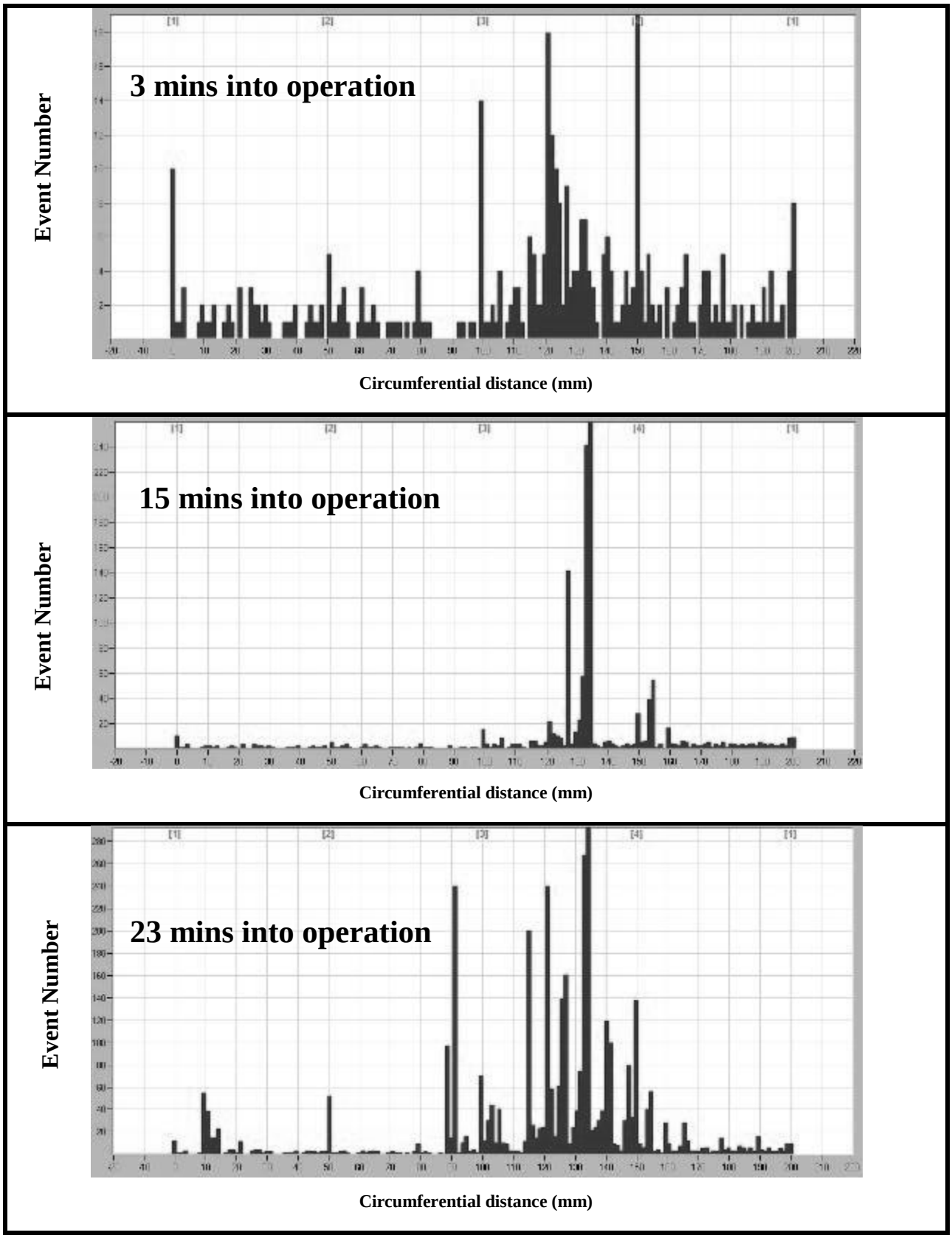

Figure 99 AE events against sensor position at different time intervals for Test-2

7.1.4 Conclusions

The applicability of both Acoustic Emission and vibration methods were studied in relation to defect identification of a naturally damaged bearing. From observation it was evident that AE was more sensitive in detecting incipient damage than vibration, reinforcing the findings of other investigators such as [13]. Furthermore, the application of SK analysis and Kurtograms was investigated and these showed the effectiveness in de-noising both AE and vibration signals. In relation to the defect prognosis, the applicability of AE for source location of bearing defect *in situ* has been demonstrated. Threshold levels above operating background levels have been shown to be sufficiently suitable for differentiating AE time-of-arrival intervals.

CHAPTER 8

8 Conclusions and Recommendations

8.1 Conclusion

This research has explored the application of AE in helical gear diagnosis. It has also investigated the use of new advanced signal processing techniques to analyze both AE and vibration signals. A series of test were conducted through which various types of defect and failures were monitored using AE and vibration.

In chapter 5 both seeded and natural defects on helical gears were monitored. In contrast with observation from spur gears [13, 94], AE and vibration technologies exhibited different diagnostic behavior. In section 5.1 it was observed that the transient AE bursts were noted to occur at the exact tooth where the defect was seeded. Also noted was the correlation between AE activities with the volume of material removed from the tooth surface. Monitoring the gradual degradation of the pinion teeth, see section 5.2, revealed some difficulties of monitoring the natural pitting with both AE and vibration. This implied that the application of advanced signal processing methods is necessary to achieve meaningful diagnosis information from AE and vibration signatures. In addition, it was found that AE possessed higher sensitivity in monitoring the seeded and natural defects as compared to vibration. This was in agreement with the similar comparative study on spur gears [13].

Chapter 6 reported on an experimental investigation in which several technologies such as AE, vibration and motor current signature analysis, were applied to identify the presence of a naturally fatigued pinion shaft in an operating gearbox. It was concluded that for this particular study a combination of these methods offers diagnostic information though successful diagnosis is very dependent on the diagnostic path taken by the investigator. Also was observed that side band energy at vicinity of GMF across the vibration spectrum registered increasing values upon the shaft fractures. Moreover, the application of envelope analysis on AE signatures revealed several harmonics of gear mesh frequency after the total loss of shaft mechanical integrity. In addition, the frequency spectrum of the enveloped AE response from the casing (sensor S2) showed the presence of the gear mesh frequency prior to fracture only. These observations present unique diagnostic capacities of AE measurements which hitherto have not been reported.

Chapter 7 provided an investigation which compared the applicability of AE and vibration technologies in monitoring a naturally degraded roller bearing. The work built on the research carried out by Elforjani and Mba on slow speed bearings [17]. It was confirmed that AE was more effective in the early diagnosis of the outer race spall as compared to vibration. Furthermore, the application of advanced signals processing techniques, such as Spectral Kurtosis, was studied on the AE and vibration signatures. It was found that band–pass filtering of both AE and vibration signal based on bandwidth and centre frequency derived from SK analysis can be a very effective tool to cancel the background noise level. This is particularly important to apply the effective envelop analysis to detect the bearing characteristic frequency. Although it is usually recommended to choose the bandwidth a few things the higher than the defect frequency of interest, the centre frequency at which the envelope analysis is carried out is selected based on the discretion of the user. The SK analysis provides an opportunity to automatically select the optimum centre frequency and bandwidth without any requirement for previous signal history and information about its frequency content. Along with advancements in silicon chips and digital technologies, the SK method can be utilized to develop intelligent condition monitoring systems which are capable of diagnosing the fault and setting an alarm reliably.

Also investigated was the defect localization capability of AET. The location of naturally occurred outer race spall was identified relative to the position of four AE Pico sensors mounted at the back of outer race. Threshold levels above operating background levels have been shown to be sufficiently suitable for differentiating AE time of arrivals intervals. The AE events number began to register high values upon the initiation of the defect. The location of this abnormally high concentration of AE events matched the location of damage upon the termination of test. This finding was first of its kind in assessing such quality of AET in a high speed application. Whilst the probability of having four AE sensors placed on a bearing race is limited it can be employed as a quality control measure for bearing manufacturers or applied on bespoke critical bearings.

In conclusion, this research has investigated different aspects of condition monitoring of gearboxes. It has been confirmed that AE is a strong diagnostic tool for early diagnosis of bearings faults. However, the application of condition monitoring for helical gear diagnosis was

fraught with some degree of complexity as compared to spur gears. This implies that condition monitoring of the gears using AET can be challenging. With the new test rig being built at Cranfield University, which aims to study worm gear diagnosis, it is expected that all aspects of AET in relation to gear diagnosis will be enlightened. On the contrary, the applicability of AET for bearing diagnosis was promising and it offered an absolute advantage over the conventional vibration diagnosis. Although effective, the author believes that AET cannot be replaced with vibration monitoring for bearing diagnosis. This is due to the fact that the effectiveness of AE can be influenced by a number of factors such as signal transmission path, sensor mounting and durability. However, it can be a complementary method to other condition monitoring technologies to ensure early and more reliable diagnosis of the bearing failures.

To conclude, the findings presented in this research aim to support ongoing investigations and to guide the future research of AET in the condition monitoring of gearboxes.

8.2 Future work and recommendation

Several aspects have been identified, which require further work and improvement. As such is the dependency between defect, surface roughness and AE activity; the surface roughness in meshing gears constantly changes due to pitting or spalling; the presence of pits or spall involves removal of material from the surface. Given the correlation between the volume of removed material and AE activity, it is an appropriate practice to achieve reasonable measures of change in surface roughness during a given time. This is thought to be an effective approach in improving the AE prognosis in relation to gears. To measure the surface roughness, the author suggests the use of a replica to cast the surface profile at regular intervals of the gearbox operation. The replica can be examined off-line using the surface profile meter.

Another key aspect of utilizing AET is the sensor placement. The tests explained in chapter 5 involved the measurement of AE signals only from the rotating pinion and bearing pedestal; due

to technical difficulties during the tests, measurements from other parts of the gearbox, i.e. casing, were not presented. Owing to the fact that, in practical application, gaining access to internal parts of the gearboxes is often associated with some limitation, it is therefore important to study the AE diagnosis from the gearbox casing. Since the signal from the gearbox casing typically experiences a high level of attenuation, it is expected that the captured signatures will exhibit lower SNR ratios, making defect identification more challenging.

The author sees the necessity of performing further tests focusing on shaft diagnosis. These tests would involve using the super finished and hardened gears to minimise the effect of pitting on induced vibration and generation of AE activity. To accelerate the shaft fatigue, the number of stress riser points can be maximised while the shaft diameter can be set to the minimum. The outcome is deemed to build on the presented research by studying the repeatability and reproducibility of the monitoring technology in detecting the fatigue crack. Furthermore, these tests are likely to offer unique opportunities to study the correlation between the growth of fatigue cracks and different signal features.

The use of the Kurtogram for AE bearing analysis was encouraging and it is hoped that future researchers will explore its full potential. The author also recommends that a similar study be performed on inner and roller defects to assess the effectiveness of SK methods in detecting such failures. To better simulate industrial condition, it is also suggested to run a similar bearing test, as explained in chapter 7, on a bearing placed inside a casing while the AE sensors are mounted on the bearing housing. The significance of this test would be to study the effect of attenuation on the diagnostic capability of an AE sensor. This will provide a reasonable opportunity to compare the effectiveness of both vibration and AE technologies.

References

[1] Rao, B.K.N., c1996., "Handbook of condition monitoring," Elsevier Advanced Technology, Oxford, pp. 603.

[2] Mine Safety and Health Administration, "Metal/Nonmetal Daily Fatality Report- Year End 2009,".

[3] Whitby, R. D., 2008, "Wind Turbine Gearbox Maintenance,".

[4] B. P. McNiff, W. D. Musial, and R. Errichello, 1990, "Variations in Gear Fatigue Life for Different Wind Turbine Braking Strategies," AWEA Wind Power 90, Anonymous Solar Energy Research Institute,.

[5] C. K. Tan, 2005, "An Investigation on the Diagnostic and Prognostic Capabilities of Acoustic Emission on Spur Gearbox,", PhD thesis, Cranfield University .

[6] Le Sueur, H. E., 1978, "AIRWORTHINESS OF HELICOPTERS." Aeronaut J, **82**(814) pp. 411-416.

[7] Hodges, D., and Pearce, J., 1995, "Gearbox Condition Monitoring," Gearing and gearbox practice today, ImechE, .

[8] M. Lebold, K. McClintic, R. Campbell, 2000, "Review of vibration analysis methods for gearbox diagnostics and prognostics," Proceedings of the 54th Meeting of the Society for Machinery Failure Prevention Technology, Virginia Beach, 634, ed. pp. 623.

[9] Ebersbach, S., Peng, Z., and Kessissoglou, N. J., 2006, "The Investigation of the Condition and Faults of a Spur Gearbox using Vibration and Wear Debris Analysis Techniques," Wear, **260**(1-2) pp. 16-24.

[10] Yesilyurt, I., Gu, F., and Ball, A. D., 2003, "Gear Tooth Stiffness Reduction Measurement using Modal Analysis and its use in Wear Fault Severity Assessment of Spur Gears," NDT and E International, **36**(5) pp. 357-372.

[11] Drosjack, M. J., and Houser, D. R., 1977, "EXPERIMENTAL AND THEORETICAL STUDY OF THE EFFECTS OF SIMULATED PITCH LINE PITTING ON THE VIBRATION OF A GEARED SYSTEM," American Society of Mechanical Engineers (Paper), (77-) pp. 11.

[12] Mba, D., and Rao, R. B. K. N., 2006, "Development of Acoustic Emission Technology for Condition Monitoring and Diagnosis of Rotating Machines: Bearings, Pumps, Gearboxes, Engines, and Rotating Structures," Shock and Vibration Digest, **38**(1) pp. 3-16.

[13] Tan, C. K., Irving, P., and Mba, D., 2007, "A Comparative Experimental Study on the Diagnostic and Prognostic Capabilities of Acoustics Emission, Vibration and Spectrometric Oil Analysis for Spur Gears," Mechanical Systems and Signal Processing, **21**(1) pp. 208-233.

[14] Tan, C. K., and Mba, D., 2005, "Limitation of Acoustic Emission for Identifying Seeded Defects in Gearboxes," Journal of Nondestructive Evaluation, **24**(1) pp. 11-28.

[15] Elforjani, M., and Mba, D., 2008, "Observations and Location of Acoustic Emissions for a Naturally Degrading Rolling Element Thrust Bearing," Journal of Failure Analysis and Prevention, **8**(4) pp. 370-385.

[16] Elforjani, M., and Mba, D., 2009, "Detecting Natural Crack Initiation and Growth in Slow Speed Shafts with the Acoustic Emission Technology," Engineering Failure Analysis, **16**(7) pp. 2121-2129.

[17] Elforjani, M., and Mba, D., 2009, "Assessment of Natural Crack Initiation and its Propagation in Slow Speed Bearings," Nondestructive Testing and Evaluation, **24**(3) pp. 261.

[18] Shigley, J.E., Mischke, C.R., Brown, Thomas H. (Thomas Hunter), 1947-, c2004, "Standard handbook of machine design electronic resource," McGraw-Hill, New York, .

[19] Seireg, A., and Dooner, D.B., c1995., "The kinematic geometry of gearing," Wiley, New York ; Chichester, pp. 450.

[20] Marshall AW, 1977, "Gear Wheels and Gear Cutting," Model & Allied Publications, Watford,UK, .

[21] Drago, T., 1988., "Fundamentals of gear design," Butterworths, Boston ; London, .

[22] Raja Hamzah, R. I., and Mba, D., 2009, "The Influence of Operating Condition on Acoustic Emission (AE) Generation during Meshing of Helical and Spur Gear," Tribology International, **42**(1) pp. 3-14.

[23] Asi, O., 2006, "Fatigue Failure of a Helical Gear in a Gearbox," Engineering Failure Analysis, **13**(7) pp. 1116-1125.

[24] Powell, G.W., and American Society for Metals., 1986., "ASM handbook." American Society for Metals, Metals Park, Ohio, pp. 843.

[25] DiMatteo, N.D., and ASM International. Handbook Committee., c1996., "Fatigue and fracture," ASM International, Materials Park, O, pp. 1057.

[26] Fernandes, P. J. L., and McDuling, C., 1997, "Surface Contact Fatigue Failures in Gears," Engineering Failure Analysis, **4**(2) pp. 99-107.

[27] British Standard, 1986, "BSI BS 436-3-Spur and Helical Gears,Part 3:Method for Calculation of Contact and Root Bending Stress Limitations for Metallic Involute Gears." .

[28] ISO, 1996, "6336-2:2006-Calcualtion of Load Capacity of Spur and Helical Gears,Part 2: Calculation of the Surface Durability of Gears(Pitting)," .

[29] American National Standard, 1995, "ANSI/AGMA 2101-C95-Fundumental Rating Factors and Calculation Methods for Involute Spur and Helical Gear Teeth.".

[30] Hutchings, I.M., 1992., "Tribology : friction and wear of engineering materials," Edward Arnold, London, pp. 273.

[31] Stachowiak, G., and Batchelor, A.W., 2000, "Engineering Tribology," Elsevier Butterworth-Heinemann, pp. 1-750.

[32] Scott, D., 1973, "Bearing Failures Diagnosis and Investigation," Wear, **25**(2) pp. 199-213.

[33] Stolarski, T.A., and Knovel, (., 2000, c1990, "Tribology in machine design electronic resource," Butterworth Heinemann, Oxford England ; Boston, pp. 298.

[34] GE Energy Co. http://www.gepower.com.

[35] Neale, M.J. and Knovel J., 1995, "The tribology handbook electronic resource," Butterworth-Heinemann, Oxford, England ; Boston, .

[36] BS 5512:1991, "Method of Calculating Dynamic Load Ratings and Rating Life of Rolling Bearings," (BS 5512:1991) .

[37] Buschow, K.H.J., 2001, "Encyclopedia of materials : science and technology." Elsevier, Amsterdam ; London, pp. 872.

[38] Harris, T.A., 1966, "Rolling bearing analysis," Wiley, New York, pp. 481.

[39] Erwin V.Zaretsky, 1997, "A.Palmgren Revisited-A basis for bearing life prediction," NASA Technical Memorandom, 107440, Kansas City,Missouri.

[40] Bhaumik, S. K., Rangaraju, R., Parameswara, M. A., 2002, "Fatigue Failure of a Hollow Power Transmission Shaft," Engineering Failure Analysis, **9**(4) pp. 457-467.

[41] American Society for Metals., and Lyman, T., 1961, "Metals handbook," American Society for Metals, Metals Park, Ohio, pp. 1300.

[42] Berndt, F., and Van Bennekom, A., 2001, "Pump Shaft Failures - a Compendium of Case Studies," Engineering Failure Analysis, **8**(2) pp. 135-144.

[43] Yacamini, R., Smith, K. S., and Ran, L., 1998, "Monitoring Torsional Vibrations of Electro-Mechanical Systems using Stator Currents," Journal of Vibration and Acoustics, Transactions of the ASME, **120**(1) pp. 72-79.

[44] Dyer, D., and Stewart, R. M., 1977, "DETECTION OF ROLLING ELEMENT BEARING DAMAGE BY STATISTICAL VIBRATION ANALYSIS." American Society of Mechanical Engineers (Paper), (77 -DET-83) .

[45] Behzad, M., AlandiHallaj, A., Bastami, A. R., 2009, "Defect Size Estimation in Rolling Element Bearings using Vibration Time Waveform," Insight: Non-Destructive Testing and Condition Monitoring, **51**(8) pp. 426-430.

[46] Ananthram Swami, Jerry M. Mendel, and Chrysostomos L. Nikias, 1995, "Higher-Order Spectral Analysis Toolbox," The Math Works ,Inc., USA, .

[47] Davies, A., 1947-, 1998, "Handbook of condition monitoring : techniques and methodology," Chapman & Hall, London, pp. 565.

[48] Braun, S. G., 1980, "SIGNATURE ANALYSIS OF SONIC BEARING VIBRATIONS." IEEE Transactions on Sonics and Ultrasonics, **SU-27**(6) pp. 317-328.

[49] Newland, D.E., 1984, "An introduction to random vibrations and spectral analysis." Longman, Harlow, .

[50] Jafarizadeh, M. A., Hassannejad, R., Ettefagh, M. M., 2008, "Asynchronous Input Gear Damage Diagnosis using Time Averaging and Wavelet Filtering," Mechanical Systems and Signal Processing, **22**(1) pp. 172-201.

[51] Crystal Instruments Co,www.go-ci.com, "Time Synchronous Averaging,".

[52] Tandon, N., and Choudhury, A., 1999, "Review of Vibration and Acoustic Measurement Methods for the Detection of Defects in Rolling Element Bearings," Tribology International, **32**(8) pp. 469-480.

[53] Smith, S., 2002, "Digital Signal Processing: A Practical Guide for Engineers and Scientists," Elsevier Newnes, pp. 1-672.

[54] Peng, Z., Kessissoglou, N. J., and Cox, M., 2005, "A Study of the Effect of Contaminant Particles in Lubricants using Wear Debris and Vibration Condition Monitoring Techniques," Wear, **258**(11-12) pp. 1651-1662.

[55] Meng, Q., and Qu, L., 1991, "Rotating Machinery Fault Diagnosis using Wigner Distribution," Mechanical Systems and Signal Processing, **5**(3) pp. 155-166.

[56] La Cour-Harbo, A.(., 1973-, c2001., "Ripples in mathematics : the discrete wavelet transform," Springer, Berlin ; London, pp. 246.

[57] Debnath, L., 1935-, c2002., "Wavelet transforms and their applications," BirkhaÌˆuser, Boston, pp. 565.

[58] Serrano, E. P., and Fabio, M. A., 1996, "Application of the Wavelet Transform to Acoustic Emission Signals Processing," IEEE Transactions on Signal Processing, **44**(5) pp. 1270-1275.

[59] Gomez, M. P., Piotrkowski, R., Ruzzante, J. E., 2007, "Estimation of the tool condition by applying the wavelet transform to acoustic emission signals," Review of Progress in Quantitative Non-destructive Evaluation, AIP, Portland, OR, USA, **894,** pp. 635-41.

[60] Chen, C., Kovacevic, R., and Jandgric, D., 2003, "Wavelet Transform Analysis of Acoustic Emission in Monitoring Friction Stir Welding of 6061 Aluminum," International Journal of Machine Tools and Manufacture, **43**(13) pp. 1383-1390.

[61] Tse, P. W., Yang, W., and Tam, H. Y., 2004, "Machine Fault Diagnosis through an Effective Exact Wavelet Analysis," Journal of Sound and Vibration, **277**(4-5) pp. 1005-1024.

[62] Rafiee, J., Rafiee, M. A., and Tse, P. W., 2010, "Application of Mother Wavelet Functions for Automatic Gear and Bearing Fault Diagnosis," Expert Systems with Applications, **37**(6) pp. 4568-4579.

[63] McInerny, S. A., and Dai, Y., 2003, "Basic Vibration Signal Processing for Bearing Fault Detection," Education, IEEE Transactions on, **46**(1) pp. 149-156.

[64] Samuel, P. D., and Pines, D. J., 2005, "A Review of Vibration-Based Techniques for Helicopter Transmission Diagnostics," Journal of Sound and Vibration, **282**(1-2) pp. 475-508.

[65] R.M. Stewart, 1977, "Some useful analysis techniques for gearbox diagnostics," MHM/R/10/77, Machine Health Monitoring Group, Institute of Sound and Vibration Research,University of southampton.

[66] McFadden, P. D., 1986, "DETECTING FATIGUE CRACKS IN GEARS BY AMPLITUDE AND PHASE DEMODULATION OF THE MESHING VIBRATION." Journal of Vibration, Acoustics, Stress, and Reliability in Design, **108**(2) pp. 165-170.

[67] Rangarao, K.V., Mallik, R.K., and Knovel., c2005, "Digital signal processing electronic resource : a practitioner's approach," John Wiley, Chichester, England ; Hoboken, NJ, pp. 191.

[68] Shin, K., and Hammond, J.K., c2008, "Fundamentals of signal processing for sound and vibration engineers," Wiley ; John Wiley distributor, Hoboken, N.J. : Chichester, pp. 403.

[69] Randall, R. B., 2005, "Applications of Spectral Kurtosis in Machine Diagnostics and Prognostics," Key Engineering Materials, **293-294** pp. 21-30.

[70] Dwyer, R. F., 1983, "A Technique for Improving Detection and Estimation of Signals Contaminated by Under Ice Noise." Journal of the Acoustical Society of America, **74**(1) pp. 124-130.

[71] Antoni, J., 2006, "The Spectral Kurtosis: A Useful Tool for Characterising Non-Stationary Signals," Mechanical Systems and Signal Processing, **20**(2) pp. 282-307.

[72] Antoni, J., and Randall, R. B., 2006, "The Spectral Kurtosis: Application to the Vibratory Surveillance and Diagnostics of Rotating Machines," Mechanical Systems and Signal Processing, **20**(2) pp. 308-331.

[73] Antoni, J., 2007, "Fast Computation of the Kurtogram for the Detection of Transient Faults," Mechanical Systems and Signal Processing, **21**(1) pp. 108-124.

[74] Miller, R.K., 1987, "Nondestructive testing handbook : volume 5 acoustic emission testing," ASNT, pp. 603.

[75] Anderson, R., "Some mechanical properties of duralumin sheet as affeted by heat treatment," Twenty-ninth annual meeting of the American society for testing materials, American society for testing materials, **26,** pp. 349-377.

[76] Holroyd, T.M., 2000., "The acoustic emission & ultrasonic monitoring handbook," Coxmoor Pub. Co., Oxford, pp. 147.

[77] Balderston, H. L., "The detection of incipient failure of bearings," 28th ASNT National Fall Conference, Oct 14-17,1968 Detroit,.

[78] Board, D. B., "Incipient failure detection in high speed machinery," 10th Symposium on NDE,23-25 April 1975,San Antonio,.

[79] Bloch, H. P., Oct 1977, "Predict Problems with Acoustic Incipient Failure Detection Systems," Hydrocarbon Processing, pp. 191-198.

[80] Williams, R.V., c1980, "Acoustic emission," Hilger, Bristol, pp. 118.

[81] Physical Acoustic Co., 2007, "PCI-2 BASED AE SYSTEM USERS's MANUAL," .

[82] Matthews, J.R., c1983., "Acoustic emission," Gordon and Breach Science, New York, pp. 167.

[83] Wheitner, J., Houser, D., and Blazakis, C., 1993, "Gear tooth bending fatigue crack detection by acoustic emission and tooth compliance," ASME, 93FTM9,.

[84] R. W. Buenneke, M. B. Slane, C. R. Dunham, 1982, "Gear Single Tooth Bending Fatigue Test," .

[85] Miyachika K., Oda S., and Koide T., 1995, "Acoustic Emission of Bending Fatigue Process of Spur Gear Teeth," Journal of Acoustic Emission, **13**(1/2) pp. S47-S53.

[86] Miyachika K., Zheng, Y., Tsubokura, K., 2002, "Acoustic Emission of bending fatigue process of supercarburized spur gear teeth," Progress in Acoustic Emission *XI*, Anonymous The Japanese Society for NDI, pp. 304-310.

[87] Singh, A., Houser, D. R., and Vijayakar, S., 1999, "Detecting Gear Tooth Breakage using Acoustic Emission: A Feasibility and Sensor Placement Study," Journal of Mechanical Design, Transactions of the ASME, **121**(4) pp. 587-593.

[88] E.Siores, and E.Negro, 1997, "Condition Monitoring of Gear Box using Acoustic Emission Testing," Material Evaluation, **55**(2) pp. 183-184,185,186,187.

[89] Singh, A., Houser, D. R., and Vijayakar, S., 1996, "Early detection of gear pitting," Proceedings of the 1996 7th International Power Transmission and Gearing Conference, ASME, New York, NY, USA, San Diego, CA, USA, **88,** pp. 673-678.

[90] Amani RAAD, Fan ZHANG, Bob RANDALL, 2003, "On the comparison of the use of AE and vibration analysis for early gear fault detection," The Eight Western Pacific Acoustics Conference, Melbourne Australia.

[91] H. Sentoku, 1998, "AE in Tooth Surface Failure Process of Spur Gears," Journal of Acoustic Emission 16, **1-4**pp. S19-S24.

[92] Badi, M. N. M., Engin, S. N., and Schonfeld, D., 1996, "Fault classification of a model driveline using time domain data," COMADEM 1996, University of Sheffield- UK, pp. 43-50.

[93] Tandon.N, and Mata.S, 1999, "Detection of Defects in Gears by Acoustic Emission Measurements," Journal of Acoustic Emission, **17**(1-2) pp. 23-24,25,26,27.

[94] Toutountzakis, T., Tan, C. K., and Mba, D., 2005, "Application of Acoustic Emission to Seeded Gear Fault Detection," NDT and E International, **38**(1) pp. 27-36.

[95] Tan, C. K., and Mba, D., 2005, "Identification of the Acoustic Emission Source during a Comparative Study on Diagnosis of a Spur Gearbox," Tribology International, **38**(5) pp. 469-480.

[96] Al-Balushi, K. R., and Samanta, B., 2002, "Gear Fault Diagnosis using Energy-Based Features of Acoustic Emission Signals," Proceedings of the Institution of Mechanical Engineers.Part I: Journal of Systems and Control Engineering, **216**(3) pp. 249-263.

[97] Al-Balushi, K. R., 1995, "The use of High Stress Waves for Monitoring Gears,", Thesis, Cranfield University .

[98] Loutas, T. H., Sotiriades, G., Kalaitzoglou, I., 2009, "Condition Monitoring of a Single-Stage Gearbox with Artificially Induced Gear Cracks Utilizing on-Line Vibration and Acoustic Emission Measurements," Applied Acoustics, **70**(9) pp. 1148-1159.

[99] Loutas, T. H., Kalaitzoglou, J., Sotiriades, G., 2006, "Diagnosis of Artificial Gear Defects on Single Stage Gearbox using Acoustic Emission," Advanced Materials Research, **13-14**pp. 415-420.

[100] Loutas, T. H., Kalaitzoglou, J., Sotiriades, G., 2008, "A Novel Approach for Continuous Acoustic Emission Monitoring on Rotating Machinery without the use of Slip Ring," Journal of Vibration and Acoustics, Transactions of the ASME, **130**(6) .

[101] Tan, C. K., and Mba, D., 2006, "A Correlation between Acoustic Emission and Asperity Contact of Spur Gears Under Partial Elastohydrodynamic Lubrication," International Journal of COMADEM, **9**(1) pp. 9-14.

[102] Boness, R. J., and McBride, S. L., 1991, "Adhesive and Abrasive Wear Studies using Acoustic Emission Techniques," Wear, **149**(1-2) pp. 41-53.

[103] Boness, R. J., McBride, S. L., and Sobczyk, M., 1990, "Wear Studies using Acoustic Emission Techniques," Tribology International, **23**(5) pp. 291.

[104] Raja Hamzah, R. I., and Mba, D., 2008, "Acoustic Emission and Specific Film Thickness (λ) for Spur Gears," Insight: Non-Destructive Testing and Condition Monitoring, **50**(11) pp. 642-644.

[105] Raja Hamzah, R. I., and Mba, D., 2008, "Acoustic emission and elastohydrodynamic film thickness for meshing of spur and helical gears," 2007 Proceedings of the ASME International Design Engineering Technical Conferences and Computers and Information in Engineering Conference, DETC2007 **7,** pp. 553-556.

[106] Raja Hamzah, R. I., 2008, "Condition Monitoring of Spur and Helical Gears using Acoustic Emission (AE) Technology,", PhD thesis, Cranfield University .

[107] Catlin, J. B. J., 1983, "The use of ultrasonic diagnostic technique to detect rolling element bearing defects," Machinery and vibration monitoring and analysis meeting, Proceedings - Machinery Vibration Monitoring and Analysis Seminar and Meeting ,Vibration institute, pp. 123-130

[108] Rogers, L. M., 1979, "The Application of Vibration Analysis and Acoustic Emission Source Location to Online Condition Monitoring of Anti Friction Bearings," Tribology International, **12**(2) pp. 51-59.

[109] Tandon, N., and Nakra, B., 1990, "Defect Detection of Rolling Element Bearings by Acoustic Emission Method," Journal of Acoustic Emission, **9**(1) pp. 25-28.

[110] Choudhury, A., and Tandon, N., 2000, "Application of Acoustic Emission Technique for the Detection of Defects in Rolling Element Bearings," Tribology International, **33**(1) pp. 39-45.

[111] Tan, C. C., 1990, "Application of acoustic emission to the detection of bearing failures," National Conference Publication - Institution of Engineers, Australia (90 pt 14), pp. 110-114.

[112] Yoshioka, T., Korenaga, A., Mano, H., 1999, "Diagnosis of Rolling Bearing by Measuring Time Interval of AE Generation," Journal of Tribology, **121**(3) pp. 468-472.

[113] Morhain, A., and Mba, D., 2003, "Bearing Defect Diagnosis and Acoustic Emission," Proceedings of the Institution of Mechanical Engineers, Part J: Journal of Engineering Tribology, **217**(4) pp. 257-272.

[114] Sakishima, H., Nagatomo, T., Ikeda, H., 2000, "Measurement of Acoustic Emission and Vibration of Rolling Bearings with an Artificial Defect," Quarterly Report of RTRI (Railway Technical Research Institute) (Japan), **41**(3) pp. 127-130.

[115] Price, E. D., 2001, "Application of High Frequency Monitoring for Classification of Rolling Element Bearing Failures," Key Engineering Materials, (204-205) pp. 173-182.

[116] Shiroishi, J., Li, Y., Liang, S., 1997, "Bearing Condition Diagnostics Via Vibration and Acoustic Emission Measurements," Mechanical Systems and Signal Processing, **11**(5) pp. 693-705.

[117] Al-Ghamdi, A. M., Cole, P., Such, R., 2004, "Estimation of Bearing Defect Size with Acoustic Emission," Insight: Non-Destructive Testing and Condition Monitoring, **46**(12) pp. 758-761.

[118] Al-Ghamd, A. M., and Mba, D., 2006, "A Comparative Experimental Study on the use of Acoustic Emission and Vibration Analysis for Bearing Defect Identification and Estimation of Defect Size," Mechanical Systems and Signal Processing, **20**(7) pp. 1537-1571.

[119] Al-Dossary, S., Hamzah, R. I. R., and Mba, D., 2009, "Observations of Changes in Acoustic Emission Waveform for Varying Seeded Defect Sizes in a Rolling Element Bearing," Applied Acoustics, **70**(1) pp. 58-81.

[120] Li, Y., Billington, S., Zhang, C., 1999, "Dynamic Prognostic Prediction of Defect Propagation on Rolling Element Bearings," Tribology Transactions, **42**(2) pp. 385-392.

[121] Sundt, P. C., 1979, "MONITORING ACOUSTIC EMISSION TO DETECT MECHANICAL DEFECTS." INTECH, **26**(12) pp. 43-44.

[122] Barclay, J., and Bannach, R., 1992, "Multiparameter condition monitoring," Noise and Vibration Worldwide, .

[123] Jamaludin N., M. D., 2001, "Condition Monitoring of Slow-Speed Rolling Element Bearings using Stress Waves," Proceedings of the Institution of Mechanical Engineers, Part E: Journal of Process Mechanical Engineering, **215**(4) pp. 245-271.

[124] WILLIAMS, T., RIBADENEIRA, X., BILLINGTON, S., 2001, "ROLLING ELEMENT BEARING DIAGNOSTICS IN RUN-TO-FAILURE LIFETIME TESTING," Mechanical Systems and Signal Processing, **15**(5) pp. 979-993.

[125] Elforjani, M., and Mba, D., 2010, "Accelerated Natural Fault Diagnosis in Slow Speed Bearings with Acoustic Emission," Engineering Fracture Mechanics, **77**(1) pp. 112-127.

[126] Couturier, J., and Mba, D., 2008, "Operational Bearing Parameters and Acoustic Emission Generation," Journal of Vibration and Acoustics, Transactions of the ASME, **130**(2).

[127] Tavakoli, M. S., 1991, "Review of bearing monitoring-Application of Acoustic Emission," 1st international conference on Acoustic Emission in manufacturing, Boston, MA, pp31-34.

[128] Miettinen, J., and Andersson, P., 2000, "Acoustic Emission of Rolling Bearings Lubricated with Contaminated Grease," Tribology International, **33**(11) pp. 777-787.

[129] Jamaludin, N., Mba, D., and Bannister, R. H., 2002, "Monitoring the Lubricant Condition in a Low-Speed Rolling Element Bearing using High Frequency Stress Waves," Proceedings of the Institution of Mechanical Engineers, Part E: Journal of Process Mechanical Engineering, **216**(2) pp. 73-88.

[130] Choy, F. K., Polyshchuk, V., Zakrajsek, J. J., 1996, "Analysis of the Effects of Surface Pitting and Wear on the Vibration of a Gear Transmission System," Tribology International, **29**(1) pp. 77-83.

[131] McFadden, P. D., 1989, "Interpolation Techniques for Time Domain Averaging of Gear Vibration," Mechanical Systems and Signal Processing, **3**(1) pp. 87-97.

[132] F. ISMAIL, H. MARTIN, F. OMAR, 1995, Proceedings of the ASME Biennial Conference on Vibration and Noise, DE-84-1, 1413, 1418, A statistical index for monitoring tooth cracks in a gearbox.

[133] Sabnavis, G., Kirk, R. G., Kasarda, M., 2004, "Cracked Shaft Detection and Diagnostics: A Literature Review," Shock and Vibration Digest, **36**(4).

[134] Maxwell, J. H., 1988, "Detecting cracked reactor coolant pump shafts with vibration monitoring," American Society of Mechanical Engineers (Paper) , pp. PVP11 6p.

[135] Lazzeri, L., Cecconi, S., Faravelli, M., 1992, "Second harmonic vibration monitoring of a cracked shaft in a turbogenerator," Proceedings of the American Power Conference , **54,** pp. 1337-1342.

[136] Prabhakar, S., Mohanty, A. R., and Sekhar, A. S., 2002, "Application of Discrete Wavelet Transform for Detection of Ball Bearing Race Faults," Tribology International, **35**(12) pp. 793-800.

[137] Combet, F., and Gelman, L., 2009, "Optimal Filtering of Gear Signals for Early Damage Detection Based on the Spectral Kurtosis," Mechanical Systems and Signal Processing, **23**(3) pp. 652-668.

[138] Barszcz, T., and Randall, R. B., 2009, "Application of Spectral Kurtosis for Detection of a Tooth Crack in the Planetary Gear of a Wind Turbine," Mechanical Systems and Signal Processing, **23**(4) pp. 1352-1365.

[139] Immovilli, F., Cocconcelli, M., Bellini, A., 2009, "Detection of Generalized-Roughness Bearing Fault by Spectral-Kurtosis Energy of Vibration Or Current Signals," IEEE Transactions on Industrial Electronics, **56**(11) pp. 4710-4717.

[140] Sawalhi, N., and Randall, R. B., 2005, "Spectral kurtosis optimization for rolling element bearings," Proceedings - 8th International Symposium on Signal Processing and its Applications, ISSPA 2005 , **2,** pp. 839-842.

[141] P. Dempsey,D. Lewicki ,H .Decker ,' Transmission Bearing Damage Detection Using Decision Fusion Analysis', NASA/TM—2004-213382,NASA, 2004.

[142] P. Dempsey, M Mosher, E Huff,' Threshold Assessment of Gear Diagnostic Tools on Flight and Test Rig Data', NASA/TM—2003-212220/REV1,NASA,2003

[143] P. Dempsey,G .Kreider,T .Fichter ,' Tapered Roller Bearing Damage Detection Using Decision Fusion Analysis', NASA/TM—2006-214380,NASA,2006.

[144] P. Dempsey,J. Zakrajsek,' Minimizing Load Effects on NA4 Gear Vibration Diagnostic Parameter', NASA/TM—2001-210671,NASA,2001

[145] Sikorska, J. Z., and Mba, D., 2008, "Challenges and Obstacles in the Application of Acoustic Emission to Process Machinery," Proceedings of the Institution of Mechanical Engineers, Part E: Journal of Process Mechanical Engineering, **222**(1) pp. 1-19.

[146] Haynes, Howard D. (Kingston, TN), and Eissenberg, David M. (Oak Ridge, TN), 1990, "Motor Current Signature Analysis Method for Diagnosing Motor Operated Devices " **07/436139** (United States Patent 4965513) .

[147] Gottlieb, I.M., 1994, "Electric motors and control techniques," TAB/McGraw-Hill, Blue Ridge Summit, PA, .

[148] Pillay, P., and Xu, Z., 1996, "Motor current signature analysis," Conference Record of the 1996 IEEE Industry Applications Conference Thirty-First IAS Annual Meeting, IEEE, San Diego, CA, USA, **1,** pp. 587-94.

[149] Kryter, R. C., and Haynes, H. D., 1989, "Condition Monitoring of Machinery using Motor Current Signature Analysis," S V Sound and Vibration, **23**(9) pp. 14-21.

[150] Benbouzid, M. E. H., 1999, "Motor Current Signature Analysis for Induction Motors Faults Detection and Diagnosis-a Review," Electromotion, **6**(4) pp. 160-74.

[151] Culbert, I. M., and Rhodes, W., 2007, "Using Current Signature Analysis Technology to Reliably Detect Cage Winding Defects in Squirrel-Cage Induction Motors," IEEE Transactions on Industry Applications, **43**(2) pp. 422-428.

[152] Thomson, W. T., and Fenger, M., 2001, "Current Signature Analysis to Detect Induction Motor Faults," IEEE Industry Applications Magazine, **7**(4) pp. 26-34.

[153] Huh, K., and Lee, K., 2000, "Cutting Force Estimation Systems Based on AC Spindle Drive," JSME International Journal.Series C: Mechanical Systems, Machine Elements and Manufacturing, **43**(1) pp. 230-236.

[154] Stein, J. L., and Wang, C., 1990, "Analysis of Power Monitoring on AC Induction Drive Systems," Journal of Dynamic Systems, Measurement and Control, Transactions ASME, **112**(2) pp. 239-248.

[154] Li, X., 2001, "Detection of Tool Flute Breakage in End Milling using Feed-Motor Current Signatures," IEEE/ASME Transactions on Mechatronics, **6**(4) pp. 491-8.

[156] Oh, Y. T., Kwon, W. T., and Chu, C. N., 2004, "Drilling Torque Control using Spindle Motor Current and its Effect on Tool Wear," International Journal of Advanced Manufacturing Technology, **24**(5-6) pp. 327-334.

[157] Rajagopalan, S., Habetler, T. G., Harley, R. G., 2006, "Current/voltage-Based Detection of Faults in Gears Coupled to Electric Motors," IEEE Transactions on Industry Applications, **42**(6) pp. 1412-20.

[158] Mohanty, A. R., and Kar, C., 2006, "Fault Detection in a Multistage Gearbox by Demodulation of Motor Current Waveform," Industrial Electronics, IEEE Transactions on, **53**(4) pp. 1285-1297.

[159] Toutountzakis, T., and Mba, D., 2003, "Observations of Acoustic Emission Activity during Gear Defect Diagnosis," NDT&E International, **36**(7) pp. 471-7.

[160] Townsend, D. P., 1985, "Lubrication and Cooling for High Speed Gears." .

[161] Kar, C., and Mohanty, A. R., 2006, "Monitoring Gear Vibrations through Motor Current Signature Analysis and Wavelet Transform," Mechanical Systems and Signal Processing, **20**(1) pp. 158-187.

[162] Zhang, Y., and Randall, R. B., 2009, "Rolling Element Bearing Fault Diagnosis Based on the Combination of Genetic Algorithms and Fast Kurtogram," Mechanical Systems and Signal Processing, **23**(5) pp. 1509-1517.

[163] Jérôme Antoni, http://www.utc.fr/~antoni/ .

[164] Vallen GmBH, "Vallen GmBH,Http://www.Vallen.de/," .

[165] LIN, J., and QU, L., 2000, "FEATURE EXTRACTION BASED ON MORLET WAVELET AND ITS APPLICATION FOR MECHANICAL FAULT DIAGNOSIS," Journal of Sound and Vibration, **234**(1) pp. 135-148.

Appendix A

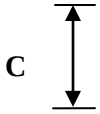

1	2	3	4
5	6	7	8

Each zone (1-8) represents the 12.5% of a tooth surface area on the pinion gear

Table A 1

Time Interval (hour)	Occurred Damage
43	Few pits were noted in Zone 5 C=7 mm
114	Deep score with size of 2 × 2 mm was noted at zone 5 while some light pits were observed in zone 6
322	Pits moving toward zone 7,similar number of pits and score in zones 5-6 but deeper
486	Deep scores with average size of 2 × 2 mm were noted in zones 1,5,2,6 and 7
658	The scores become deeper and a new scores was noted at zone 8
778	50 % pitting was reached and Almost every tooth has large pits across face width

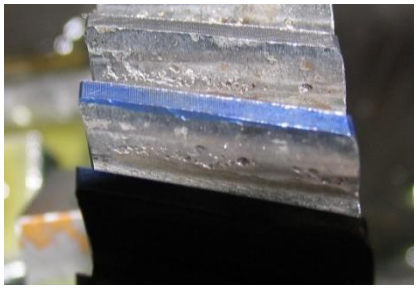

Figure A 1 pitting damaged occurred on the tooth face

Table A 2 Pitting progress

Test 1		Test 2	
Pitting %	**Time(h)**	**Pitting %**	**Time(h)**
0	12	0	20
5.7	24	3	43
6	30	11	78
6.4	41	12.5	97
7	52	12.	114
8	64	13	134
8.5	76	13	157
10	89	13	204
10.5	101	18	276
12	114	22	322
12	125	22	345
12	138	22	389
13	147	22	415
13	161	22	437
16	174	24	460
17	185	26	486
17.5	197	26	513
18	213	30	554
18	233	36	601
18.5	246	38	658
20.5	260	40	682
22	272	48	778
24	295		
24	318		

Appendix B

Table B 1 AE r.m.s and standard deviation (STD) values associated with each defect at different conditions

Condition / Defect No	D		A		B		C	
Defect Free	r.m.s	0.3408	r.m.s	0.3408	r.m.s	0.2954	r.m.s	0.2382
	std	0.0423	std	0.0423	std	0.0568	std	0.0256
Defect 1	r.m.s	0.4087	r.m.s	0.3614	r.m.s	0.3349	r.m.s	0.2971
	std	0.0491	std	0.036	std	0.067	std	0.0645
Defect 2	r.m.s	0.4607	r.m.s	0.4094	r.m.s	0.369	r.m.s	0.2734
	std	0.0295	std	0.0375	std	0.0842	std	0.039
Defect 3	r.m.s	0.5118	r.m.s	0.4352	r.m.s	0.3813	r.m.s	0.3454
	std	0.0845	std	0.046	std	0.0839	std	0.0815
Defect 4	r.m.s	0.5055	r.m.s	0.4241	r.m.s	0.467	r.m.s	0.4366
	std	0.0547	std	0.0475	std	0.0669	std	0.0799
Defect 5	r.m.s	0.4775	r.m.s	0.4108	r.m.s	0.4535	r.m.s	0.4124
	std	0.0615	std	0.0423	std	0.0776	std	0.0463
Defect 6	r.m.s	0.5303	r.m.s	0.4326	r.m.s	0.5437	r.m.s	0.4444
	std	0.0571	std	0.0387	std	0.0576	std	0.0649
Defect 7	r.m.s	0.5416	r.m.s	0.4679	r.m.s	0.5463	r.m.s	0.4801
	std	0.0679	std	0.0445	std	0.0745	std	0.0652

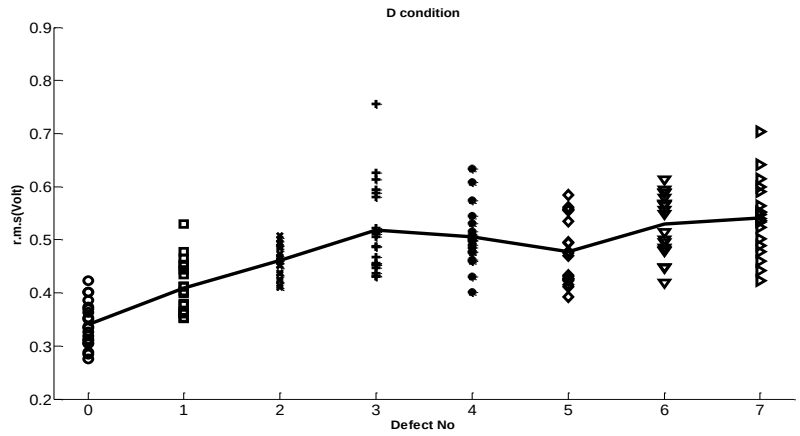

Figure B 1 AE r.m.s level associated with defect condition 'D'

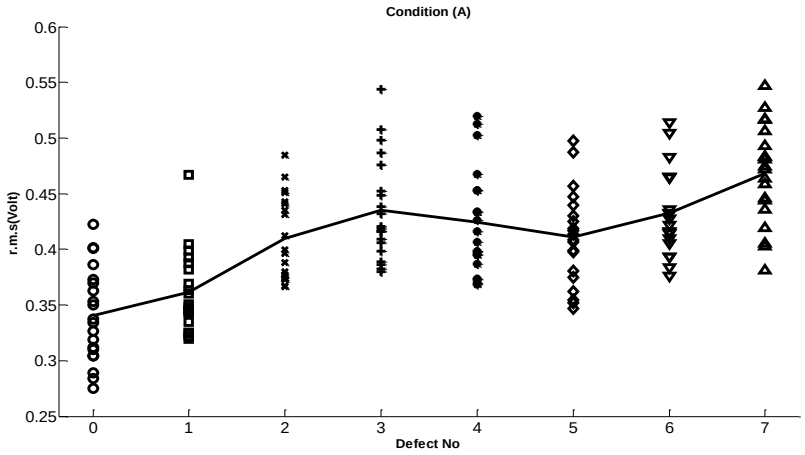

Figure B 2 AE r.m.s level associated with defect condition 'A'

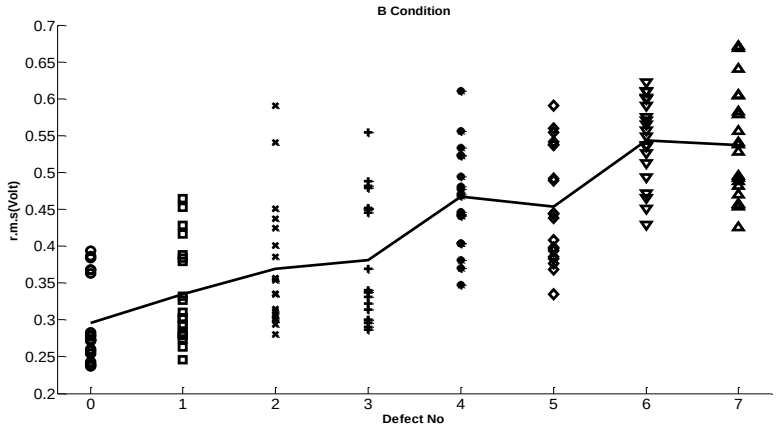

Figure B 3 AE r.m.s level associated with defect condition 'B'

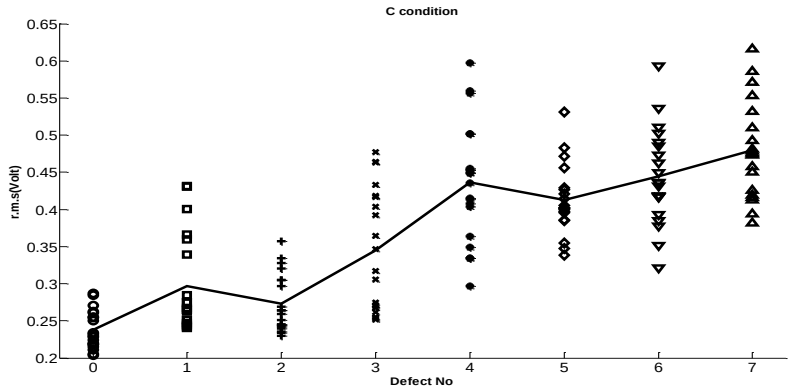

Figure B 4 AE r.m.s level associated with defect condition 'C'

Appendix C

Table C 1 lists the values of shear stress yield shear stress for different materials. Also listed the maximum externally applied pressure (P) values below which the deformation within the contact zone is within the elastic region. These values are determined from Equation 4 and 5. The values are calculated for three different radius of curvature of 5, 10 and 15 mm.

Table C 1 Indicative values of stress within the contact zone

Material	**Young modulus (GPa)**	**Ultimate tensile stress (MPa)**	**Yield stress (Mpa)**	**Yield shear stress (Mpa)**	**Maximum external pressure (Gpa)**		
					5 mm	**10 mm**	**15 mm**
Alloy steel (AISI 4340)	200	744	472	273	204	818	1840
Aluminium alloy (AA 2011)	75	295	380	209	251	1000	2267
Ductile iron	190	414	256	192	77	308	694